Dispersion of a Tracer

in the Eastern Tropical South Pacific

- an Investigation of Interactions from the Benthic Boundary Layer to the Ocean Interior -

Dissertation
to obtain the Doctoral Degree
at the Faculty of Mathematics and Natural Sciences
at the Christian-Albrechts-University of Kiel

submitted by
Madeleine Freund
Kiel, 2020

Dispersion of a Tracer

in the Eastern Tropical South Pacific

- an Investigation of Interactions from the Benthic Boundary Layer to the Ocean Interior -

Dissertation
zur Erlangung des Doktorgrades
der Mathematisch-Naturwissenschaftlichen Fakultät
der Christian-Albrechts-Universität zu Kiel

vorgelegt vom
Madeleine Freund
Kiel, 2020

Erster Gutachter: Prof. Dr. Martin Visbeck
Zweiter Gutachter: Prof. Dr. Andreas Oschlies

Tag der mündlichen Prüfung: 27.04.2020
Zum Druck genehmigt: 27.04.2020

---

gez. Prof. Dr. Frank Kempken, Dekan

Abstract

Wind and buoyancy driven oceanic circulation and turbulent diffusion distribute heat, salt, and other dissolved constituents such as oxygen, carbon dioxide, or nutrients in the ocean. However, natural variability of physical processes, and the nutrient fluxes are complex, highly dynamic and difficult to observe directly. Especially, how the physical processes affect overall biogeochemical tracers is still an important subject of research. The region of interest is the Eastern Tropical South Pacific where anoxic conditions on the continental shelf off Peru and Chile lead to a release of nutrients from the sediments into the water directly above. The fate of these nutrients is not well understood, yet. This thesis summarizes the studies inferring the spread of an artificial dissolved constituent, a tracer potentially representing such nutrients, using a so called tracer release experiment performed to quantify the benthic pelagic exchanges in the Peruvian oxygen minimum zone. This provides the physical basis to identify and quantify pathways potentially used by the nutrients. The Peru-Chile undercurrent and mesoscale eddy activity are found to dominate the lateral tracer dispersion and are responsible for a fast and wide tracer spread to the south and in the offshore ocean. The tracer transport velocity in the Peru-Chile undercurrent near by Callao ($\sim$12°S) is 3-5 cm s^{-1} and 7-17 cm s^{-1} southward from Paracas headland (14-17.5°S). Anticyclonic eddies (mainly the subsurface ones) capture 21-54% of the tracer in their cores which reaches the offshore ocean. This way the eddies denote the connection between the Peruvian shelf and the offshore ocean, but the Peru-Chile undercurrent acts first and place the tracer into the eddy generation hot spot. In the vertical, there is an upward tracer motion. It happens basically diapycnal, i.e. across density surfaces, and thus is accompanied by a lightening of tracer tagged-water. In the process, the tracer crawls upward the shelf along the slope within the bottom boundary water layer. Thus the theory by Ferrari et al. (2016); Holmes et al. (2019) seems to sufficiently explain the observed behavior. Overall 10-30$\pm$10% of the tracer rise, even high enough to reach the surface waters. In contrast, the open ocean diapycnal diffusivity coefficient is $(1.4 \pm 0.4) \cdot 10^{-5}$ m^2 s^{-1}, representative for calm open ocean regimes. Thus it cannot account for the upward motion but fills in a geographic gap of such values. With this physical basis it is possible to conclude on the nutrient constrains. Typical nutrient concentration pattern over the Peruvian shelf not only waft back and forth or recirculate locally but need to be permanent reestablished by a source, namely their release from the sediments, as the substances in the water column are permanently transported away. The upward motion is especially important as it shows a pathway into the euphotic surface waters provided by ocean physics. Thus nutrients released from the shelf sediments could potentially be used for primary production in these realms.

German Abstract - Zusammenfassung

Die durch Wind und Dichteveränderungen getriebenen Meeresströmungen sowie turbulente Diffusion bestimmen die Verteilung von Wärme, Salzgehalt, und anderen gelösten Substanzen wie Sauerstoff, Kohlendioxid oder Nährstoffen im Ozean. Jedoch sind natürliche Variabilitäten der physikalischen Prozesse und Nährstoffflüsse komplex, sehr dynamisch und schwierig direkt zu beobachten. Insbesondere wie physikalische Prozesse auf biogeochemische Stoffe wirken ist ein wichtiges Thema in der gegenwärtigen Forschung. Als Untersuchungsgebiet wurde der tropische Süd-Ost Pazifik gewählt, da dort sauerstoffarme Bedingungen am Kontinentalhang vor Peru und Chile dazu führen, dass Nährstoffe aus dem Sediment in die darüber liegende Wasserschicht frei gesetzt werden. Der Verbleib dieser Nährstoffe ist bis jetzt noch ungeklärt. In dieser Doktorarbeit sind die Studien zusammen gefasst, die die Ausbreitung einer künstlichen, gelösten Substanz untersuchen. Diese Substanz ist ein Marker, der die Nährstoffe repräsentiert, und wurde in einem so genannten "Tracer Release" Experiment ausgebracht, um Interaktionen von der benthischen Grenzschicht ins Freiwasser zu bestimmen. Dies bildet eine physikalische Grundlage, um mögliche, den Nährstoffen zur Verfügung stehende, Wege zu identifizieren und zu quantifizieren. Der Peru-Chile Unterstrom und mesoskalige Wirbelaktivität dominieren die laterale Marker-Verteilung und verursachen eine schnelle und weit reichende Marker-Ausbreitung nach Süden und in den offenen Ozean. Die Transport-Geschwindigkeit mit dem Peru-Chile Unterstrom beträgt nahe Callao (∼12°S) 3-5 cm s^{-1} und 7-17 cm s^{-1} von der Paracas Landspitze südwärts (14-17.5°S). Antizyklonal drehende Wirbel (vorrangig die in mittlerer Wassertiefe) schließen 21-54% des Markers in ihren Kernen ein, der so in den offenen Ozean gebracht wird. Auf diese Weise bilden die Wirbel die Verbindung zwischen dem Peruanischen Kontinentalhang und dem offenen Ozean, aber es ist der Peru-Chile Unterstrom der zuerst den Marker beeinflusst und in das Gebiet mit der höchsten Wirbelbildungsrate bringt. In der Vertikalen bewegt sich der Marker aufwärts. Das geschieht hauptsächlich durch kleinskalige turbulente Vermischung über Dichteflächen hinweg, so dass das markierte Wasser leichter wird. Dabei kriecht der Marker am Kontinentalhang entlang der Flanke, in der Bodenwassergrenzschicht nach oben. Somit erklärt die theoretische Grundlage von Ferrari et al. (2016); Holmes et al. (2019) das beobachtete Verhalten des Markers ausreichend gut. Insgesamt steigen 10-30±10% des Markers zur Meeresoberfläche auf. Im Gegensatz dazu ist der diapycnische Diffusions-Koeffizient im offenen Ozean $(1.4 \pm 0.4) \cdot 10^{-5}$ m^2 s^{-1} repräsentativ für wenig dynamische Bereiche des Ozeans. Deshalb kann die aufwärtige Bewegung nicht durch die Prozesse stattfinden, die durch den Koeffizienten repräsentiert werden. Der Koeffizient füllt jedoch eine Lücke in der geographischen Abdeckung solcher Werte. Auf Basis der physikalischen Ergebnisse kann folgendes für die Nährstoffbelange geschlussfolgert werden: Typische Verteilungsmuster der Nährstoffkonzentration über dem Peruanischen Kontinentalhang wabern nicht einfach hin und her und zirkulieren auch nicht an Ort und Stelle, sondern diese Verteilungsmuster müssen sich beständig aus einer Nährstoffquelle, den Sedimenten, erneuern; da die Stoffe in der Wassersäule beständig abtransportiert werden. Die nach oben gerichtete Bewegung ist besonders wichtig, da sie zeigt, dass physikalisch ein Verbindungsweg in lichtreiche Wasserschichten an der Oberfläche besteht. Damit könnten in diesen Schichten

Nährstoffe aus den Sedimenten am Boden des Kontinentalhanges für Primärproduktion (also Algenblüte, etc.) genutzt werden.

Contents

Abstract **I**

List of Figures **XII**

List of Tables **XIII**

List of Abbreviations **XIV**

1 Introduction **1**

1.1 Motivation, Frame, and the Scientific Key Questions 1

1.2 The Study Area - Eastern Tropical South Pacific (ETSP) 2

1.2.1 The Peru Current System 3

1.2.2 The ETSP subsurface OMZ and anoxic sediments on the continental shelf 4

1.2.3 Eddies in the ETSP 5

1.2.4 El Niño Dynamics 7

1.2.5 Offshore Diapycnal Diffusivity 8

1.3 Vertical Tracer Motion at a Continental Shelf 10

1.4 Tracer Release Experiments (TREs) 12

2 Data and Methods **15**

2.1 The Observational 'Peruvian Oxygen-minimum-zone System Tracer Release Experiment' (POSTRE) 15

2.1.1 Tracer Injection and Initial Conditions 15

2.1.2 Tracer Survey 17

2.2 Modeled TREs (moTREs) 18

2.2.1 Overview and Strategy 18

2.2.2 ROMS/CROCO model for moTRE1 and moTRE2 20

2.2.3 NEMO model for moTRE3 and moTRE4 22

2.2.4 Data Processing 22

2.2.4.1 Model Data and Tracer Units 22

2.2.4.2 Model Tracer in Shallow Waters 23

2.2.4.3 Hovmoeller Diagrams 23

3 Advective Regimes and the Connectivity from the Shelfbreak to the Open Ocean **27**

Abstract of the Chapter . . . 27
3.1 Lateral Tracer Distribution . . . 28
3.1.1 POSTRE Tracer Distribution after 17 months . . . 28
3.1.2 moTREs Tracer Distributions after 17 months in Comparison to POSTRE 28
3.1.3 A First Description of the Time Development of the moTREs Tracer Distributions . . . 32
3.2 Depth Dependent Lateral Tracer Distribution . . . 35
3.3 Spatio-Temporal Tracer Spread in the moTREs . . . 38
3.4 Coast-Parallel Tracer Export by the PCUC . . . 43
3.5 Offshore Tracer Export by Mesoscale Eddy Activity . . . 46
3.5.1 POSTRE Tracer Captured in Anticyclonic (Mode-Water) Eddies . . . 46
3.5.2 moTREs Tracer Relation to Mesoscale Eddies . . . 48
3.6 Discussion . . . 51

4 Upward Tracer Motion and the Connectivity from the Bottom Boundary to the Euphotic Zone 54
Abstract of the Chapter . . . 54
4.1 The Observational TRE - POSTRE . . . 55
4.1.1 Tracer Distribution in Depth Space, and Upward Tracer Motion . . . 55
4.1.2 Isopycnal Heave from Injection to Survey, El Niño Influence, and the Stratification Conditions of POSTRE . . . 56
4.1.3 Tracer Distribution in Density Space, and Lightening of Tracer-Tagged Water . . . 59
4.1.4 Tracer Distribution in Temperature - Salinity Space, and Property Changes of the Lightening Tracer-Tagged Water . . . 59
4.2 The moTREs in Comparison to POSTRE . . . 62
4.2.1 Tracer Distribution in Depth Space, and Upward Tracer Motion . . . 62
4.2.2 Tracer Distribution in Density Space, and Lightening of Tracer-Tagged Water . . . 64
4.2.3 Tracer Distribution in Temperature - Salinity Space, and Property Changes of the Lightening Tracer-Tagged Water . . . 65
4.2.4 moTREs' Focus on the Coastal Region and the Early Stages of the Experiments . . . 68
4.3 Summary and Discussion . . . 69

5 Eastern Tropical South Pacific Diapycnal Diffusivity within the Offshore Oxygen Minimum Zone 73
Abstract of the Chapter . . . 73
5.1 Preamble . . . 74
5.2 Data Analysis and Result . . . 74
5.3 Discussion . . . 78

6 Summary and Outlook **82**

Appendices **85**

A moTREs in Depth-, Density-, and θ-S-Space at Full Horizontal Resolution 85

B Supporting Information - Data Set: The Processed Tracer Injection Data 89

References **91**

Acknowledgements **XVII**

Expression of Thanks **XX**

Declaration **XXI**

List of Figures

1.1 **Overview about relevant processes governing the tracer distribution in the ETSP.** The tracer and its behavior is indicated in red; shelf/land in brown, the water (including its motions: surface current at the shelf, PCUC, and eddies) in blue. 3

1.2 "**Oxygen concentration** (μmol kg^{-1}) **in the eastern tropical Pacific** at σ_θ = 26.8 kg m^{-3} (close to the deep oxygen minimum) as obtained from the MIMOC climatology (Schmidtko et al., 2013) **with circulation schematic** superimposed. Current bands displayed are, for the surface layer (white solid arrows), the South Equatorial Current (SEC), the Equatorial Undercurrent (EUC), the Peru-Chile or Humboldt Current (PCC/HC), the Peru Oceanic Current (POC), and for the thermocline layer (white dashed arrows), the North Equatorial Intermediate Current (NEIC), the North Intermediate Countercurrent (NICC), the Equatorial Intermediate Current (EIC), the South Intermediate Countercurrent (SICC), the primary and secondary Southern Subsurface countercurrents (pSSCC,sSSCC), the deeper layer of the SEC, the Chile-Peru Coastal Current (CPCC), the Peru-Chile Undercurrent (PCUC) and the Peru-Chile Countercurrent (PCCC). The location of the $\sim$ 86°W section is marked by the black line." (Brandt et al. 2015, their Fig. 2) 4

1.3 "[... The] sampling locations (triangles) on the Peruvian margin at 12°S during January 2013. [...] **Cross-section of dissolved oxygen concentrations [... and] distributions of [...] nitrate [and] nitrite** [...]. The white contours show the potential density (kg m^{-3}). [...]" (modified from Sommer et al., 2016, their Figs. 1 & 3) 5

1.4 **Subsurface eddy generation spots** (dots) **and propagation pathways** (gray and red tracks) for eddies existing at least 9 months. Climatological dissolved oxygen on the 26.7 kg m^3 isopycnal shaded and contoured in white. Modified from Frenger et al. (2018); the gray box denote their eddy tracking region. 7

1.5 **Schematic ENSO conditions** (e.g. McPhaden, 2004). 8

1.6 **Global maps of diapycnal diffusivity estimates** (a) averaged between 250-500 m water depth, over five years (2006-2011), and over 1.5° square bins of ARGO data (Whalen et al., 2012, their Fig. 2a); and (b) averaged between the mixed layer depth and 1000 m water depth (Waterhouse et al., 2014, their Fig.1a). It shows the need to improve the data coverage and to further gain diffusivity estimates in the (South) Pacific and especially the ETSP. 9

1.7 "A longitude-depth section of the near-boundary region of the ocean above rough topography is characterized by enhanced turbulence generated by tidal and geostrophic flows impinging over topography. [BBL and SML are indicated. ...] A typical vertical profile of the turbulent density flux $F_\rho^{(z)}$ through the BBL and SML is sketched on the upper-right corner of the figure. [...] The black arrows indicate **the diabatic sinking of waters in the SML and the diabatic along-boundary upwelling in the BBL.**" (Ferrari et al. 2016, their Fig. 2) 11

2.1 (a) **The region of interest** with the survey area highlighted (red rectangle) and a zoom in for the POSTRE injection sites. **The modified OTIS** is shown - Photo: C. Marandino, 2015. (b) **The time-dependent density changes during the injection**, i.e. over the duration the tracer got pumped into the ocean (updated from Marandino, 2016, their Fig. 7.10.2). 16

2.2 **Tracer-density relation during the injection** (a) in potential Temperature (θ) - Salinity - space (for clarity only 3-min means are shown). The barplot (b) shows the amount of tracer (in mol) released versus potential density anomaly interval summed over all injections, and a Gaussian fit. The single release sites are identified by gray shades. 17

2.3 **Visualized difference between the s- und z- coordinates** by Shchepetkin and McWilliams (2005, their Fig.1 a&d): "Examples of vertical coordinate systems: (a) S-coordinate of Song and Haidvogel (1994) [...] (d) z-coordinate system toward the S-coordinate." 18

2.4 **Normalized ROMS tracer rushing down the shelf by following the coordinates gradient.** 19

2.5 **Normalized NEMO tracer without the bias** to compare with Fig. 2.4. Thus the tracer does not rush down the shelf. 20

2.6 **Distance from the reference point Callao** (12.03°S, 77.1°W) for each point in lat.-lon.-space in the ETSP. The arrows denote simplified tracer transport directions to give their context to the Hovmoeller diagrams in Figs. 2.7 & 3.6-3.9. 24

2.7 **Hovmoeller diagrams of the moTREs**; (a) moTRE1-ROMS, (b) moTRE2-CROCO, (c) moTRE3-NEMO, (d) moTRE4-NEMO. The y-axis denotes the distance to the geographical reference point Callao (12.03°S, 77.1°W). Please note the different color axis between the ROMS/CROCO TREs (moTRE1 and moTRE2) and the NEMO TREs (moTRE3 and moTRE4). 25

3.1 **Lateral tracer distribution by the vertical column integral** in nmol m^{-2} 17 months after injection; (a) POSTRE (filled circles for the measurement at each station and smoothed), (b) moTRE1-ROMS, (c) moTRE2-CROCO, (d) moTRE3-NEMO, (e) and moTRE4-NEMO. The 2000m-isobath and injection sites (asterisks and stars) are indicated. Please note the different color axis for the NEMO TREs (moTRE3 and moTRE4) compared to POSTRE and the ROMS TREs (moTRE1 and moTRE2). 29

3.2 **moTREs subsampled at the observational stations** and smoothed equivalently; (a) moTRE1-ROMS, (b) moTRE2-CROCO, (c) moTRE3-NEMO, (d) moTRE4-NEMO. Stars denote the model, asterisks the observational injection sites. Please note the different color axis for the NEMO TREs (moTRE3 and moTRE4) compared to POSTRE and the ROMS TREs (moTRE1 and moTRE2). 31

3.3 **Time dependent lateral tracer distribution** by the vertical column integral normalized with the maximum tracer concentration; after 1.5, 3, and 6 months for the moTREs. Continued on the next page for 12, 18, and 24 months after injection. 33

3.3 Continuing - **Time dependent lateral tracer distribution** by the vertical column integral normalized with the maximum tracer concentration; after 12, 18, and 24* months for the moTREs. *Please note for moTRE3, the last available time step is 22.5 months after injection, not 24. 34

3.4 **Depth dependent lateral tracer distribution exemplary for the POSTRE tracer** along 17°S after 17 months. The color coded dots denote the actually measured concentration on top of the interpolated field. The shelf is indicated in gray at about 72°W. 35

3.5 **Depth dependent lateral tracer distribution exemplary for the moTREs tracers** along 17°S after 1.5, 3, 6, 12, 17, and 24 months; (a) moTRE1-ROMS, and (b) moTRE2-CROCO. Continuing on the next page with (c) moTRE3-NEMO, and (d) moTRE4-NEMO. The shelf is indicated in gray at about 72°W. 36

3.5 Continuing - **Depth dependent lateral tracer distribution exemplary for the moTREs** tracers along 17°S after 1.5, 3, 6, 12, 17, and 22.5/24 months; (c) moTRE3-NEMO, and (d) moTRE4-NEMO. The shelf is indicated in gray at about 72°W. 37

3.6 **Hovmoeller diagram of moTRE1-ROMS** with markers for points to derive the slopes indicating the tracer transport distances over time and thus the velocity. 39

3.7 **Hovmoeller diagram of moTRE2-CROCO** with markers for points to derive the slopes indicating the tracer transport distances over time and thus the velocity. 40

3.8 **Hovmoeller diagram of moTRE3-NEMO** with markers for points to derive the slopes indicating the tracer transport distances over time and thus the velocity. 41

3.9 **Hovmoeller diagram of moTRE4-NEMO** with markers for points to derive the slopes indicating the tracer transport distances over time and thus the velocity. 42

3.10 **Averaged** (over three years) **velocity field from the ROMS-CLIM configuration**. (a) Mean horizontal velocities over the depth range around 130±15 m with absolute velocity values in color and directions denoted by arrows. (b) Meridional velocity component along 15°S. 44
3.11 **The velocity field as measured during the tracer survey in March 2017**, averaged over 600s-bins in the depth range around 130±15 m. (a) The absolute value velocity. (b) The meridional velocity component. 44
3.12 **Aligning the tracer to the PCUC** exemplary along 21°S 17 months after injection for (a) moTRE2-CROCO, and (b) POSTRE; via meridional velocity, salinity and tracer concentration. Please note the different color axis for the tracer concentration. 45
3.13 **Eddies measured during the tracer survey** with SLA (shaded) on 17. March 2017 with ship position (x) during survey cruise. Two eddies (A, B) tracked backward (white and black track) to their origin (dot). Sections of observed tracer and hydrography shown in Fig. 3.14 indicated. (Schütte, F., 2017 - personal correspondence) 46
3.14 **Eddy activity** (and PCUC) **found for POSTRE** by observed meridional velocity, tracer, salinity, and oxygen along 18°S, 19°S, and 21°S. Please note the shelf to be at the right side of each section: at 18°S it is at about 70.4°W, at 19°S it is at about 71°W, and at 21° it is at about 70.3°W. 47
3.15 **Representative examples of the eddy-tracer relation in the ROMS/CROCO experiments** (continued in Fig. 3.16), shown here in moTRE2-CROCO. Namely, the tracer distribution is related to salinity and meridional velocity. This is section 21°S, 17 months after injection, showing the tracer captured in an AMW at 74-75°W just detached from the PCUC. 49
3.16 Continuing - **Representative examples of the eddy-tracer relation in the ROMS/CROCO experiments**, shown here in moTRE1-ROMS. Namely, the tracer distribution is related to salinity and meridional velocity. (a) 24°S, 17 months after injection, showing the tracer captured in an ANT at 73-74°W. (b) 19°S, 12 months after injection, showing the CYC at 74.5-76°W free of tracer. (c) 15°S, 17 months after injection, showing a tracer-tagged filament at 82-84°W, and a tracer free AMW at ∼80°W generated on an already tracer freed shelf. (d) 17°S, 17 months after injection, showing CYCs at ∼80°W capturing tracer after its distribution all over the place. Compare to the related lateral tracer distribution map Fig. 3.1 for e.g. the shape of filament and for the already tracer freed shelf. 50

4.1 **Surveyed tracer depth distribution.** Injection depth indicated as blue line, the 50 m isobath dashed in red, the tracer weighted mean dash dotted in brown. 55
4.2 **Well mixed coastal profiles** as indication for enhanced mixing at the shelf. . . 55

4.3 (a) **The depth of 26.3-isopycnal** in March, June, October, December. And (b) the depth difference of 26.3-isopycnal depth between October and March. . . 56
4.4 **Comparing the observed and climatological** (a) depth of 26.3-isopycnal in October and (b) the depth of the 26.17-isopycnal in March. The shades in the maps are derived from the MIMOC climatology (Schmidtko et al., 2013); the overlaid dots are the observed properties of the injection and survey cruises labeled with SO243 and M135, respectively. 57
4.5 **Surveyed tracer density distribution.** Injection depth indicated as blue line, the tracer weighted mean dash dotted in brown. 59
4.6 **Properties** (potential temperature, salinity, and oxygen) **of POSTRE tracer-tagged water.** 60
4.7 θ**-S relation of** (a) **the surveyed tracer samples** color coded by concentration and injection in blue; and of (b) the related oxygen content. Isopycnals in gray. The bluish lines in (b) show the mean θ-S profiles averaged over five regions within the study area: (1) from the southernmost station up to including 22°S, (2) over 20°S to 21°S, (3) over 19°S to 18°S, (4) over 16°S to 17°S, and (5) from including 15°S to the northernmost station. 60
4.8 **Tracer depth distribution 17 months after injection** for (a) POSTRE, (b) moTRE1-ROMS, (c) moTRE2-CROCO, (d) moTRE3-NEMO, and (e) moTRE4-NEMO. Injection depth indicated as blue line, the 50 m isobath dashed in red, the tracer weighted mean (of the full moTREs) dash dotted in brown. The moTREs' samples are shown with surface tracer, but subsampled at the stations of the observation. 63
4.9 **Tracer weighted mean depth over time.** 64
4.10 **Tracer density distribution 17 months after injection** for (a) POSTRE, (b) moTRE1-ROMS, (c) moTRE2-CROCO, (d) moTRE3-NEMO, and (e) moTRE4-NEMO. Injection depth indicated as blue line, the tracer weighted mean (of the full moTREs) dash dotted in brown. The moTREs' samples are subsampled at the stations of the observation. 65
4.11 θ-S relation of POSTRE (a & b) as in Fig. 4.7. θ**-S relation of the tracer concentration after 17 months** for (c) moTRE1-ROMS, (d) moTRE2-CROCO, (e) moTRE3-NEMO, (f) moTRE4-NEMO; subsampled on the observational stations. The injection is shown in blue. Isopycnals in gray. 67
4.12 **Tracer at the shelf in the early stages of the experiment**, exemplary for (a) moTRE1-ROMS at 17°S and (b) moTRE3-NEMO at 15°S, i.e. in both cases about 1-1.5° of latitude south of the southern most injection site. 68

5.1 (a) Vertical column integral to show **the stations used here**; with injection sites (asterisks), and the 2000 m isobath (black line). Stations not used are in gray. Bathymetry and topography are shown in blue, green, and brown.
(b) **Vertical profiles of the density-depth conditions** for the open ocean stations of the survey cruise (gray) and its mean (black). 75

5.2 **Buoyancy frequency (N) in March**, whereas N is calculated for the depths layers between the 26.17 and 26.348 - isopycnals, from hydrographic profiles using the toolbox by McDougall and Barker (2011). The shades in the maps are derived from the MIMOC climatology (Schmidtko et al., 2013); the overlaid dots are the observed properties of the survey cruises labeled with M135. The injection sites are indicated by asterisks. 75

5.3 **Vertical tracer profiles as a function of density (a) and distance from their respective peak density (b)**; with the mean surveyed profile in blue, its Gaussian fit in red, and the Gaussian fitted injection profile (cp. Fig. 2.2b) in black. 77

6.1 **Summarizing the relevant processes governing the tracer distribution and their quantified effect on the tracer in the ETSP.** The tracer and its behavior is indicated in red; shelf/land in brown, the water (including its motions: PCUC, and eddies) in blue. 83

A.1 **Tracer depth distribution 17 months after injection** for (a) POSTRE, (b) moTRE1-ROMS, (c) moTRE2-CROCO, (d) moTRE3-NEMO, and (e) moTRE4-NEMO. Injection depth indicated as blue line, the 50 m isobath dashed in red, the tracer weigthed mean dash dotted in brown. The moTREs are shown with surface tracer. Note the different y-axis for NEMO. 86

A.2 **Tracer density distribution 17 months after injection** for (a) POSTRE, (b) moTRE1-ROMS, (c) moTRE2-CROCO, (d) moTRE3-NEMO, (e) moTRE4-NEMO. Injection depth indicated as blue/black line, the tracer weigthed mean dash dotted in brown. Note the different y-axis for NEMO. 87

A.3 **θ-S relation** of (a) moTRE1-ROMS, (b) moTRE2-CROCO, (c) moTRE3-NEMO, (d) moTRE4-NEMO. The injection is shown in blue. The tracer concentration 17 months after the injection is color coded. Isopycnals in gray. 88

List of Tables

1.1 **Summary of relevant eddy properties in the ETSP.** References in this table are sort cut with CZ18 for Czeschel et al. (2018), ST13 for Stramma et al. (2013), FR18 for Frenger et al. (2018), and CH05, CH08, CH11 for Chaigneau and Pizarro (2005); Chaigneau et al. (2008, 2011), respectively. 6

2.1 **Summarizing POSTRE's injection.** 16

2.2 **Injection sites and depth, and the tracer weighted mean injection density** in comparison between the observational and each model experiment. 21

4.1 **Tracer weighted mean values of depth, density, salinity and temperature compared between injection and 17 months after and the differences in these properties.** 69

5.1 **Bulk investigations** to get an impression of **how strong the initial mixing could affect the open ocean diapycnal diffusivity**. Presumed values are written in red, the bulk results from it are black. 79

B.1 **Processed tracer injection data, which is used to infer the initial conditions** as shown in Fig. 2.2 (a and b) of the main text. 90

Abbreviations

AAIW - Antarctic Intermediate Water

(vm)ADCP - (vessel mounted) Acoustic Current Doppler Profiler

ANT - Anticyclonic eddy

AMW - Anticyclonic mode water eddy

BBL - Bottom Boundary Layer

CTD - Conductivity-Temperature-Depth sensor

CYC - Cyclonic eddy

density - refers to potential density anomaly in kg m^{-3}

ENSO - El Niño Southern Oscillation

ESPIW - Eastern South Pacific Intermediate Water

ESSW - Equatorial SubSurface Water

ETSP - Eastern Tropical South Pacific

ETNA - Eastern Tropical North Atlantic

GC/ECD - gas chromatograph equipped with an electron capture detector

MIMOC - Monthly, Isopycnal/Mixed-layer Ocean Climatology

moTREs - 'modeled TREs', four TREs performed in numerical simulations, with

- **moTRE1** - based on ROMS with climatological driven configuration
- **moTRE2** - based on CROCO with interannually forced configuration, and capturing the 1997/98 El Niño
- **moTRE3 & moTRE4** - based on NEMO, interannually forced and injected in two different years

NEDEs - New England Dye Experiments by Houghton (1997), Houghton and Visbeck (1998), and Houghton et al. (2006)

NEMO - Nucleus for European Modelling of the Ocean

OMZ - Oxygen Minimum Zone

OTIS - Ocean Tracer Injection System

PCUC - Peru-Chile UnderCurrent

POSTRE - Peruvian Oxygen-minimum-zone System Tracer Release Experiment (referred to the observation)

ROMS/CROCO - 'Regional Ocean Model System' and its new version 'Coastal and Regional Ocean COmmunity model'

ROMS-CLIM configuration - climatological driven configuration based on ROMS used for moTRE1

SF_5CF_3 - trifluoromethyl sulfur pentafluoride as current standard tracer for TREs

SF_6 - sulfur hexafluoride former tracer of TREs, replaced by SF_5CF_3

SFB754 - Collaborative Research Center 754 "Climate - Biogeochemistry Interactions in the Tropical Ocean"

SI-videos - Supporting Information: Video Supplement; showing the time development of the modeled lateral tracer distributions in full time resolution

SLA - Sea Level Anomaly

SML - Stratified Mixing Layer

SPESTMW - South Pacific Eastern Sub-Tropical Mode Water

SST - Sea Surface Temperature(s)

temperature - refers to potential temperature (θ) in °C

transport velocity - refers to absolute value tracer transport velocity

TRE - Tracer Release Experiment

1 Introduction

1.1 Motivation, Frame, and the Scientific Key Questions

Oceanic water motions are governed by three dimensional physical processes. Up front, the most important processes are advection and turbulent diffusion which transport and mix water properties, respectively, in the horizontal and the vertical. Among others, relevant water properties are heat and dissolved constituents such as salt, oxygen, carbon dioxide, and nutrients.

The region of interest is an Ekman-driven boundary upwelling region located in the Eastern Tropical South Pacific (ETSP). Here, nutrients distributions are important for the development and maintenance of an Oxygen Minimum Zone (OMZ) and for overall oxygen and especially nitrogen budgets. In particular, the anoxic conditions of the marine sediments on the continental shelf off Peru and Chile lead to a release of nutrients from the sediments into the water directly above, the Bottom Boundary water Layer (BBL). Thus (beyond the general upwelling and OMZ mechanisms) a nutrient behavior in question is a positive feedback loop hypotized by Ingall and Jahnke (1994). This means, when nutrients come up, leave the bottom water, and reach the euphotic zone, they could fuel primary production in the surface waters. This would enlarge the export of organic matter in subsurface waters and thus increase the oxygen consumption. The higher oxygen demand results in an expansion of the anoxic conditions (also over the shelf). In turn, this yields higher nutrient fluxes which release more nutrients from the sediments into the BBL.

The natural variability of physical processes, and the nutrient fluxes in the ETSP are complex, highly dynamic and difficult to observe directly. To investigate the nutrient fluxes and to prove if the feedback loop applies in the ETSP, an artificial tracer is used. In the case regarded in this thesis, the tracer is meant to mimic nutrients released from the anoxic sediments off Peru, and by its nature capture all relevant ocean physics affecting the nutrients.

The use of an artificial tracer provides the possibility to get an overall idea of advection pathways and integrated mixing aspects. It is an integral approach, used to cover and depict the overall situation and enabling long-term and large-range evidence. The evaluation of the tracer fate gives insight in the connectivity between the bottom water and the water column interior or even the surface waters, and in the connectivity between the shelf region and the offshore ocean. It allows quantifications on constituents exchange as a basis for e.g. nutrient or productivity studies and budget constrains. It is also a useful frame for studies investigating single details of

the depicted concept. Though, it is neither the aim of this thesis nor a possibility of the method to disentangle all process contributions.

This thesis contributes to the understanding of the physical processes and pathways in the ETSP as basis for nutrient distributions. The tracer is only affected by ocean physics and by that it is an ideal tool to separate between physical and biogeochemical processes when it comes to nutrient constrains. This will be a basis to better estimate the behavior of biogeochemical constituents, e.g. (a) if nutrients out of the sediments reach the euphotic zone, (b) if they can be transported over wide distances, (c) under which conditions unusual pattern appear, or (d) if oxygen depleted waters from the shelf feed the offshore OMZ.

The overarching aim can be addressed guided by following **scientific key questions**:

1) Which Advective Regimes in the ETSP transport chemical constituents originating from sediments of the continental shelf and connect their dispersion pathway(s) over the shelfbreak to the open ocean; and how effective are these transport paths? (Chapter 3 - Results from a Tracer Release Experiment in the Ocean and Models)

2) How can the upward tracer motion - and its inherent connectivity from the bottom boundary to the euphotic zone - be explained; and how large is the affected portion of chemical constituents? (Chapter 4)

3) Is the diapycnal diffusivity within the offshore OMZ of the ETSP representative for calm open ocean regimes, and what is its best estimate? (Chapter 5)

1.2 The Study Area - Eastern Tropical South Pacific (ETSP)

The ETSP is the oceanic region offshore the western coast of South America. In this thesis it is referred approximately between 5-30°S and 70-90°W. The region's mean state is characterized by the Peru Current System (section 1.2.1) and an OMZ (section 1.2.2) as recently summarized by Brandt et al. (2015, their Fig. 2) and shown below in Fig. 1.2. It is a highly variable region affected by a lot of intraseasonal impacts. Ocean dynamics are associated most importantly with mesoscale eddies (e.g. Penven et al., 2005), coastal trapped waves, strong El Niño events and the atmospheric meridional displacement of the mid latitude South East Pacific Anticyclone (Echevin et al., 2014). In this thesis mesoscale eddy activity (section 1.2.3) and El Niño events (section 1.2.4) are of special interest.

Major local processes shaping chemical constituents are sketched in Fig. 1.1. The Peru-Chile UnderCurrent (PCUC - e.g. Brink et al., 1983; Huyer et al., 1991) and mesoscale eddy activity (e.g. Chaigneau et al., 2009, 2011; Stramma et al., 2013; Czeschel et al., 2018; Frenger et al., 2018, and references therein) are well known advections to govern the lateral distributions of chemical constituents, e.g. the tracer and the nutrients. In the open ocean the turbulent diapycnal diffusion (section 1.2.5) is of interest in comparison to similar measurements to get a global view. The vertical tracer mixing in the coastal areas potentially give new insights to the related processes (expecting the concepts of Ferrari et al., 2016; Holmes et al., 2019, to be

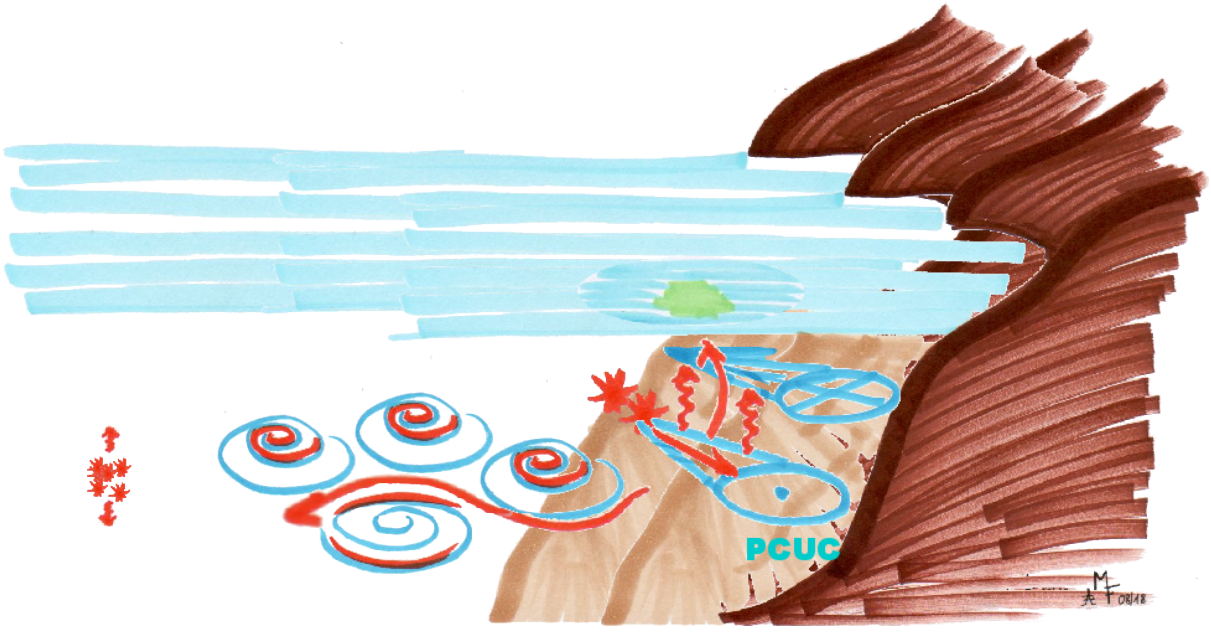

Figure 1.1: Overview about relevant processes governing the tracer distribution in the ETSP. The tracer and its behavior is indicated in red; shelf/land in brown, the water (including its motions: surface current at the shelf, PCUC, and eddies) in blue.

applicable - section 1.3).

1.2.1 The Peru Current System

The Peru Current System denotes the northern part of the Humboldt Current System between 5°S and 20°S (e.g. Brandt et al., 2015; Penven et al., 2005, refer to Fig. 1.2 for details). Off the shelf, there is nearly no meridional flow from the subtropics to the tropics (Karstensen et al., 2008). In contrast, the (Peruvian) shelf is strongly influenced by the surface Humboldt Current (identical to the Peru-Chile Current) and the subsurface Peru-Chile UnderCurrent (PCUC).

The PCUC flows south- / poleward (e.g. Brandt et al., 2015; Penven et al., 2005, and references therein), transporting nutrient rich and oxygen depleted (e.g. Brink et al., 1983; Huyer et al., 1991) Equatorial SubSurface Water (ESSW - Hormazabal et al., 2013). It shows only weak seasonal variability off Peru which gets stronger in austral summer and autumn (e.g. Pizarro et al., 2002; Thomsen et al., 2016; Chaigneau et al., 2013; Penven et al., 2005). However, this eastern boundary current is generally weak and thus affected by eddy and extratropical Rossby wave induced recirculations or the propagation of coastal trapped waves which strongly complicate the PCUC circulation such that the mean state is hard to measure (Chaigneau et al., 2008; Dewitte et al., 2008; Chaigneau et al., 2013).

The equatorial ocean and its currents (e.g. Lukas, 1986) are directly connected to the Peru Current System. These equatorial currents feed especially the PCUC via the lower branch of the Equatorial Undercurrent and the Southern Subsurface Counter Currents (Montes et al., 2010).

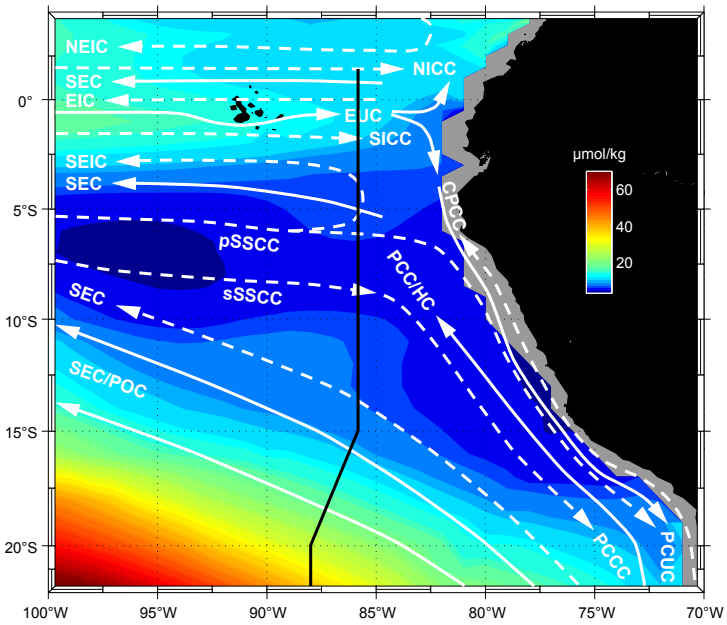

Figure 1.2: "Oxygen concentration (μmol kg^{-1}) in the eastern tropical Pacific at σ_θ = 26.8 kg m^{-3} (close to the deep oxygen minimum) as obtained from the MIMOC climatology (Schmidtko et al., 2013) with circulation schematic superimposed. Current bands displayed are, for the surface layer (white solid arrows), the South Equatorial Current (SEC), the Equatorial Undercurrent (EUC), the Peru-Chile or Humboldt Current (PCC/HC), the Peru Oceanic Current (POC), and for the thermocline layer (white dashed arrows), the North Equatorial Intermediate Current (NEIC), the North Intermediate Countercurrent (NICC), the Equatorial Intermediate Current (EIC), the South Intermediate Countercurrent (SICC), the primary and secondary Southern Subsurface countercurrents (pSSCC, sSSCC), the deeper layer of the SEC, the Chile-Peru Coastal Current (CPCC), the Peru-Chile Undercurrent (PCUC) and the Peru-Chile Countercurrent (PCCC). The location of the $\sim$ 86°W section is marked by the black line." (Brandt et al., 2015, their Fig. 2)

1.2.2 The ETSP subsurface OMZ and anoxic sediments on the continental shelf

As general upwelling and OMZ mechanisms in the ETSP, almost constantly favorable conditions for Ekman-driven eastern boundary coastal upwelling (e.g. Strub et al., 1998) yield year-round high productivity, most intense between 4°S and 16°S (Chavez and Messié, 2009). As common for the eastern boundary upwelling systems of the tropical oceans, it holds an OMZ in intermediate water depths (Fig. 1.2, Brandt et al., 2015; Karstensen et al., 2008). The ETSP OMZ core appears as a double minimum located north of 10°S in about 400 m depth, and south of 10°S near 300 m. The oxygen values are below 4.5 μmol kg^{-1} (Karstensen et al., 2008).

It is known that the ventilation of OMZs generally takes place due to lateral and vertical mixing and zonal advection (e.g. Brandt et al., 2015). The oxygen-rich water is supplied from the western basin by the near equatorial current system (Karstensen et al., 2008). However, the specific ventilation of the ETSP OMZ is still part of ongoing research (e.g. Brandt et al., 2015; Llanillo et al., 2018).

The subsurface OMZ appears in the offshore ocean (Karstensen et al., 2008) but covers also wide ranges of the Peruvian shelf (Fig. 1.3). Anoxic marine sediments on the continental shelf release significant amount of ammonium, phosphorus, reduced iron and silicate (e.g. Bohlen et al., 2011; Noffke et al., 2012; Lomnitz et al., 2016). Therefore, the water layer directly influenced by the

sediments, the BBL, contains high concentrations of nutrients and is particular dynamic in terms of nitrogen cycling (e.g. Kalvelage et al., 2013). To get an impression, representative nitrate and nitrite distributions over the shelf are shown in Fig. 1.3. If the positive feedback loop postulated by Ingall and Jahnke (1994) is applicable in the ETSP, the complex processes responsible for the dispersion of nutrients from the BBL to the surface ocean are additionally potential important for the development and maintenance of the OMZ, on top of the general mechanisms related to the Ekman-driven upwelling. However, these processes partly still lack of understanding and the occurance of the feedback loop is a mechanism in question. And, also the nutrient flux from the continental shelf into the offshore ocean is part of ongoing scientific discussion (e.g. Conway et al., 2018).

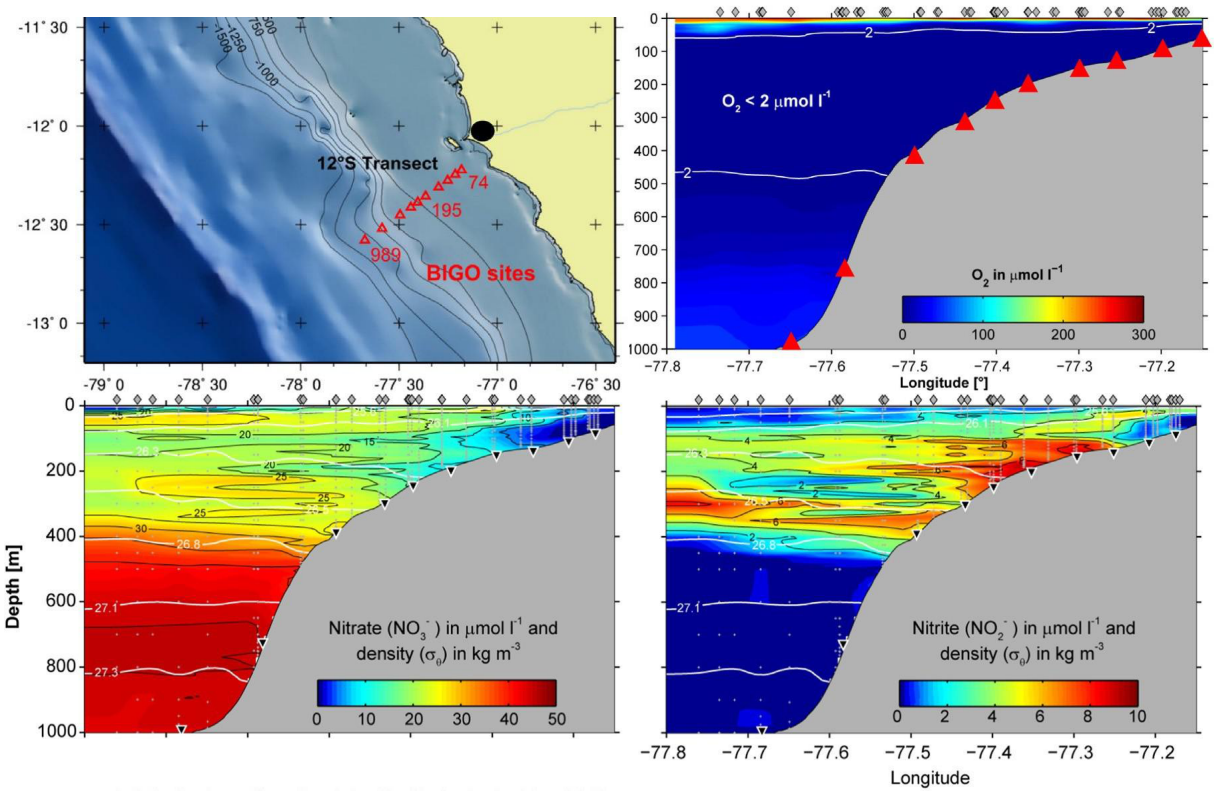

Figure 1.3: "[... The] sampling locations (triangles) on the Peruvian margin at 12°S during January 2013. [...] Cross-section of dissolved oxygen concentrations [... and] distributions of [...] nitrate [and] nitrite [...]. The white contours show the potential density (kg m^{-3}). [...]" (Modified from Sommer et al., 2016, their Figs. 1 & 3)

1.2.3 Eddies in the ETSP

The ETSP mesoscale eddy activity is well explored in general (e.g. Chaigneau and Pizarro, 2005; Chaigneau et al., 2008, 2011; Stramma et al., 2013; Czeschel et al., 2018; Frenger et al., 2018). The most important eddy properties are summarized in Tab. 1.1. In general, an eddy is a non-linear coherent vortex denoted by a rotational speed that exceeds the translation speed (e.g. Chelton et al., 2007). Thus eddies inherent the possibility to trap water properties (such as

momentum, heat, mass, near surface chlorophyll, biological productivity, oxygen, or nutrients) in their cores, and not only stir through the water (e.g. Czeschel et al., 2018; Chaigneau et al., 2011; Frenger et al., 2018).

Table 1.1: Summary of relevant eddy properties in the ETSP.
References in this table are sort cut with CZ18 for Czeschel et al. (2018), ST13 for Stramma et al. (2013), FR18 for Frenger et al. (2018), and CH05, CH08, CH11 for Chaigneau and Pizarro (2005); Chaigneau et al. (2008, 2011), respectively.

Property	**Value**	**Reference**
regions of most frequent eddy appearance	9-10°S and 16-22°S max. at 15-18°S, east of 90°W	CH08, CZ18, ST13
number of eddies formed	228 to ∼310 per year	CZ18, CH11
... of which	∼18% getting older than 3 month 25.7% reach the offshore area	CH11 CZ18
fraction of eddy types	∼49% CYCs and ∼51% ANTs 60-80% of subsurface eddies are AMWs	CZ18 FR18
average eddy radius	50-70 km	FR18, CH11, CZ18
vertical extent	240 m for CYCs and 530 m for ANTs	CH11
mean propagation distance	700 km	CH11
max. propagation distance	>1000 km	ST14
intrinsic propagation	govern ∼80% of the distance	FR18
propagation velocity	∼3 cm s^{-1} to ∼6 cm s^{-1}	CH05

The ETSP eddies propagate everything westward and offshore into the open ocean OMZ (e.g. Klein and Lapeyre, 2009). They are an important part of the advection from the shelf into the offshore ocean and act especially as a carrier for nutrients and oxygen depleted waters along this pathway (e.g. Chaigneau et al., 2011; Stramma et al., 2013; Thomsen et al., 2016; Frenger et al., 2018). Their cores exhibit distinct physical and biogeochemical water anomalies. Whereas Frenger et al. (2018) also speculate that "subsurface eddies maintain greater coherence than surface eddies and are therefore particularly efficient at transporting material properties over long distances."

The eddy generation area in the ETSP is close to the Peruvian and Chilenian coast (e.g. Chaigneau et al., 2011; Czeschel et al., 2018; Frenger et al., 2018). This is nicely demonstrated by Frenger et al. (2018) for subsurface eddies in their model (Geophysical Fluid Dynamics Laboratory - GDFL - with 0.1° spatial resolution and 50 vertical levels; their Fig. 6) and shown here as Fig. 1.4. For the purpose of this thesis it is interesting that no eddy is generated north of about 13.7°S and the majority of eddies is generated south of Arica (ca. 18.5°S) all the way south along the coast until about 40-45°S. Overall these eddies propagate to the west but also slightly northward reaching up to 10°S in the offshore region.

The eddies are formed by boundary current separation due to the sharp topographic bend (Molemaker et al., 2015; Thomsen et al., 2016). The anticyclones (ANTs) are generated due to instabilities of the PCUC (Colas et al., 2012; Johnson and McTaggart, 2010) and cyclones (CYCs) arise from meanders of equatorward surface currents (Chaigneau et al., 2011; Hormaz-

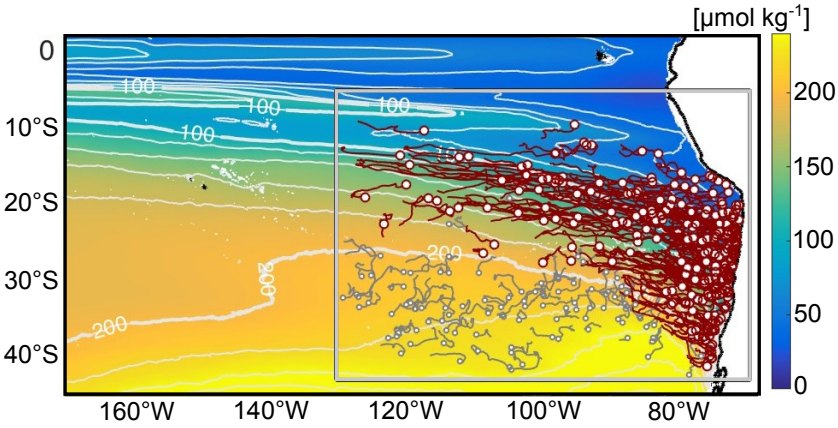

Figure 1.4: Subsurface eddy generation spots (dots) and propagation pathways (gray and red tracks) for eddies existing at least 9 months. Climatological dissolved oxygen on the 26.7 kg m^3 isopycnal shaded and contoured in white. Modified from Frenger et al. (2018); the gray box denote their eddy tracking region.

abal et al., 2013; Johnson and McTaggart, 2010; Chaigneau et al., 2013). The instability of the PCUC has been especially observed to generate the anticyclonic mode-water (i.e. subsurface or also called intrathermocline) eddies (AMWs - Combes et al., 2015; Hormazabal et al., 2013; Johnson and McTaggart, 2010; Frenger et al., 2018).

According to their generation area and source waters the cores of ANTs contain Eastern South Pacific Intermediate Water (ESPIW) and ESSW (Hormazabal et al., 2013; Chaigneau et al., 2011). Similarly, the AMWs carry the biogeochemical signatures typical for the PCUC and appear as warm-salty, low-oxygen and high-nutrient anomalies. They tend to preserve the material properties of their source waters and release them where they dissolve farther offshore (Combes et al., 2015; Frenger et al., 2018). The CYCs capture the cold and fresh upwelled water from the Chile and Peru surface currents (Colas et al., 2012; Johnson and McTaggart, 2010) associated with thermocline water above the ESPIW (Chaigneau et al., 2011).

Please note, this thesis highlights only the relation between the tracer and the eddy behavior; and keep restricted to that rather than investigating the eddy properties any further.

1.2.4 El Niño Dynamics

In the Pacific, El Niño dynamics modulate near surface temperatures (SST), salinity and density (e.g. Stramma et al., 2016; Fuenzalida et al., 2009). Generally, El Niño - Southern Oscillation (ENSO) denotes a coupled ocean-atmosphere system with periods of anomalous climate conditions. The periods are called El Niño and La Niña (Fig. 1.5). El Niño occurs quasi-periodic in 2-7 year intervals. Due to a decreased pressure difference between the atmospheric South Pacific High and the Indonesian Low, the thermocline collapse, and unusually warm SST establish off Peru and Ecuador from Christmas onwards. La Niña succeeds El Niño as an intensified 'normal' condition (e.g. McPhaden, 2018; Colling, 2001). Strong El Niño events appeared in 1972/73, 1982/83, 1991/92, 1997/98 and 2015/16 (e.g. Colling, 2001; Stramma et al., 2016).

Off Peru, El Niño strengthens the poleward along-coast flow (PCUC), deepens the thermocline and reduces or reverses the upwelling induced land-sea temperature gradient. Although the upwelling favorable winds are not greatly reduced and the water continues to be drawn from 50-

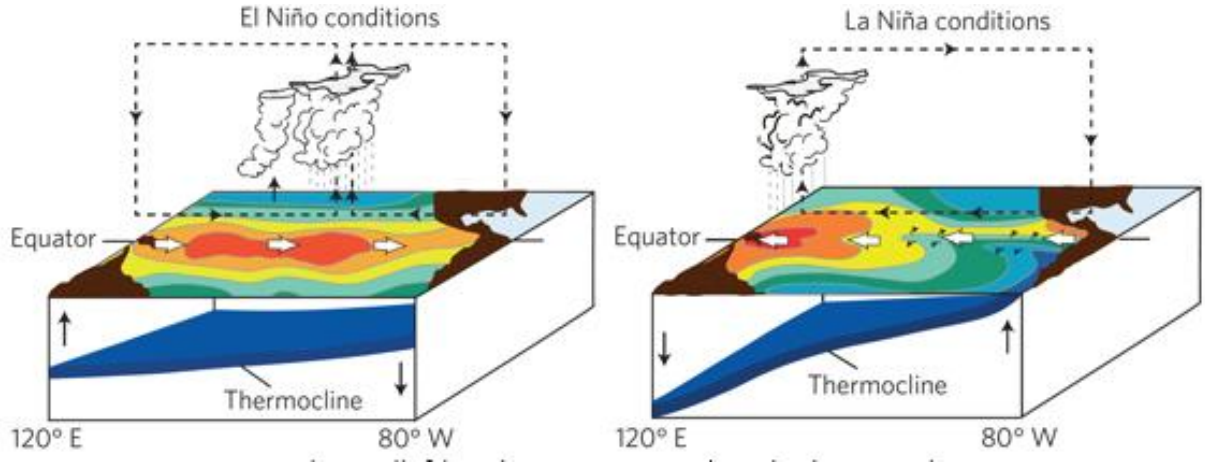

Figure 1.5: Schematic ENSO conditions (e.g. McPhaden, 2004).

100 m depth to the surface, the water mass change yields an upwelling of warm, saline, nutrient poor and oxygen deplete water (e.g. Strub et al., 1998). However, as temperature and salinity increase in the upper ocean in contrast to the seasonal cycle, the density decrease correlated (e.g. Stramma et al., 2016; Fuenzalida et al., 2009). Thus the upper ocean oxygen increases due to modulations of the mixed layer depth which modulates the oxycline depth and the vertical extent of the OMZ. Just below 400 m depth the El Niño influences become negligible on oxygen changes (Czeschel et al., 2012; José et al., 2019).

Regarding the conditions in the past few years, a strong El Niño event developed in early 2015 with SST anomalies along the equator towards South America and southward off Peru. In October 2015 the oceanic conditions at the Peruvian shelf between 9-16°S showed a transition to a typical El Niño (Stramma et al., 2016). It became one of the strongest events of the record (L'Heureux et al., 2017; Timmermann et al., 2018). But instead of a strong La Niña afterwards, a strong coastal El Niño appeared in spring 2017 (Rodríguez-Morata et al., 2018). Coastal El Niños are, as their name suggests, localized at the South American coast without basin scale signals. Before the 2017 event, the last event documented was in 1925 (Ramírez and Briones, 2017; Takahashi and Martínez, 2017).

The series of events from 2015 to 2017 coincide with the time frame of the (observational) investigations of this thesis and definitely influenced the tracer usage. But, an El Niño signal is not as clear represented in the tracer data as one would expect when thinking of a strong event like in 2015/16. Even if ENSO defines unusual climate conditions, these were well understood, until basically 2014. Since then events happened very unusual for their definition (Xie and Fang, 2019; McPhaden, 2015; Rodríguez-Morata et al., 2018). Thus the influence of the El Niño signal might cannot be clearly identified due to its unusual properties.

1.2.5 Offshore Diapycnal Diffusivity

Relevant data to estimate the strength of diapycnal mixing in the ETSP is rare. Whalen et al. (2012) addressed this issue in their global study using ARGO floats and suggesting values in

orders of 10^{-6}-10^{-5} m^2 s^{-1}. Albeit, studies like Waterhouse et al. (2014) still present a lack of data. And generally, about vertical diffusivity much less is known in the South Pacific than e.g. in the Atlantic, Indic or even the North (West) Pacific (Whalen et al., 2012; Waterhouse et al., 2014, their maps Fig. 2a and Fig. 1a, respectively - shown here in Fig. 1.6). Providing a large-scale and long-term representative value for the ETSP fills the data gap, supports the ARGO estimates, and thus can complete the global view.

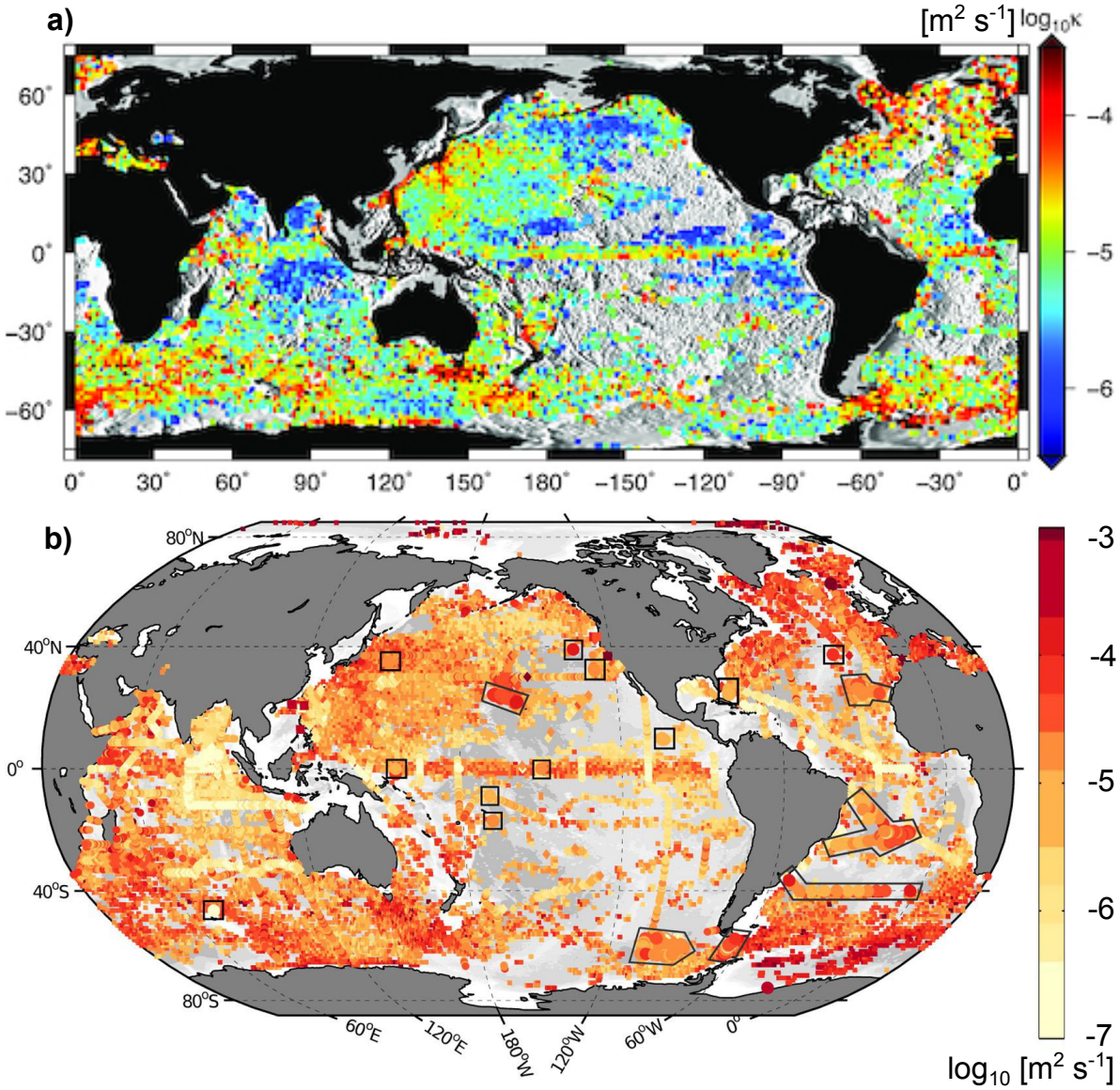

Figure 1.6: Global maps of diapycnal diffusivity estimates (a) averaged between 250-500 m water depth, over five years (2006-2011), and over 1.5° square bins of ARGO data (Whalen et al., 2012, their Fig. 2a); and (b) averaged between the mixed layer depth and 1000 m water depth (Waterhouse et al., 2014, their Fig.1a). It shows the need to improve the data coverage and to further gain diffusivity estimates in the (South) Pacific and especially the ETSP.

The diapycnal diffusivity coefficient quantifies the turbulence-induced mixing rate at which tracers spread across density surfaces (e.g. Mashayek et al., 2017, and references therein). In the

open ocean this cross-density spread represents vertical mixing. It is a key parameter that controls basin scale ocean stratification, the depth of the thermocline, vertical biogeochemical fluxes, the rate of the meridional overturning circulation (e.g. Munk, 1966; Ferrari et al., 2016; Mashayek et al., 2017, and references therein), and plays a significant role in the ventilation of OMZs (e.g. Fischer et al., 2013; Brandt et al., 2015; Banyte et al., 2012; Köllner et al., 2016; Duteil and Oschlies, 2011). A diapycnal diffusivity estimate for the ETSP open ocean is particular essential for oxygen and nutrient budgets of the related OMZ (cp. Llanillo et al., 2018).

In offshore ocean areas over smooth bathymetry the dynamic regimes are calm; only breaking internal waves induce turbulence and diapycnal diffusivity (e.g. Alford et al., 2016, and references therein). Such calm regimes were measured in the Eastern Tropical North Atlantic (Banyte et al., 2012; Köllner et al., 2016), in the extra tropical North Atlantic (e.g. Ledwell et al., 1998), and in the Pacific sector of the Southern Ocean (Ledwell et al., 2011). The commonalities in the physical regimes of open ocean areas lead to the expectation of a global standard for diapycnal mixing (e.g. Munk, 1966). Fulfilling the expectation supports the improvements made since Munk (1966), postulating that open ocean regimes over abyssal plains are calm whereas by about one order of magnitude enhanced diapycnal mixing act at the basin boundaries (with their highly dynamic shelf regions, rough topography, or seamounts and ridges - e.g. Toole et al., 1994; Polzin et al., 1997; Holtermann et al., 2012; Watson et al., 2013).

Dynamic interactions with boundary features result in highly localized diapycnal diffusivity estimates. The enhanced boundary mixing is known to account for the missing link in the buoyancy budgets (e.g. Ferrari et al., 2016; McDougall and Ferrari, 2017; Ledwell, 2018). However, these distinct local diffusivities are restricted to the regions with additional turbulence-generation-mechanisms caused by boundary features. They are not meaningful for the overall open ocean regime. Previous investigations in the ETSP derived diapycnal diffusivity estimates only in the coastal areas for very shallow waters (e.g. Schlosser et al., 2018, Supporting Information), and as intermediate steps which, for unknown reasons, were not published (e.g. Loginova et al., 2019; Steinfeldt et al., 2015).

1.3 Vertical Tracer Motion at a Continental Shelf

Tracer mixing in coastal areas is a complex topic of ongoing scientific discussions but with several new insights within the last few years. The theoretical background was recently summarized and further evaluated by Ferrari et al. (2016), McDougall and Ferrari (2017), and Holmes et al. (2019). It is assumed to be applicable to the Peruvian shelf and the tracer investigations of this thesis. Especially, vertical tracer motion related to ocean boundaries appears to be unusual compared to offshore ocean mixing. Though, for the purpose of this thesis only a continental shelf like boundary and near the boundary point-releases of tracer is important and regarded.

To understand the differences between the offshore and the shelf mixing one can imagine a water parcel in the ocean interior. Based on the observational evidence that dissipation increases with depth (e.g. Toole et al., 1994; Polzin et al., 1997; Ledwell et al., 2000; St. Laurent et al., 2012;

Waterhouse et al., 2014), the water parcel becomes denser by vertical mixing. More heavy water from below than lighter water from above causes the density changes. Contrary, a water parcel at a solid boundary become lighter, as the density flux have to vanish at the solid ground and vertical mixing can only act from above (Ferrari et al., 2016).

Focusing on the continental shelf (Fig. 1.7 - in a simplified view while neglecting sediments, etc.), there is the BBL on top of the solid boundary of the sea floor. The isopycnals intersect the boundary at right angles and thus turn on top of the BBL. The BBL has a thickness in order of tens of meters. Above the BBL, there is the stratified mixing layer (SML). The SML is a few hundred meters thick (Polzin et al., 1997; St. Laurent et al., 2012; Ferrari et al., 2016, and references therein). Both regimes are thought to be related to enhanced boundary mixing processes in which a diapycnal buoyancy flux is maximum at the top of the BBL. It decreases exponentially with height in the SML, and decrease linearly to vanish at the solid boundary (Ferrari et al., 2016; McDougall and Ferrari, 2017, and references therein). The interplay between these two regimes emerges within a few hundred kilometers of the continental boundaries, whereas in the bulk of the ocean interior only weak turbulence rates appear (McDougall and Ferrari, 2017).

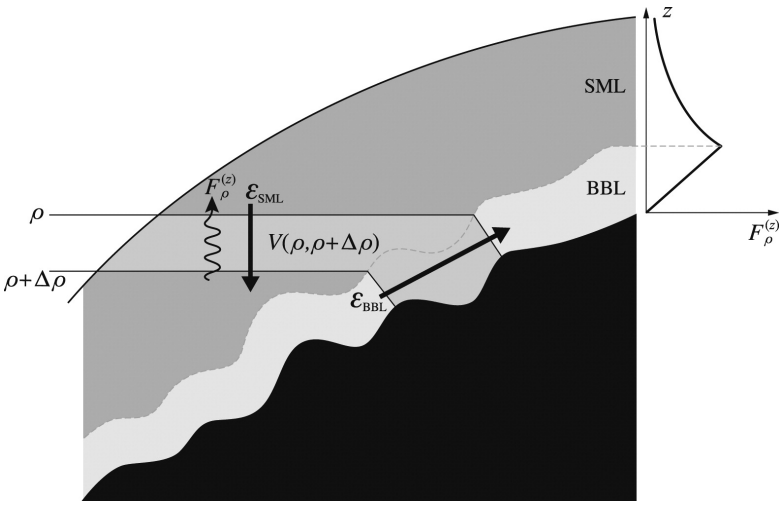

Figure 1.7: "A longitude-depth section of the near-boundary region of the ocean above rough topography is characterized by enhanced turbulence generated by tidal and geostrophic flows impinging over topography. [BBL and SML are indicated. ...] A typical vertical profile of the turbulent density flux $F_\rho^{(z)}$ through the BBL and SML is sketched on the upper-right corner of the figure. [...] The black arrows indicate the diabatic sinking of waters in the SML ($\mathcal{E}_{SML}$) and the diabatic along-boundary upwelling in the BBL ($\mathcal{E}_{BBL}$)." (Ferrari et al., 2016, their Fig. 2)

Consequently, water in the BBL lightens, the positive diapycnal velocity is across the isopycnals that intersect the ocean bottom, and an along boundary flow emerge. Thus the lightened water in the BBL rises along the boundary of the continental slope (Ferrari et al., 2016). In the SML, water parcels get heavier as described above for the ocean interior. Thus a diapycnal downward transport vertically drops the water at some distance of the boundary but within the enhanced dissipation regime of the SML. A net diapycnal volume transport results from the cancellation between upwelling in the BBL and downwelling in the SML and is typically several times smaller than the upward transport in the BBL (McDougall and Ferrari, 2017).

Regarding now a tracer to get distributed in the regimes of the BBL and SML, idealized model

experiments were used by Holmes et al. (2019) to test several hypotheses. In doing so, their results revealed important consequences which necessarily need to be taken into account when analyzing the tracer in this thesis. Thus according to Holmes' et al. (2019) model investigations the following issues of the theory need to be highlighted: As just now described in general, tracer-tagged water moves upslope and the tracer diffuse into lighter waters. In detail, a tracer patch near the boundary does not spread linearly, i.e. not like a half-Gaussian. On the one hand, the patch expand due to diapycnal upward transport of tracer-tagged water in the BBL but is than squeezed by diapycnal downward tracer motion in the SML. On average the tracer tend to show a net upward motion as the BBL transport exceeds this of the SML, and the net diapycnal volume transport brings almost the entire tracer distribution above the injection density. On the other hand, a diapycnal diffusivity averaged over the patch and estimated from the increase of the second moment would be much less than to expect. Or rather, even in presence of large diapycnal mixing the tracer patch would not show enough net vertical spreading due to the interplay between BBL and SML transports to quantify a sufficient diffusivity coefficient if its calculation is based on the increase in second moment. Additionally, at the continental shelf the tracer based diffusivity estimate includes contributions from advection, from accumulation of tracer on the boundary, from the vertical gradient in the diffusivity, and from the BBL buoyancy perturbation. Thus, on the continental shelf the diffusivity resulting based on the tracer spread is initially a few times (but generally less than on order of magnitude) smaller than the isotropic diffusivity (Holmes et al., 2019). This is a major difference to diffusivity estimates derived in the offshore ocean by the overall spreading rate of a tracer across the isopycnals. As apart from the shelf, such an estimate is representative to the tracer weighted isotropic diffusivity (e.g. Fischer et al., 2013; Köllner et al., 2016).

Finally, Holmes et al. (2019) investigated more hypotized influencing factors on tracer spreading and found the following relations. The topographic slope has almost no influence on the diapycnal tracer spreading. The slope of the isopycnals in the SML has minor impact on the diapycnal tracer dispersion, if the tracer does not extend the BBL/SML regimes into the far-field ocean interior. Along-isopycnal diffusion enhances the tracer spreading rate. Advective and diffusive fluxes have equivalent influence, and on average the tracer is diapycnally diffused and advected in the same direction. The BBL velocity indirectly influence the tracer spreading normal to the slope as it transports tracer upslope and across the isopycnals, after which it diffuses vertically out of the BBL (Holmes et al., 2019).

1.4 Tracer Release Experiments (TREs)

To address the research questions the tracer is used in a so called Tracer Release Experiment (TRE). This is essentially an observational approach based on a deliberate release of a tracer into the ocean. The survey of the tracer reflect the total transport, advective and diffusive, inherently depends on the entire history of mixing events, and capture integrated information about the circulation. Thus it provides stable estimates of comprised information in orders of

month to years and hundreds to thousands kilometers (Watson and Ledwell, 2000; Haine and Hall, 2002; Banyte et al., 2012; Ho, 2019). Starting from the mid 1980's TREs became a method which enables something of the precession of land based laboratory investigations (Watson and Ledwell, 2000).

The tracer is a chemical that enable to mark unambiguously large water bodies and to track particular water parcels. By demand, the tracer is a stable compound, reliable conservative (i.e. inert in seawater and mixed conservatively or with specified biogeochemical sinks), non-toxic, easy to analyze, has an exceptionally low detection limit, and a low marine background concentration (Watson and Ledwell, 2000; Ho et al., 2008). The currently used standard chemical is trifluoromethyl sulfur pentafluoride (SF_5CF_3), replacing sulfur hexafluoride (SF_6), as decided on the Ocean Sciences Meeting 2006 in Hawaii (Ho, 2019). SF_5CF_3 is artificially produced for the use in TREs only and has proven itself as an ideal tracer with long-term stability, no discernible sinking effects or chemical decay even in anoxic conditions (Ho et al., 2008; Holtermann et al., 2012).

To get the tracer dissolved in subsurface seawater an injection package, the Ocean Tracer Injection System (OTIS), was designed. It was originally constructed at Woods Hole Oceanographic Institution to conduct the North Atlantic TRE, the first large scale TRE at the sea (Watson and Ledwell, 2000; Ledwell et al., 1993). When OTIS is lowered into the water the tracer is pumped at high pressure through fine orifices and spayed out, yielding an emulsion with seawater and finally a dissolution (Watson and Ledwell, 2000).

During the survey, water samples are taken and their tracer concentration is measured with a purge-and-trap gas chromatograph equipped with an electron capture detector (GC/ECD - Watson and Ledwell, 2000).

TREs are a well established method to estimate turbulent diapycnal diffusivity (as a measure of vertical ocean mixing in the open ocean) and are classical examples which found such mixing small in the ocean interior and by orders of magnitude larger towards the basin boundaries. More precise, the North Atlantic TRE (e.g. Ledwell et al., 1998), the Guinea Upwelling TRE (Banyte et al., 2012), and the Oxygen Supply TRE (Köllner et al., 2016) conducted in the (tropical) North Atlantic prove the ocean interior as dynamically calm regime. Whereas the Brazil Basin TRE conducted in the South Atlantic showed evidence for enhanced diapycnal diffusivity due to the influence of rough bottom topography (Polzin et al., 1997; Ledwell et al., 2000). The small scale Baltic Sea TRE supported this finding by evidence of increased diapycnal diffusivity related to basin walls (Holtermann et al., 2012). DIMES, the 'Diapycnal and Isopycnal Mixing Experiment in the Southern ocean', was designed to show the difference between calm ocean regions over smooth bathymetry and enhanced mixing over rough topography. DIMES started in the Pacific sector but is clearly related to the Southern Ocean (Ledwell et al., 2011; Watson et al., 2013).

No tracer signal that remained in the ocean by DIMES or any other previous experiment conducted in the Pacific do contaminate the data or interfere the results of the TRE in the ETSP

investigated in this thesis. The global distribution of TREs (e.g. Ho, 2019) highlight the ETSP as an ideal region for a conduction, and also point out some data and knowledge gaps in the study area to be addressed with a TRE. Despite DIMES, the TREs in the Pacific were mostly small scale releases like in the Santa Monica (Ledwell and Watson, 1991; Ledwell and Hickey, 1995) and Santa Cruz Basin (Ledwell and Bratkovich, 1995) as well as on the East Pacific Rise at 9-10°N (Jackson et al., 2010). All of them are far away from the area of interest here, and except DIMES they used SF_6 which do not interact with the SF_5CF_3 signal.

In the ETSP the 'Peruvian Oxygen-minimum-zone System Tracer Release Experiment' (POSTRE) was conducted from October 2015 to April 2017 to quantify benthic pelagic exchanges in the Peruvian OMZ. POSTRE is a large scale experiment related to boundary influence. It is one of the few TREs done in the Pacific and one of the sparse "coastal" TREs. The tracer was injected directly into the BBL and at least partly injected into a boundary current, the PCUC. POSTRE is the first experiment where the tracer was injected at fixed stations (e.g. Fig. 3.1) instead of along streaks on a target density. POSTRE is the third TRE done within the Collaborative Research Center 754 "Climate - Biogeochemistry Interactions in the Tropical Ocean" (SFB754). Though, its connection to the (ventilation of) OMZs is different than for the two previous TREs, the Guinea Upwelling TRE (injected 2008 - Banyte et al., 2012, 2013) and the Oxygen Supply TRE (injected 2012 - Köllner et al., 2016). POSTRE is highly affected by advection and among others describes the transport of the oxygen depleted ESSW of the PCUC from the shelf into the offshore OMZ. Nevertheless, as it was also possible to derive an offshore diapycnal diffusivity estimate, POSTRE provides the first possibililty to compare large mixing TREs from the Atlantic and the Pacific to get a global overview.

As the ETSP is a very dynamic region, the conditions under which a tracer is injected and spread affect the whole experiment significantly. Thus it would be ideal to perform several TREs like POSTRE under slightly changed conditions during the injection and thereafter. This is impossible in the real ocean, whereas numerical simulations are predestined for it. So, 'modeled TREs' (moTREs) help to show how much influence the injection conditions have on the overall experiment and highlight properties of the tracer distribution to be persistent despite several states of natural variabilities. In turn, modeled tracer dispersions related to a comparable observational TRE can help to evaluate the model performance in terms of such distributions which are potentially applicable for dissolved constituents like nutrients or gases.

Four moTREs were perfomed in the most advanced models. All four model data sets and the observation together are thought to give a good representation of this highly dynamic region, filling their respective issues and provide persistent results representative even in this dynamic region with changing environmental conditions. Moreover, using different models and configurations in comparison to the observations helps to identify where and how their short comings afflict the tracer behavior unrealistically. This provides a better basis for the results shown here than just one model or one configuration could do.

2 Data and Methods

The scientific key questions are addressed in the context of a TRE performed in the ocean (section 2.1) and four analog 'modeled TREs' (moTREs) performed in numerical simulations (section 2.2). As already introduced, the tracer mimic nutrients coming out of the anoxic marine sediments of the continental shelf. Hence physical pathways in the ocean interior available for these nutrients can be traced and benthic-pelagic exchanges in the Peruvian OMZ can be quantified. Therefore, the tracer was injected at fixed stations, directly into the BBL.

2.1 The Observational 'Peruvian Oxygen-minimum-zone System Tracer Release Experiment' (POSTRE)

2.1.1 Tracer Injection and Initial Conditions

The tracer (68.5 kg of SF_5CF_3) was injected at three locations along the Peruvian shelf (10°42.9'S, 78°14.1'W; 12°21.87'S, 77°26.25'W and 14°02.16'S, 76°31.67'W - Fig. 2.1a, Tabs. 2.1 & 2.2) in October 2015 (expedition SO243 with RV Sonne II; Marandino, 2016). Therefore, the GEOMAR OTIS (e.g. Holtermann et al., 2012; Banyte et al., 2012; Köllner et al., 2016) was adapted by removing the buoyancy devices and adding four legs (Fig. 2.1a). It was lowered to the shelf bottom and released the tracer directly into the anoxic BBL (roughly 0.6 m above the bottom at about 250 m water depth). The tracer typically was pumped by two dual-head HPLC pumps with high pressure (∼22 MPa) through twelve fine orifices (25 μm ID) into the ocean. Once in contact with seawater an emulsion emerges and the tracer droplets begin to dissolve. Any possible droplet "settling error" can be neglected since the injection was located near the bottom. A Conductivity-Temperature-Depth (CTD) sensor was mounted on the frame of the OTIS to document the ambient water mass conditions during the injection. It was calibrated similar to Banyte et al. (2012) by aligning the temperature-salinity relation to that of the well-calibrated profiling CTD and correcting for an offset of 0.007 psu and 0.003 psu on the salinity data of two respective sensors. The profiling CTD calibration yielded an r.m.s. uncertainty of 0.001 psu for salinity. The temperature sensors, calibrated by the manufacturer, are assumed to have an accuracy better than 0.002°C (Stramma et al., 2016). This is equivalent to a density r.m.s. of 0.0001 kg m^{-3}.

Table 2.1: Summarizing POSTRE's injection.

POSTRE (observed)	latitude	longitude	depth [m]	date	start time (UTC)	duration	tracer amount
injection at	10.7°S	78.2°W	250	Oct. 13	01:15	10h 48min	25 kg
	12.4°S	77.4°W	250	Oct. 15	21:48	8h 16min	28 kg
	14.4°S	76.5°W	250	Oct. 18	01:13	7h 55min	15.5 kg

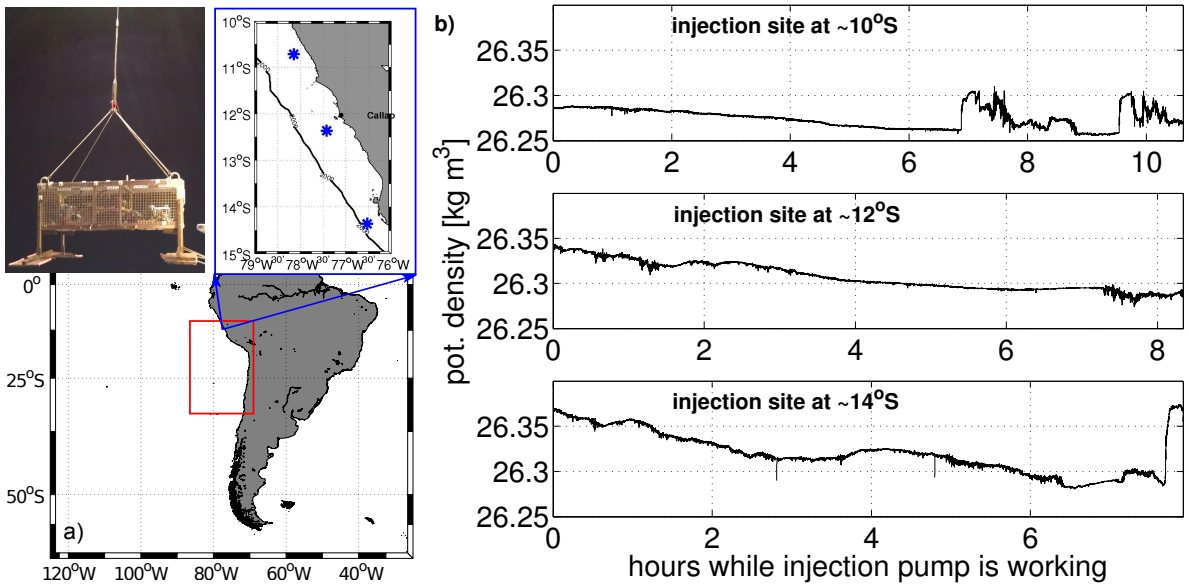

Figure 2.1: (a) The region of interest with the survey area highlighted (red rectangle) and a zoom in for the POSTRE injection sites. The modified OTIS is shown - Photo: C. Marandino, 2015. (b) The time-dependent density changes during the injection, i.e. over the duration the tracer got pumped into the ocean (updated from Marandino, 2016, their Fig. 7.10.2).

The initial conditions inferred from the OTIS' mounted CTD data showed the signal of the highly dynamic shelf regime. The injections cover a potential density range from 26.24 to 26.38 kg m^{-3} (Figs. 2.1b & 2.2). The injected tracer amount as a function of density is shown in Fig. 2.2b as the total sum and the individual contribution of the three sites. The tracer peak of this function's Gaussian fit is at 26.29±0.03 kg m^{-3} (where the uncertainty gives the standard deviation). The width of this injection is about one order of magnitude larger than those of previous ocean mixing TREs where the injection was executed narrowly on a density surface (cp. e.g. Ledwell et al., 1998; Banyte et al., 2012; Köllner et al., 2016) due to this study's modified injection setup. Fortunately, the overall distribution revealed a Gaussian shape.

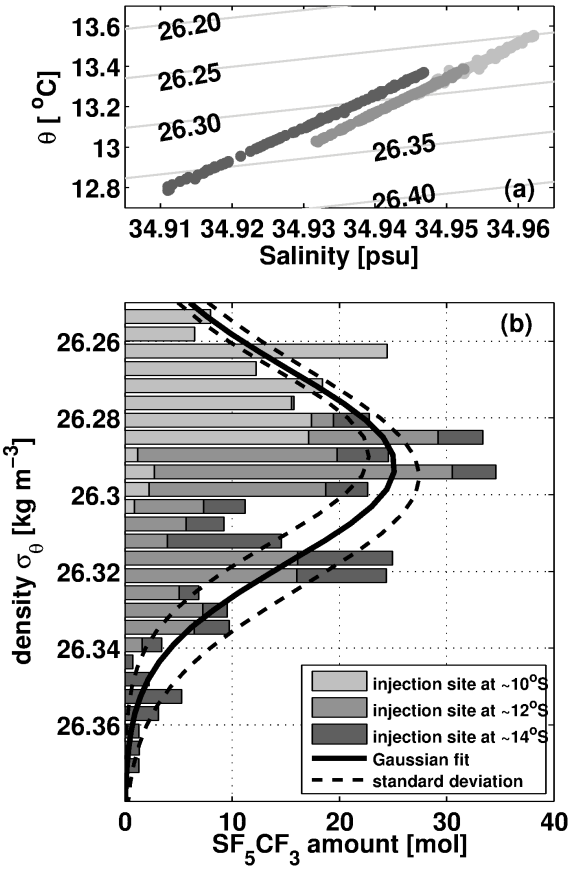

Figure 2.2: Tracer-density relation during the injection (a) in potential Temperature (θ) - Salinity - space (for clarity only 3-min means are shown). The barplot (b) shows the amount of tracer (in mol) released versus potential density anomaly interval summed over all injections, and a Gaussian fit. The single release sites are identified by gray shades.

2.1.2 Tracer Survey

The large scale tracer survey was performed about 17 months after the release (1. March to 8. April 2017 - expedition M135 with RV Meteor; Visbeck, under review). The sampling grid spans from about 10.7°S to 30°S and from the Peruvian-Chilenian coast offshore towards 81°W for most sections (red rectangle in Fig. 2.1a). Offshorewards the stations are about one degree apart. Coastwards their distance reduces to 0.5, 0.25, and even 0.1 degree closest to the shelf. The 2000 m isobath parallel to the coast is sampled at approximately every degree of latitude. The former WOCE section along 17°S (Talley, 2007) was repeated offshorewards until 86°W. Every section along a latitude covers at least a distance of about 4° longitude from coast.

In total 132 CTD-stations were sampled and analyzed for its tracer content at typically 21 depths. The uncertainty of the salinity sensor was estimated to be 0.001 psu after calibration and 0.002°C for temperature yielding a density r.m.s. uncertainty of 0.0001 kg m^{-3}. Water for tracer measurements was sampled in 250 ml ground glass syringes and stored in a water bath of about 5°C before processing on board within 12 hours after sampling. The tracer concentration was measured with two purge-and-trap systems including gas chromatographs equipped with an electron capture detector (GC/ECD). Overall, 3172 samples were measured. This includes 165 samples for determination of the inter-system precision (0.11 fmol kg^{-1}) as well as 80 and 63 replicates, respectively, for single instrument precisions (0.05 fmol kg^{-1} & 0.06 fmol kg^{-1}), yielding 2864 data points of SF_5CF_3 (Visbeck, under review).

Simultaneous to the tracer, CTD (Schmidtko et al., 2019) and vmADCP (vessel mounted Acoustic Doppler Current Profiler, using here 75 kHz - Visbeck et al., 2018), as well as oxygen measurements (Tanhua and Visbeck, 2018; Schmidtko et al., 2019) give insight in the hydrographic conditions of the experiment.

In the following POSTRE, the short name under which the observational experiment was performed, recalls always the observation in the ocean, not the numerical simulations.

2.2 Modeled TREs (moTREs)

2.2.1 Overview and Strategy

Additionally to the observation, four moTREs were simulated. A benefit of the first moTRE was to prepare the observational tracer survey. However, all of them are useful to address a major short coming in the POSTRE experimental setup: The very poor temporal resolution. The moTREs support the POSTRE results as they provide much higher temporal and spatial resolution as ever possible in observation. This gives especially more insights on the temporal tracer evolution, which cannot be gained from POSTRE.

The moTREs are based on two models: ROMS/CROCO (Regional Ocean Model System and its new version Coastal and Regional Ocean COmmunity model - section 2.2.2) and NEMO (Nucleus for European Modelling of the Ocean - section 2.2.3). The essential difference between these two models is the vertical coordinate system as ROMS/CROCO has topography following 's-coordinates' and NEMO has 'regular' geopotential depth 'z-coordinates'. The difference is nicely shown by Shchepetkin and McWilliams (2005, their Fig.1 a&d - shown here in Fig. 2.3).

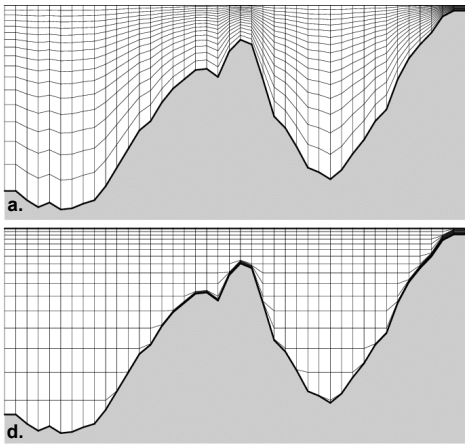

Figure 2.3: Visualized difference between the s- und z-coordinates by Shchepetkin and McWilliams (2005, their Fig.1 a&d): "Examples of vertical coordinate systems: (a) S-coordinate of Song and Haidvogel (1994) [...] (d) z-coordinate system toward the S-coordinate."

ROMS/CROCO is well established for ETSP research questions, and a tool promising a sufficient degree of realism (e.g. Penven et al., 2005; Montes et al., 2010; Echevin et al., 2014; Montes et al., 2014). As the most important argument to use ROMS/CROCO, the squeeze of s-coordinates in shallow waters leads to a high vertical resolution over the shelf and in the coastal areas (Song and Haidvogel, 1994). Unfortunately when having the s-coordinate system, tracers tend to distribute topography following along the coordinates rather than e.g. along isopycnals, as they

follow the along-coordinate gradient (Fig. 2.4 - Shchepetkin and McWilliams, 2005; Beckmann, 1998; Willebrand et al., 2001; Shchepetkin and McWilliams, 2003). To evaluate the effects of this bias it needs comparable moTREs in a vertical z-coordinate system (Fig. 2.5). Although, the regular vertical coordinate in NEMO results in a comparable coarse resolution of the shelf and near coastal regions.

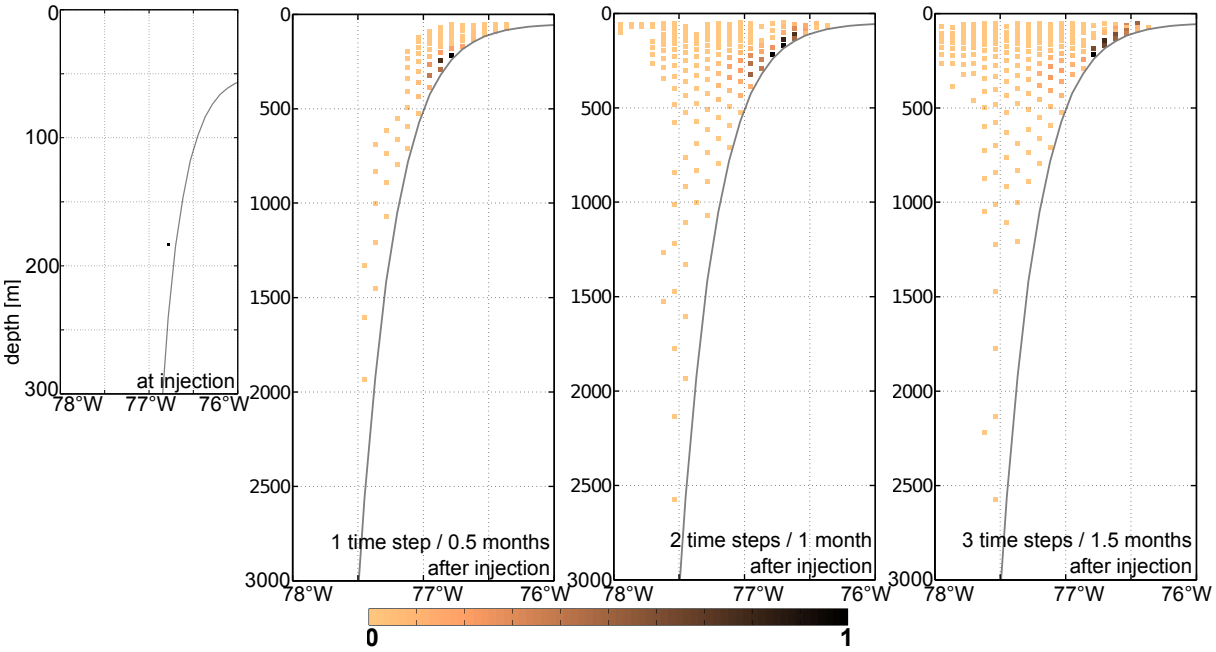

Figure 2.4: Normalized ROMS tracer rushing down the shelf by following the coordinates gradient. Please note the different vertical axis between the time steps and in comparison to Fig. 2.5.

All moTREs are online runs and got different forcing to provide a variety of possible scenarios. A climatological forced simulation (called moTRE1-ROMS) is made to present a mean state. This is compared and supported by interannually forced simulations of usual conditions (called moTRE4-NEMO and moTRE3-NEMO and started in 1994 and 1995, respectively). As the observational POSTRE coincide with the El Niño event from 2015/16 one of the interannual forced simulations (called moTRE2-CROCO) is made to represent the moTRE under El Niño conditions.

For the interannual forcing no realistic data is available for the time of the observation, yet. To have suitable conditions to perform moTREs these are dated back in time. 1994 and 1995 are years with very usual environmental conditions in the ETSP and thus can be used in reference to the climatological run as a mean state, and for year to year differences without noteworthy anomaly to take into account. To reproduce the moTRE under El Niño conditions the event of 1997/98 was chosen. This was also one of the strongest events in the record, and at the beginning the 2015/16 El Niño developed similarly to the 1997/98 El Niño suggesting similar influences on the tracer distribution.

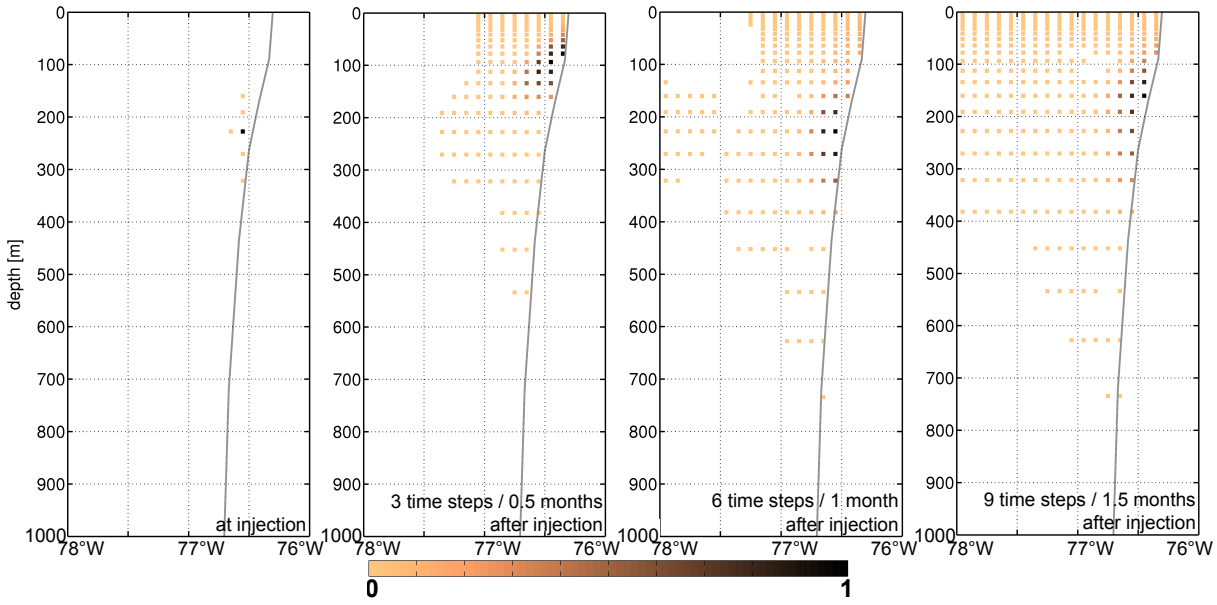

Figure 2.5: Normalized NEMO tracer without the bias to compare with Fig. 2.4. Thus the tracer does not rush down the shelf. Please note the different vertical axis in comparison to Fig. 2.4.

2.2.2 ROMS/CROCO model for moTRE1 and moTRE2

Two regional model configurations based on ROMS/CROCO are used to evaluate the tracer propagation: a climatological (ROMS-CLIM) and an interannual (CROCO-ENSO) forced simulation. ROMS/CROCO is a French ROMS_AGRIF model with a split-explicit, free-surface, topography-following vertical coordinate model that is well suited to represent coastal and regional processes (Shchepetkin and McWilliams, 2005).

ROMS-CLIM configuration applies a 2-way nesting (Debreu et al., 2012) to simulate the dynamics of the ETSP using the ROMS model. The large scale domain has 0.25° resolution and extends from 9°W-120°W in longitude and from 18°N-40°S in latitude (José et al., 2017). The high resolution grid has around 0.08° and extends from 69°W-102°W in longitude and 5°N-31°S in latitude, covering the equatorial dynamics and the core of the OMZ. This model configuration has 32 vertical levels. The topography is derived from GEBCO1 (General Bathymetric Chart of the Oceans at 1 minute resolution - IOC et al., 2003). ROMS-CLIM configuration is forced at the surface with heat and fresh water fluxes from COADS (Comprehensive Ocean-Atmosphere Data Set - Worley et al., 2005) and wind fields from the QuickSCAT product (Liu et al., 1998). The open boundaries of the large scale domain are nudged toward tracers and velocity field from SODA (Simple Ocean Data Assimilation - Carton and Giese, 2008). A detailed description of this model configuration is given in José et al. (2017).

CROCO-ENSO configuration is forced at interannual basis and has 0.08° horizontal resolution. The model domain extends from 12°N to 35°S in latitude and 69°W to 118°W in longitude. It connects at the open boundaries to the monthly SODA reanalysis data product (Carton et al., 2018). At the surface, CROCO-ENSO configuration uses the heat fluxes, humidity, precipita-

tion rates, atmospheric and surface ocean temperature from CFSR (Climate Forecast System Reanalysis - Saha et al., 2010) data, as well as the winds from CCMP (Cross-Calibrated Multi-Platform) product derived from observations (Atlas et al., 1996). CROCO-ENSO configuration is similar as described in José et al. (2019) but with 45 instead of 32 vertical levels.

To perform a TRE in ROMS/CROCO the PASSIVE_TRACER tool is applied (Penven et al. (2008) & Penven and Tan (2003) for ROMS_TOOLS; CROCO_TOOLS are provided by https://www.croco-ocean.org or rather https://gitlab.inria.fr/croco-ocean/croco_tools). That means, there are particles injected. The tracer advection is computed from the velocity fields at each time step. However, the particles are not subject to diffusion, which contributes to the mixing processes in the model.

For the TRE in ROMS-CLIM (moTRE1), $3{\cdot}10^4$ passive tracer particles were injected at the seafloor of three locations along the central Peruvian shelf, around 12.1°S, 13.9°S and 15.4°S (Tab. 2.2). moTRE1 started mid November of climatological year 15 and ran for 3 additional years. Half month snapshots are analyzed.

For the TRE in CROCO-ENSO (moTRE2), a total of $3{\cdot}10^6$ passive tracer particles were injected at the seafloor of three locations along the Peruvian shelf, at 10.4°S, 12.2°S and 14.0°S (Tab. 2.2), on 15. October 1997, coinciding with the beginning of 1997/98 El Niño event. 3 day snapshots are analyzed from October 1997 to 1999.

When interpreting the outputs, it is important to keep in mind that in ROMS/CROCO the tracer distribution along the s-coordinate lead especially in moTRE1-ROMS to tracer rushing down the shelf (Fig. 2.4) in early stages of the moTRE. For moTRE2-CROCO the higher vertical resolution largely reduces this effect. Over time, the along coordinate gradient reduce and the concentrations in the very deep waters dilute. Thus especially moTRE1 gives a more realistic tracer pattern after the first 6 months of lapse time (not shown).

Table 2.2: Injection sites and depth, and the tracer weighted mean injection density in comparison between the observational and each model experiment.

	latitude	longitude	depth [m]	density [kg m^{-3}]
POSTRE	10.7°S	78.2°W	250	
(observed)	12.4°S	77.4°W	250	26.3±0.03
	14.4°S	76.5°W	250	
moTRE1	12.1°S	77.8°W	187.9	
(ROMS-CLIM)	13.9°S	76.8°W	183.3	26.27±0.14
	15.4°S	75.6°W	271.7	
moTRE2	10.4°S	79.1°W	260	
(CROCO-ENSO)	12.2°S	78.0°W	260	26.42±0.15
	14.0°S	77.1°W	260	
moTRE3 &	10.7°S	78.3°W	300	27.30±0.02 &
moTRE4	12.4°S	77.4°W	300	27.16±0.04
(NEMO-TROPAC)	14.1°S	76.6°W	300	

2.2.3 NEMO model for moTRE3 and moTRE4

The Tropical Pacific (TROPAC) configuration used here builds on the NEMO v3.6 code (Madec et al., 2008). NEMO-TROPAC includes a base model called ORCA05, characterized by a coarse horizontal resolution (0.5° in latitude and longitude). In this base model, a two ways AGRIF (Adaptive Grid Refinement In Fortran) nest (Debreu et al., 2008) has been implemented in the whole Pacific Ocean, from 49°S to 31°N. The nested area is eddy resolving (0.1° resolution). The configuration includes 46 vertical levels, with increasing thickness from 6 m at the surface to 250 m at depth. The Gent and McWilliams (1990) parameterization is used solely in the base model. TROPAC is forced by the interannually varying atmospheric data given by the Coordinated Ocean-Ice Reference Experiments (CORE) v2 reanalysis products (Large and Yeager, 2009) over the period 1948-2007. The initial fields for the physical variables are given by the final state of an 80 year climatological spin-up. TROPAC has been compared to observations of the eastern Pacific Ocean in Czeschel et al. (2011).

Two tracer release experiments have been performed with a conservative tracer (no decay). The passive tracer has been released at 300 m depth on 15. October 1994 and 1995 at 10.7°S (127 mol l^{-1}), 12.4°S (143 mol l^{-1}), 14.1°S (79 mol l^{-1}) (Tab. 2.2). To differentiate between the two experiments, they are called moTRE3 (starting in 1995) and moTRE4 (starting in 1994). moTRE3 ran for 22.5 months and moTRE4 ran for two years. 5 day averages are analyzed.

2.2.4 Data Processing

2.2.4.1 Model Data and Tracer Units

The models, the configurations and even the tracer experiments are remarkably different. To get the tracers on a comparable basis (1) for the ROMS/CROCO tracer (given in particles per grid cell) the number of particles were equaled to the observational injected tracer amount of 349 mol, normalized by the sum over all particles, and converted into a concentration of unit mol kg^{-1} by using the grid cell size, layer thickness and density. (2) For the NEMO tracer (given in mol l^{-1}) a scaling factor need to be derived by using the grid cell volume to get the total tracer amount in mol and scale it with the total observational injection amount of 349 mol. The scaled NEMO tracer (in mol l^{-1}) is converted into mol kg^{-1} with regard to the density field. This way each moTRE gets the same units which were made to match the observations but naturally are no real values to deal with. It is necessary, as the focus is on the pattern and related processes of the tracer distributions. To account for the artificial units, percentage values are used in the statements about the tracer portions affected by single processes or in special regions. It is beyond the scope of this thesis to go into the details of model comparison. However, the figures show the artificial tracer units as a reference for further model improvements.

The moTREs give insight in the basic behavior of the tracer and can be used reliable when set in context to observations. It is important to realize (1) that the moTREs tracer results are generally similar to each other and to POSTRE despite all of the differences. And, (2) the details of the different results show the important points of possible improvements to address

them in the future.

Simultaneous to the tracer, both models contain standard variables of ocean physics such as temperature, salinity, and velocity to give insight in the hydrographic conditions of the experiments.

2.2.4.2 Model Tracer in Shallow Waters

Tracer outgasing is an important process acting in the observational experiment. In the real ocean, tracer entering the mixed layer quickly equilibrate with the atmosphere, i.e. gases out within a few weeks and is irrecoverable. In the case of POSTRE it is a major way of tracer loss, quantified in 4.2.1. However, outgasing is not implemented in the models. Thus model tracer brought into shallow waters accumulates there. For a better comparability between POSTRE and the moTREs it is mandatory to define a bulk outgasing applicable to the model outputs.

In this thesis the bulk outgasing is defined via the tracer amount within a certain shallow water layer. As depth of this layer is chosen to be 50 m. This value is based on the modeled tracer distributions and hydrography. For the purpose of this thesis a value constant over time is wanted which can be used in all model configurations despite the intra-, interannual, and ENSO variabilities. Additionally, this constant need to be applicable in both models despite their different vertical coordinate systems. It could be argued, using the mixed layer with a depth of might 20 m would be more realistic in the real ocean. However, it is questionable if a value derived from CTD data of one cruise or an abitrary number of cruises gives a more representative estimate for the models, especially with regard to the vertical model resolution. Instead it was decided to orientate on the moTREs whereat I am aware of a number of improvements on the value of the shallow water layer depth which might be applicable in the future.

At the time, the bulk outgasing is applied by removing the tracer in the upper 50 m as presented in most graphics and results. The only case where this removal was not applied (Fig. 4.8) is indicated with the label "with surface tracer".

2.2.4.3 Hovmoeller Diagrams

To effectively quantify the distances the tracer covers in given times and to derive a tracer transport velocity out of that, so called Hovmoeller diagrams are used (section 3.3). A Hovmoeller diagram shows a quantity in a space spanned by a temporal and a spatial axis and thus gives information about an evolution. In the case of the moTREs the tracer distributes along three spatial axes: longitude, latitude, and depth. As the interest is in an absolute value tracer transport distance and velocity, these three spatial axes need to be merged into one dimension.

The transformation of longitude, latitude, and depth into one spatial dimension is achieved when (1) using the vertical column intergal of the tracer and by that eliminating the depth. (2) Giving each point in lat.-lon.-space a distance from a reference point in the same geographical space. Without loss of generality, Callao (12.03°S, 77.1°W) can be chosen as reference (Fig. 2.6). The direction of the tracer transport gets lost or rather the tracer transport directions over time get

known from the investigations of the tracer distributions and spreading in the sections 3.1 & 3.2, can and need to be regarded from this. Therefore it is not necessary to include the tracer transport direction in the Hovmoeller diagrams. Finally, to get unique tracer values for each time step and each distance from the reference point, the tracer is summed over same distances from reference.

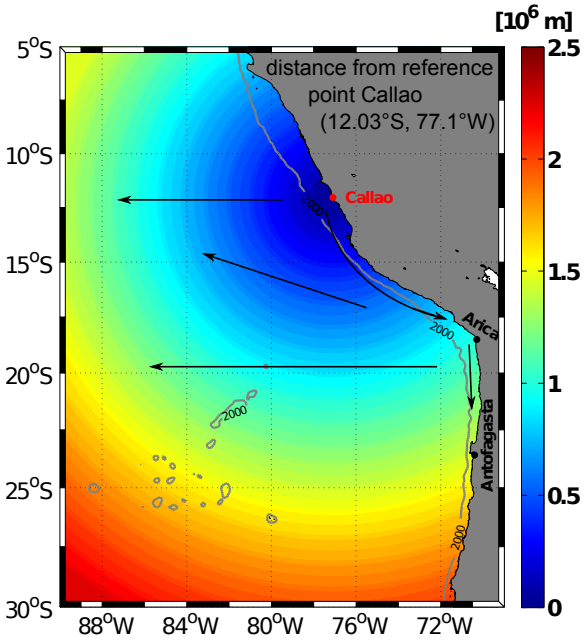

Figure 2.6: Distance from the reference point Callao (12.03°S, 77.1°W) for each point in lat.-lon.-space in the ETSP. The arrows denote simplified tracer transport directions to give their context to the Hovmoeller diagrams in Figs. 2.7 & 3.6-3.9.

The tracer transport distances can be derived between two time steps as the difference of the distances from the reference point to the location of a local tracer maximum. The difference in time between the two steps gives a duration how long the tracer needed to cover the distance. Thus the tracer transport velocity can be directly read from the slopes in the Hovmoeller diagrams.

The Hovmoeller diagrams of all moTREs (Fig. 2.7) show an increase in distance from Callao (as geographical reference point) over the first few months of the experiments, a decrease afterwards, and again an increase in the late stages. These are just effects of changing tracer transport directions. Regarding the (time dependant) tracer pattern and transport directions (sections 3.1 & 3.1.3), it is reasonable that the injection spots are located in different parts of a coast parallel water flow, the PCUC (section 3.4). The tracer transport velocities in the early experiments stages thus denote the transport within this current, as the tracer is on the shelf first. Later it gets into the offshore ocean after it turns direction. Due to the coastline bend, the geographical points west of the area where the tracer most efficiently leaves the shelf are closer to Callao than the geographical points on the shelf. Thus the distance decrease. When the tracer gets far offshore, the geograpical points are located at increasing distance from Callao (Fig. 2.6).

Although, Hovmoeller diagrams provide a smart way to read out velocities, they are hard to capture on a first glace and tricky to display in the easiest way. Especially as in this thesis,

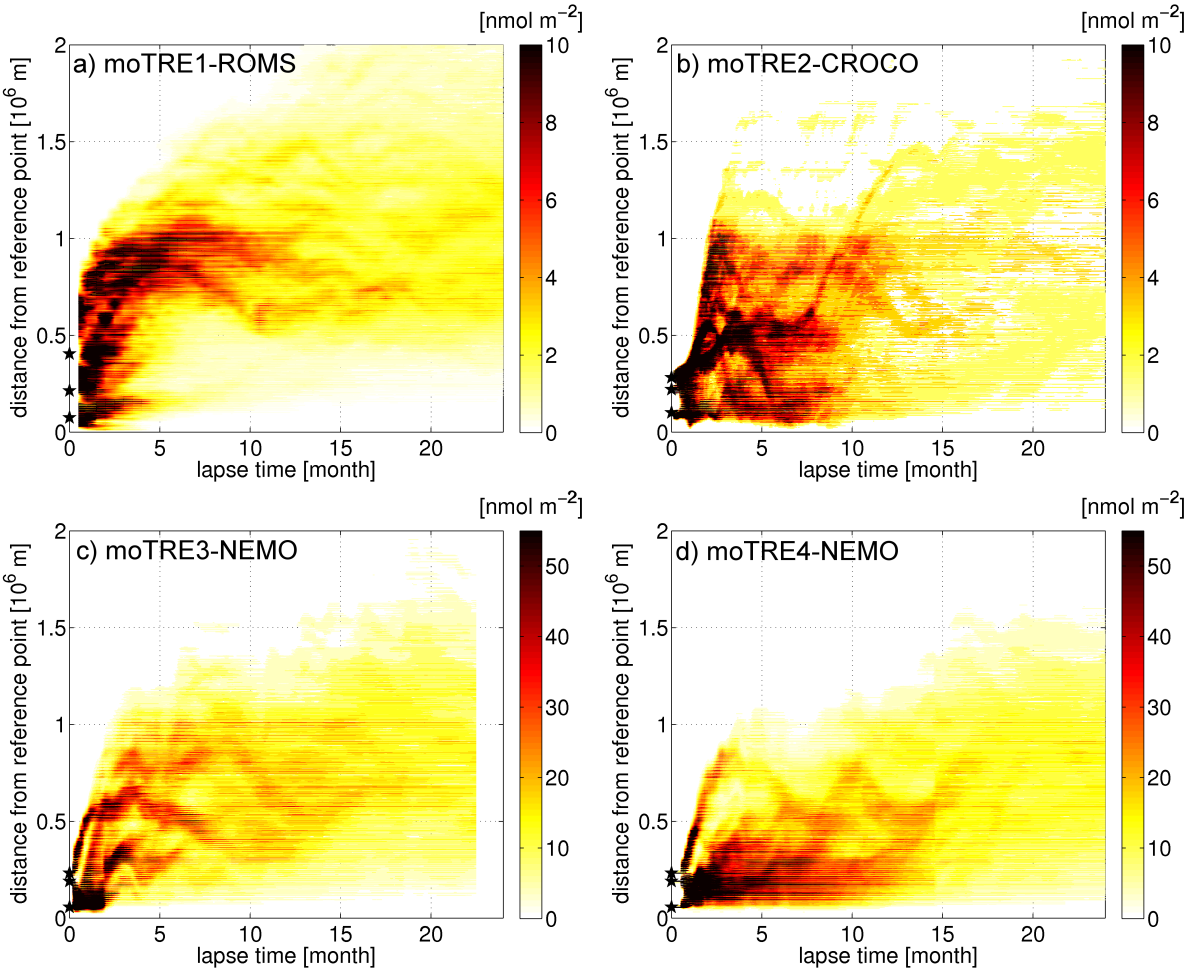

Figure 2.7: Hovmoeller diagrams of the moTREs; (a) moTRE1-ROMS, (b) moTRE2-CROCO, (c) moTRE3-NEMO, (d) moTRE4-NEMO. The y-axis denotes the distance to the geographical reference point Callao (12.03°S, 77.1°W). Please note the different color axis between the ROMS/CROCO TREs (moTRE1 and moTRE2) and the NEMO TREs (moTRE3 and moTRE4).

the 4D tracer motion needs to be broken down into the two plot-dimensions. There are several display possibilites, but in any case information got lost or rather need to be regarded from other analyses. Thus the interpretation of the hovmoeller diagrams requires a detailed understanding of the tracer pattern over time and requires to keep it in mind holisticly. For instance, even if the hovmoeller diagrams do not include transport directions, the transport velocities can be related to them over the transport distances. That means, a velocity derived in the first 6 months of every moTRE belongs to the PCUC because the major tracer distribution over this time is coast parallel and along the shelf. Thus the covered transport distance inherently represent this transport process. The other way round in later stages of the experiments, if there is no tracer left in the northern parts of the shelf, the transport velocity belongs to the eddy induced offshore tracer spread inherent in the transport distance which is again unique for specified times of the (mo)TRE(s).

Depending on the research question to be answered with such an approach many improvements are possible. For a focus on the PCUC, a seperation of the tracer using only this on the shelf is strait foreward. However, this was beyond the time frame of the thesis. And, as there are several possible questions to address details far beyond the general frame of this thesis, the diagrams as shown in Figs. 2.7 & 3.6-3.9 are chosen to display the overall tracer potential of further analyses.

3 Advective Regimes and the Connectivity from the Shelfbreak to the Open Ocean

Abstract of the Chapter. Advection denotes the transport due to the general wind and buoyancy driven oceanic circulation. In the ETSP the advection is highly dynamic and consists of interacting regimes. Such regimes are well known as surface and subsurface currents along the shelf and mesoscale eddy activity. However, the integral effect of the advective regimes on the transport of dissolved constituents from the shelf into the offshore ocean is hard to observe. Here the connection between the Peruvian shelf and the offshore ETSP is demonstrated based on the long-term lateral tracer distribution, by inferring the advective regimes and quantifying their efficiency. The PCUC is dominant in the first few months to half of a year of the (mo)TRE(s) in a latitudinal range from the injection sites at about 10°S to about 16-18°S. Its integral tracer transport velocity near by Callao (∼12°S) is 3-5 cm s^{-1} and 7-17 cm s^{-1} southward from Paracas headland (14-17.5°S). The mesoscale eddy activity takes over in the later stages of the experiments. About 80% of the tracer is influenced by eddies and 21-54% of the tracer reach the offshore ocean captured in the cores of surface and mainly subsurface anticyclones. It is found that a dissolved substance spreading from the sediments of the Peruvian shelf by ocean physics can move unexpected fast and wide to the south and in the offshore ocean.

3.1 Lateral Tracer Distribution

3.1.1 POSTRE Tracer Distribution after 17 months

Seventeen months after the injection the tracer could be measured over the entire sampling area. During the observational survey only at two out of 132 stations there were no samples with tracer concentrations above the detection limit. From the release sites the tracer spread more than 2000 km southward and more than 1400 km offshore, covering an area of more than $2{\cdot}10^6$ km^2. The observed lateral tracer distribution is shown in Fig. 3.1a by a map of the vertical column integral concentrations. For this map an interpolation between the stations is applied, using Gaussian weights with 0.5 degree radii of influence and 1.5 degree cut-off radii.

In the southern most part of the sampling region, 24°S to 30°S, only one section along the coast was executed. The tracer amount increases northward, while the vertical tracer spread enlarges. Nevertheless, the vertical column integral tracer concentrations remain lower than 0.1 nmol m^{-2} for all stations south of 24°S. North of 24°S the tracer distribution shows some inhomogenity in which single stations show comparable high tracer amount. The overall tracer maximum is between 19°S and 21°S near the coast.

The observed center of mass of the tracer patch has shifted from 12.22°S and 77.48°W at the injection to 18.44°S and 74.13°W 17 months later. This is a direct line distance of about 780 km. It would need a drift velocity of about 0.02 m s^{-1} along this line, pointing on strong advection influencing the lateral tracer distribution.

3.1.2 moTREs Tracer Distributions after 17 months in Comparison to POSTRE

Regarding the moTREs 17 months after the injection (Fig. 3.1 b-e) their overall shape is very similar to each other and to the observation. It can be seen that all moTREs represent POSTRE well. The plume of highest tracer concentration is at the coastline bend near Arica (ca. 18.5°S) for all moTREs, in accordance to POSTRE. All moTREs as well as POSTRE show a coast parallel southward transport and an eye-catching shape with a sharp cut south of 20°S. In the ROMS/CROCO experiments (moTRE1 and moTRE2) eddy activity is well visible. For NEMO (moTRE3 and moTRE4) the eddy activity is indicated but less pronounced. In NEMO there is no tracer west of 76°W at latitudes higher 20°S. In ROMS/CROCO single eddies pass to the west through this area. These eddies seem to have the tracer captured in their cores.

In accordance to the literature the "eddy channel" between 15-20°S (Chaigneau et al., 2008; Czeschel et al., 2018; Stramma et al., 2013) is measured in the observations. Additional but weaker offshore transport is found between 10-15°S. Conformable, in both ROMS/CROCO experiments the eddy channel between 15-20°S is well represented. In moTRE2-CROCO there is additional weaker offshore transport between 10-15°S, which cannot be found in moTRE1-ROMS. In NEMO there is only weak offshore transport between 15-20°S but strong between 10-15°S. Overall, the eddy related offshore transport is strongest in moTRE2-CROCO, reaching offshore to about 105°W, whereas the tracer in moTRE1-ROMS, moTRE3-NEMO and

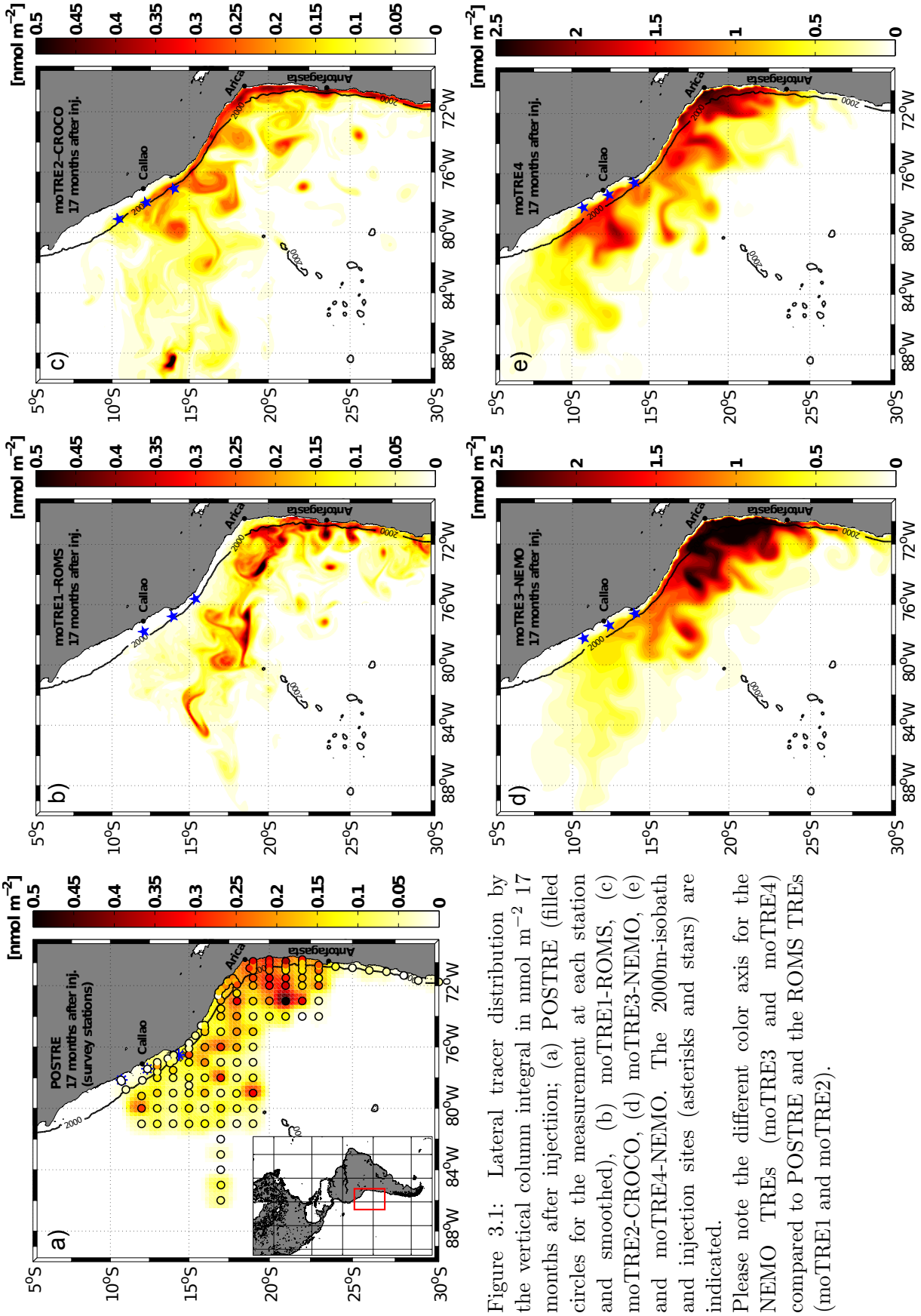

Figure 3.1: Lateral tracer distribution by the vertical column integral in nmol m^{-2} 17 months after injectiion; (a) POSTRE (filled circles for the measurement at each station and smoothed), (b) moTRE1-ROMS, (c) moTRE2-CROCO, (d) moTRE3-NEMO, (e) and moTRE4-NEMO. The 2000m-isobath and injection sites (asterisks and stars) are indicated.
Please note the different color axis for the NEMO TREs (moTRE3 and moTRE4) compared to POSTRE and the ROMS TREs (moTRE1 and moTRE2).

moTRE4-NEMO do not get further offshore than 90.5-94°W.

Looking in each scenario in more detail, moTRE1-ROMS is a surprisingly close representation of the observations. This is despite the different injection sites, while moTRE1-ROMS was made with the initial station plan before the observational injection. A subject to restriction in the representation of the observation is that the modeled shelf is widely free of tracer from the injection sites southward to about 17.5°S. This might be a direct effect from the different injection sites as the southernmost station (15.4°S) is affected by strong current velocities all the time (Fig. 3.10 - section 3.4). moTRE2-CROCO has highest tracer concentrations attached over the shelf with comparable low concentrations in the open ocean but nevertheless reaching furthest to the west of all moTREs. In moTRE4-NEMO the tracer patch is located most northern, reaching 5-10°S but not 30°S. These differences most likely occur due to the different forcings. Additionally, it should be named that, despite the comparable shapes of the tracer patches, the NEMO TREs have about five times higher tracer concentrations than the ROMS/CROCO TREs and POSTRE which cannot be explained by the tracer dispersions. It is an eye-catching difference to investigate in future model comparison and for improvements.

Focusing now on the tracer within the boundaries of the observations, i.e. from 10-30°S and from the coast to 80°W, the difference in distribution between the moTREs gets more detailed. For moTRE1-ROMS the majority of tracer could have been found with the sampling grid. For moTRE2-CROCO the tracer spread very far offshore with a high tracer amount reaching further westwards than 80°W. Although, highest column integral tracer concentrations seems to be attached to the shelf. A rather small amount of tracer in moTRE2-CROCO passes the southern and northern boundaries. For moTRE3-NEMO up to about 30% of tracer distribute to the north and to the west beyond the boundaries of the observation. For moTRE4-NEMO about half of tracer with up to 56% is outside of the regarded boundaries, and again distributed to the north and to the west.

In both ROMS/CROCO experiments and moTRE3-NEMO the southward transports reach beyond 30°S but only negligible tracer amount ($\sim$1% for moTRE1-ROMS, $\sim$6% for moTRE2-CROCO, $\sim$1% for moTRE3-NEMO) passes this boundary. moTRE4-NEMO reaches south toward 28°S. In the observations the first and southern most station was at 30°S, where a small tracer concentration was found. Testing this statement further the subsampled moTREs (Fig. 3.2) indicate an over-estimation of the modeled tracer amount in the southern part of the sampling grid for the ROMS/CROCO TREs and moTRE3-NEMO.

Looking in more detail to the western edge , about 20% (moTRE1-ROMS), 36% (moTRE2-CROCO), 18% (moTRE3-NEMO), and 32% (moTRE4-NEMO) of the modeled tracer passes 80°W. This shows the offshore transport pathway to be very effective. Compared to 30$\pm$10% extrapolated as observational tracer loss beyond the sampling grid, the moTRE estimates are close. The moTRE values might be slightly smaller because the observed tracer is already lost west of 74°W for stations south of including 20°S.

With that, the southward transport is captured very well. The offshore transport was too

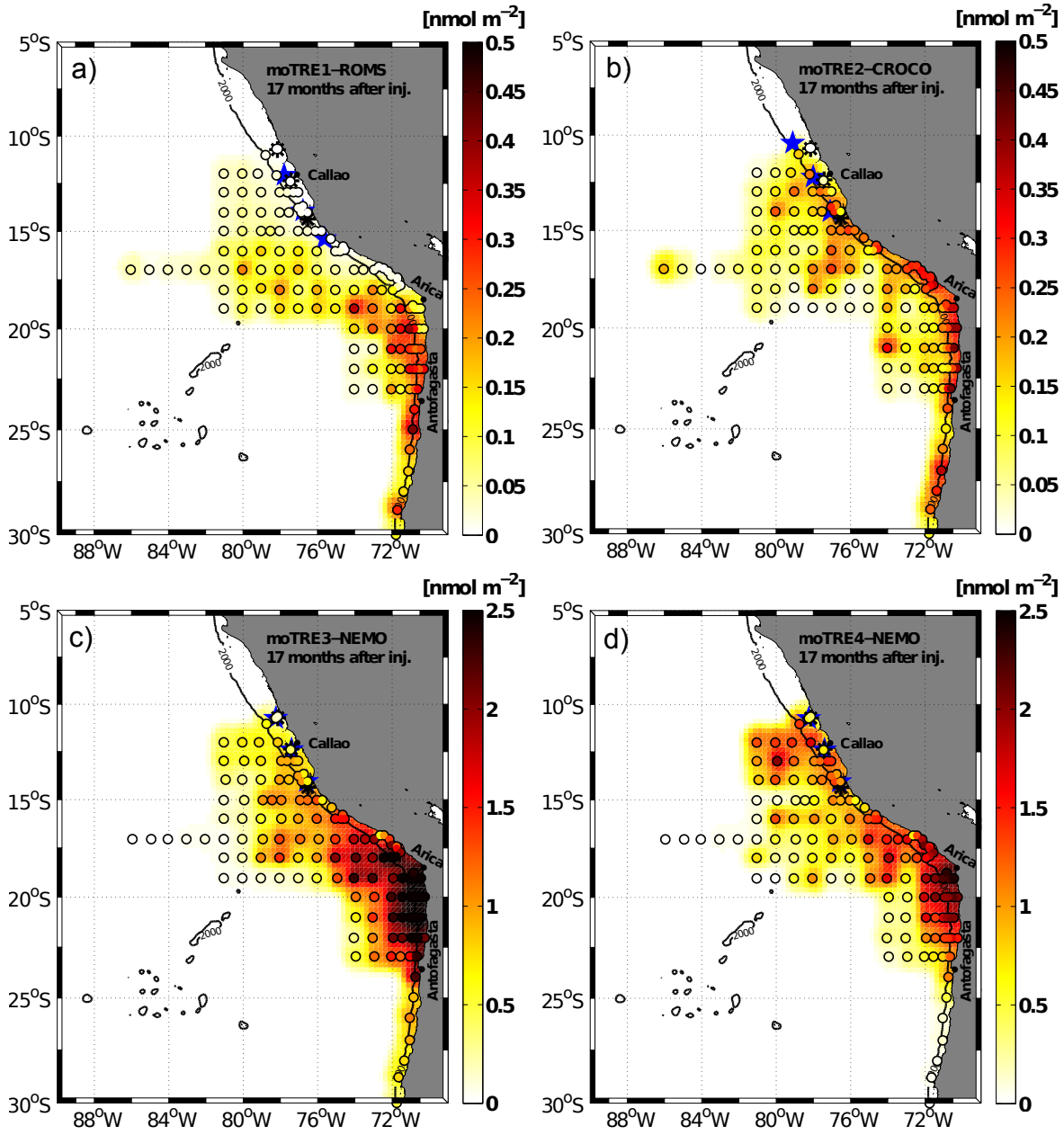

Figure 3.2: moTREs subsampled at the observational stations and smoothed equivalently; (a) moTRE1-ROMS, (b) moTRE2-CROCO, (c) moTRE3-NEMO, (d) moTRE4-NEMO. Stars denote the model, asterisks the observational injection sites.
Please note the different color axis for the NEMO TREs (moTRE3 and moTRE4) compared to POSTRE and the ROMS TREs (moTRE1 and moTRE2).

strong for observational sampling and need to be supported by the modeled tracer patches. A northward transport appears only in NEMO but for both, moTRE3 and moTRE4, with slightly different strength, having a tracer loss of about 7% (moTRE3-NEMO) and ∼21% (moTRE4-NEMO) to the north (compared to 0.3% and ∼2% in moTRE1-ROMS and moTRE2-CROCO, respectively). This northward motion also seems to shift the westward transport about 5° of latitude towards the equator in the NEMO experiments compared to the ROMS/CROCO ex-

periments. Regarding this in context to the literature (e.g. Frenger et al., 2018, Fig. 1.4) the northward transport in relation to the westward transport is most likely a component of the mesoscale eddy activity and its representation in NEMO.

Consistently, 17 months after the injection the centers of masses moved over remarkable distances, showing the dominance of advective processes on the lateral tracer distribution. The centers of masses for each of the moTREs are farther offshore than in the observations. This is probably because the observational survey did not cover the entire distance over which the tracer was transported offshore.

3.1.3 A First Description of the Time Development of the moTREs Tracer Distributions

To highlight the chronological order of important transport processes relevant snapshots (Fig. 3.3) of the supplement videos are shown. In the first few months to almost half of a year the tracer keeps on the shelf and goes coast parallel to the south. In the ETSP this relates to the PCUC (section 3.4). Afterwards more and more eddies are visible by their tracer content. The eddies take the tracer offshore but appear to be of similar importance like the shelf related transport between about 6 to 18 months. After the first one and a half year the eddy related tracer distribution is dominant, spreading the tracer all over the region. All of the moTREs agree generally on this order of tracer transport processes.

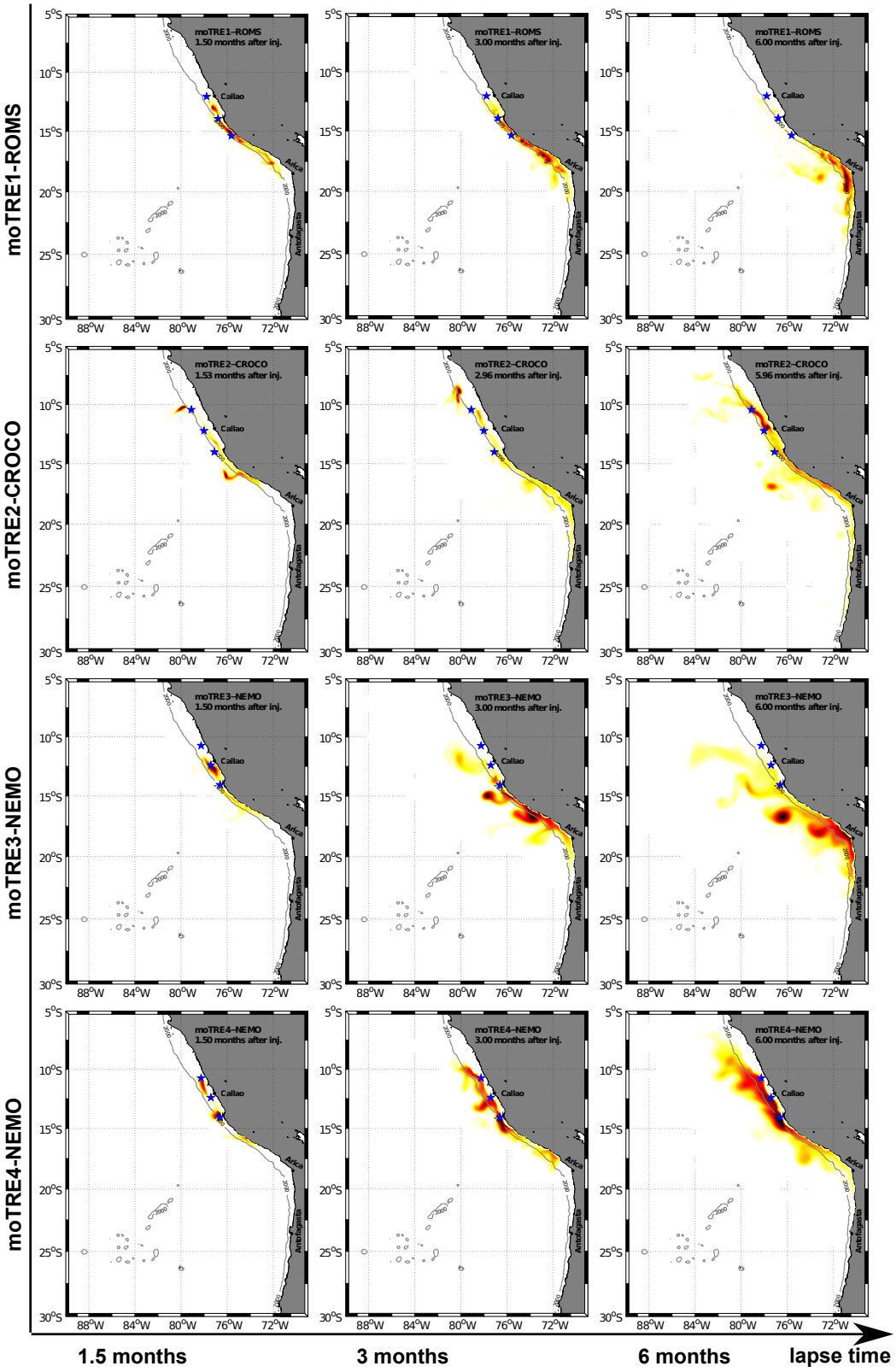

Figure 3.3: Time dependent lateral tracer distribution by the vertical column integral normalized with the maximum tracer concentration; after 1.5, 3, and 6 months for the moTREs. Continued on the next page for 12, 18, and 24 months after injection.

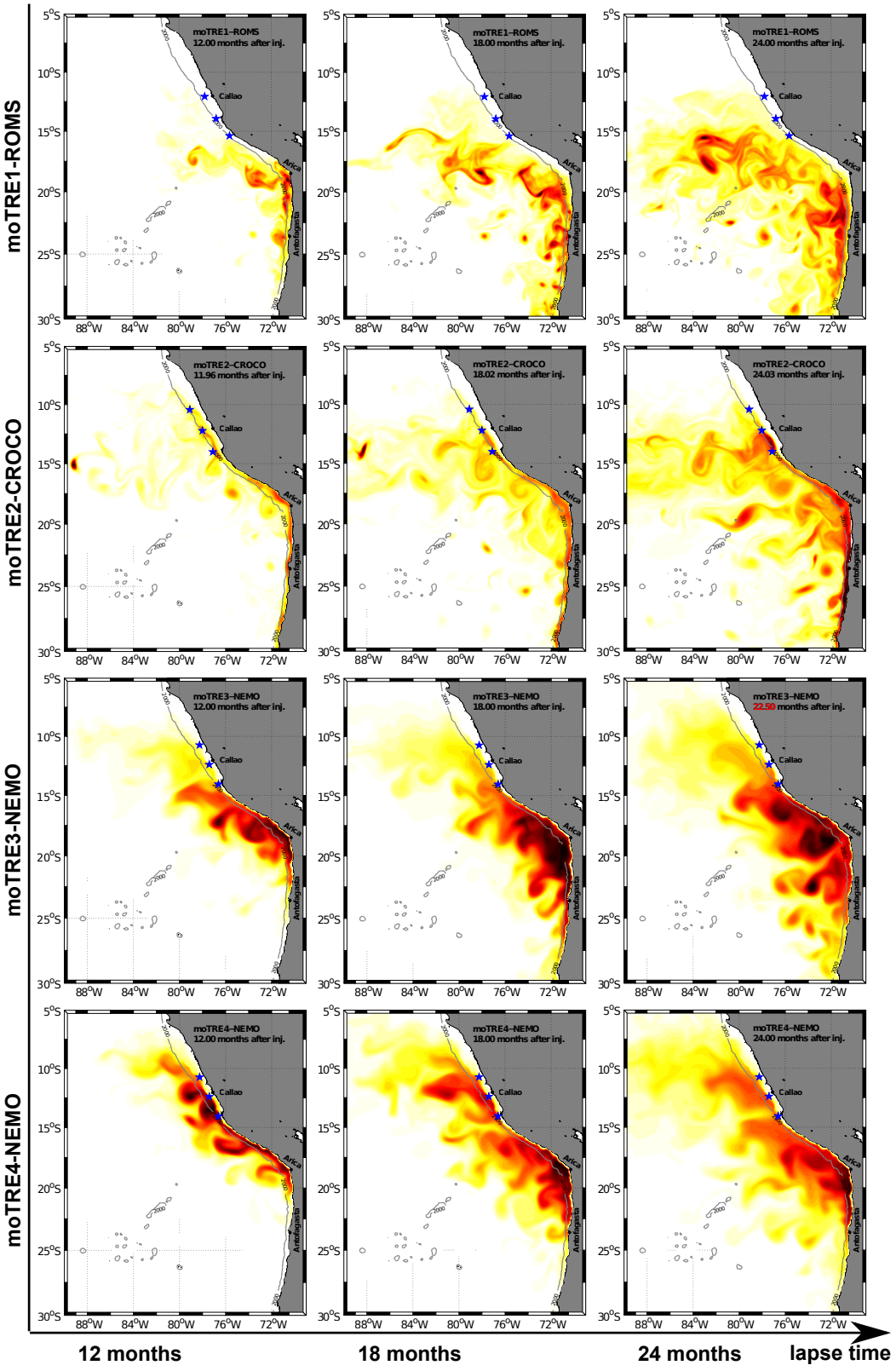

Figure 3.3: Continuing - Time dependent lateral tracer distribution by the vertical column integral normalized with the maximum tracer concentration; after 12, 18, and 24* months for the moTREs. *Please note for moTRE3, the last avilable time step is 22.5 months after injection, not 24.

3.2 Depth Dependent Lateral Tracer Distribution

Beyond the vertical column integral as a measure for the lateral tracer distribution, it is of interest to look into the depth dependent lateral tracer distribution. Therefore sections of exemplary selected latitudes are investigated.

Starting with the observation, the section along 17°S is chosen (Fig. 3.4) as it is longest and has the most stations into the offshore ocean. Near the coast the tracer is distributed with almost equally high concentration over the entire upper 300 m of the water column. Offshoreward the isopycnals squeeze and the depth range covered with tracer narrows. However, the tracer seems to stay in the same range of isopycnals, nicely showing the different stratification regimes in the offshore ocean versus near the shelfbreak. Highest tracer concentrations are associated with tracer clusters. These clusters are related to mesoscale activity (section 3.5). Interestingly, these clusters seem to coincide with a tracer weighted mean survey density of 26.17 kg m^{-3} (bold line in Fig. 3.4). This is lighter (and thus shallower) than the tracer weighted injection density of 26.3 kg m^{-3} (dotted line in Fig. 3.4). As the clusters seem to propagate offshore along-isopycnal, the vertical tracer spread on the shelf has to cause the change in densities before the tracer leaves it. I will come back to this in the next chapter and keep the focus of this chapter on the lateral tracer dispersion.

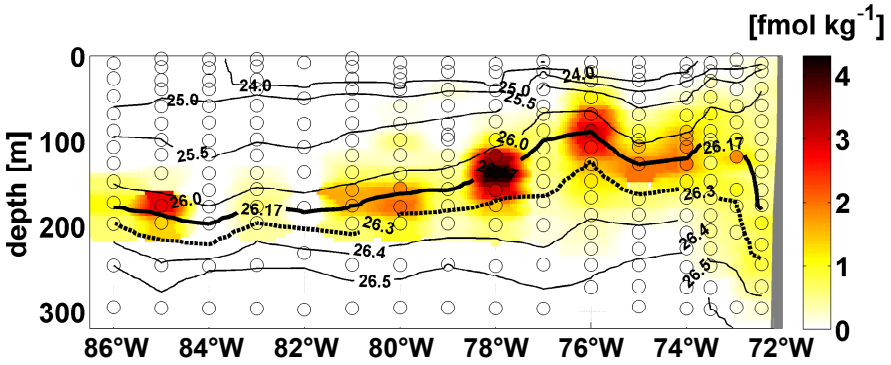

Figure 3.4: Depth dependent lateral tracer distribution exemplary for the POSTRE tracer along 17°S after 17 months. The color coded dots denote the actually measured concentration on top of the interpolated field. The shelf is indicated in gray at about 72°W.

For the moTREs the depth dependent lateral tracer distribution can be regarded over time. For better comparability to the observations the section along 17°S is chosen again and shown 1.5, 3, 6, 12, 17, and 24 months after the injection (Fig. 3.5). At the continental shelf the isopycnals of none of the moTREs show the observed stratification pattern. In the ROMS/CROCO TREs a shelf related widening of the isopycnal distance is partly represented but not as strong as in the observations. In the NEMO TREs it is not visible at all. Thus ROMS/CROCO might capture some dynamics resulting from the different stratification regimes between shelf and offshore areas. For NEMO this might not be possible or visible by the model properties of the regular vertical z-coordinate giving a comparable coarse resolution in the coastal areas, and of the model

output in 5 day averages.

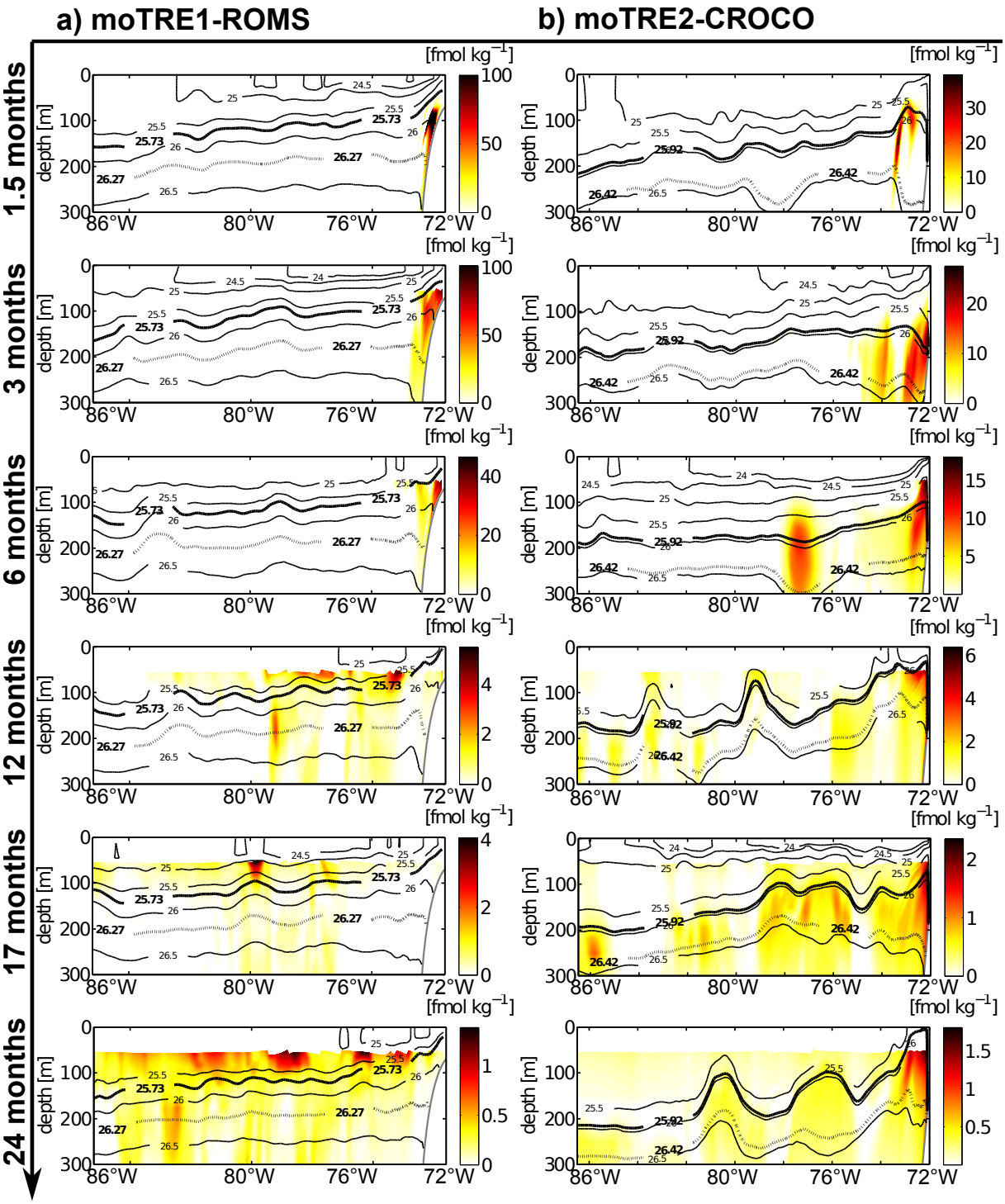

Figure 3.5: Depth dependent lateral tracer distribution exemplary for the moTREs tracers along 17°S after 1.5, 3, 6, 12, 17, and 24 months; (a) moTRE1-ROMS, and (b) moTRE2-CROCO. Continuing on the next page with (c) moTRE3-NEMO, and (d) moTRE4-NEMO. The shelf is indicated in gray at about 72°W.

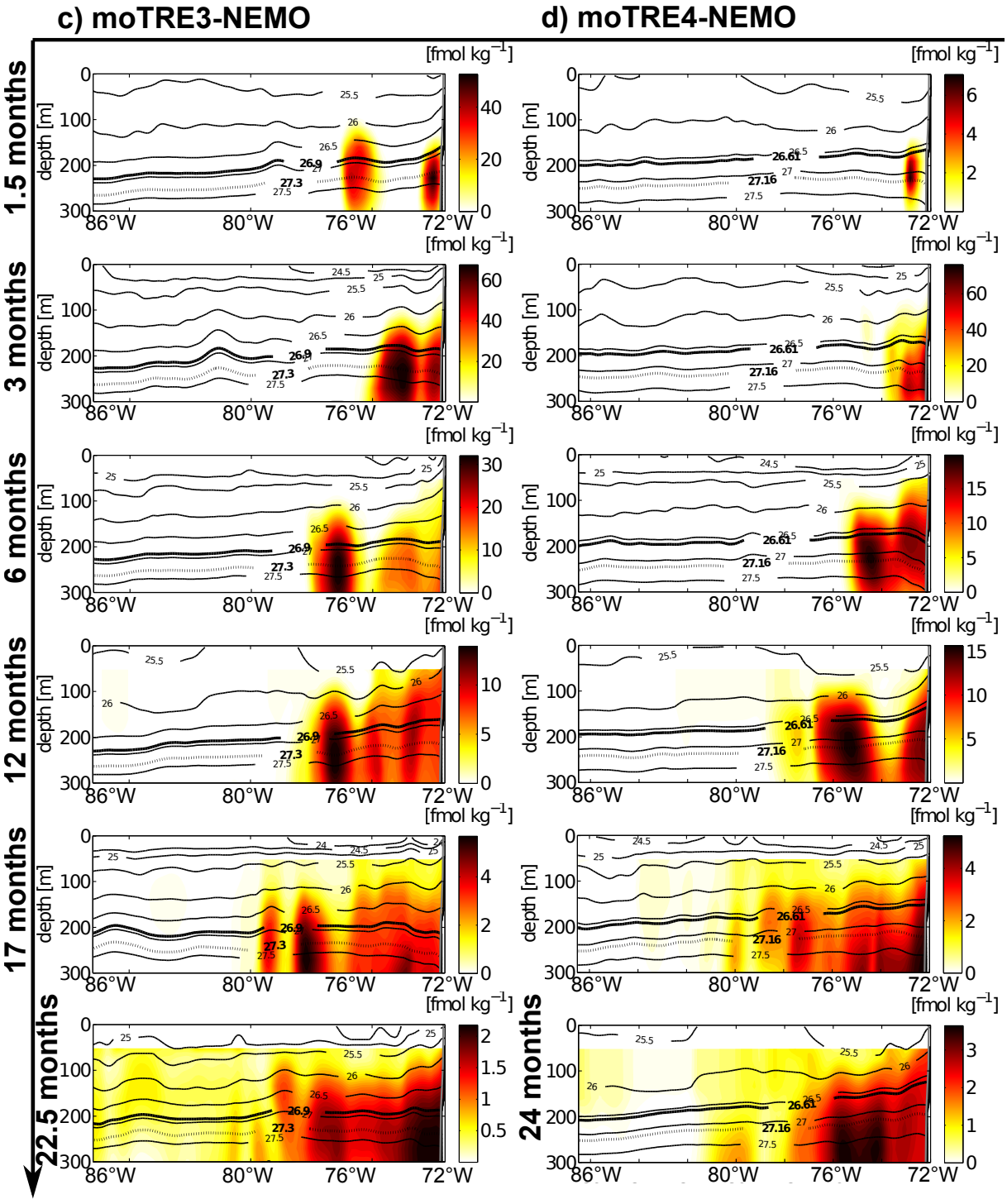

Figure 3.5: Continuing - Depth dependent lateral tracer distribution exemplary for the moTREs tracers along 17°S after 1.5, 3, 6, 12, 17, and 22.5/24 months; (c) moTRE3-NEMO, and (d) moTRE4-NEMO. The shelf is indicated in gray at about 72°W.

For moTRE1-ROMS (Fig. 3.5a), the tracer is related to the shelf in the first 6 months after the injection. Later, it distributes in the offshore ocean with high tracer concentrations in the surface and equally high tracer concentrations in the deeper ranges (100-300 m). Mesoscale activity is indicated but not very clear.

For moTRE2-CROCO (Fig. 3.5b), a clear high tracer signal attached to the shelf is present through all time steps. At the shelf there is no indication of tracer covering the entire upper water column similar to the observations. Apart from the shelf, tracer cluster appear similar to the observation, indicating them to be most likely related to mesoscale activity and to follow along-isopycnal motions. moTRE2-CROCO represents best the depth dependent lateral tracer distribution of POSTRE.

The NEMO TREs (Fig. 3.5 c&d) behave very similar to each other. The tracer appears first attached to the shelf. Later clusters appear and cover the offshore longitudes increasingly in number. However, since the NEMO data was saved only as five day averages, the related short term motions shaping the tracer seems to blur and merge into each other. Thus it is not possible to relate the tracer behavior reliable and clearly to the hydrography and therefore the isopycnals do not seem to react in relation to the tracer behavior.

3.3 Spatio-Temporal Tracer Spread in the moTREs

To infer an absolute value tracer transport distance and velocity (in the following simply referred as transport distance and velocity) Hovmoeller diagrams are used. The overview for all moTREs is shown in Fig. 2.7, the details for each of the moTREs in Figs. 3.6-3.9. For the detailed graphics the tracer distribution within the first few months is split from the later to better visualize the local tracer maxima. Additionally, the splitting is done where the tracer turns and reminds on separate transport directions. The geographical reference point to derive the distance is Callao.

Focusing on moTRE1-ROMS in the first five months of the experiment (Fig. 3.6a) three local tracer maxima naturally starting at the injection sites can be tracked. The northernmost injection side is close to Callao ($\sim$12°S). Its tracer signal propagates only slowly with 1 cm s^{-1} while covering a transport distance of $0.03 \cdot 10^6$ m in 1 month. The tracer signals starting from two more injection sides are much faster. The one from the $\sim$14°S-site shows a transport distance of $0.36 \cdot 10^6$ m covered in 2 months yielding a transport velocity of 7 cm s^{-1}. After 2.5 months lapse time it slows down slightly, covering a further transport distance of $0.21 \cdot 10^6$ m in 2 more months, i.e. with a transport velocity of 4 cm s^{-1}. Starting from the southern most injection site ($\sim$15.4°S) the transport distance is $0.3 \cdot 10^6$ m, covered in 2.5 months, yielding a transport velocity of 5 cm s^{-1}. However, the tracer signals of the single injection sites merge together early. Thus a second signal starting from this southern most injection shows a distance of $0.22 \cdot 10^6$ m to be covered in 4 months, i.e. with a transport velocity of 2 cm s^{-1}.

In the later months after the injection (Fig. 3.6b) several local maxima show the major transports. The turn in transport direction from mainly south to mainly west appears at about 5 months lapse time (section 3.1). Afterwards local tracer maxima

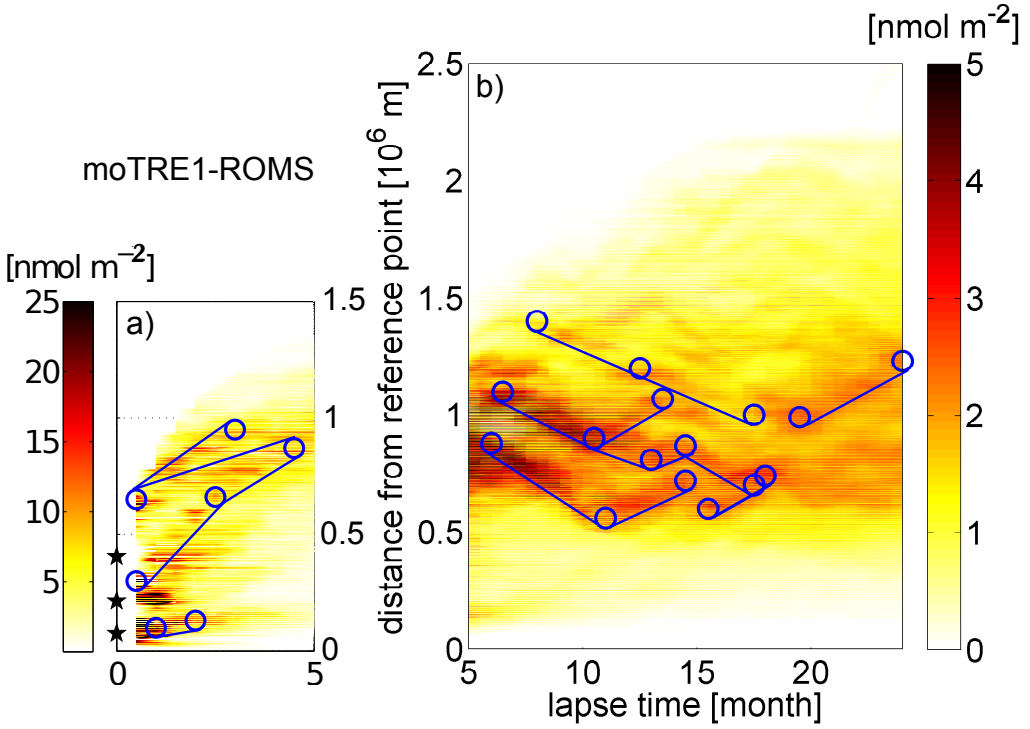

Figure 3.6: Hovmoeller diagram of moTRE1-ROMS with markers for points to derive the slopes indicating the tracer transport distances over time and thus the velocity.

between the lapse times of	denote transport distances of	yield transport velocities of
8.0 to 17.5 months	$0.4{\cdot}10^6$ m	2 cm s^{-1}
6.5 to 13 to 14.5 to 17.5 months	$(0.29, 0.06, 0.17){\cdot}10^6$ m	2 cm s^{-1} (respectively)
6.0 to 11 to 14.5 months	$(0.32, 0.16){\cdot}10^6$ m	2 cm s^{-1} (respectively)
10.5 to 13.5 months	$0.17{\cdot}10^6$ m	2 cm s^{-1}
15.5 to 18 months	$0.14{\cdot}10^6$ m	2 cm s^{-1}
19.5 to 24 months	$0.24{\cdot}10^6$ m	2 cm s^{-1} .

This means in the first part of the experiment, where the tracer transport relates to the coast parallel spreading (with the PCUC), the transport velocity is between 4 and 7 cm s^{-1}, but over time it slows down to 2 cm s^{-1}. In the later stages where the tracer transport relates to the offshore spreading (with the eddy activity), the transport velocity is about 2 cm s^{-1}.

For moTRE2 to moTRE4 an important difference is that the injection sites are distributed north of, close by and south of Callao (∼10°S, ∼12°S, ∼14°S). Thus the site close to zero distance from the geographical reference point, Callao, is actually this one in the middle. The tracer signal starting from the northern most site, north of Callao, decreases its distance to Callao first and increases it after passing by.

In detail the following values are found for moTRE2-CROCO (Fig. 3.7). In the early stages of the experiment (Fig. 3.7a) there is a tracer signal staying close to Callao (∼12°S) for about 1.13 months but not covering any distance. Starting from the two injection sites apart and also looking for local tracer maxima after the tracer merged in one patch, gives

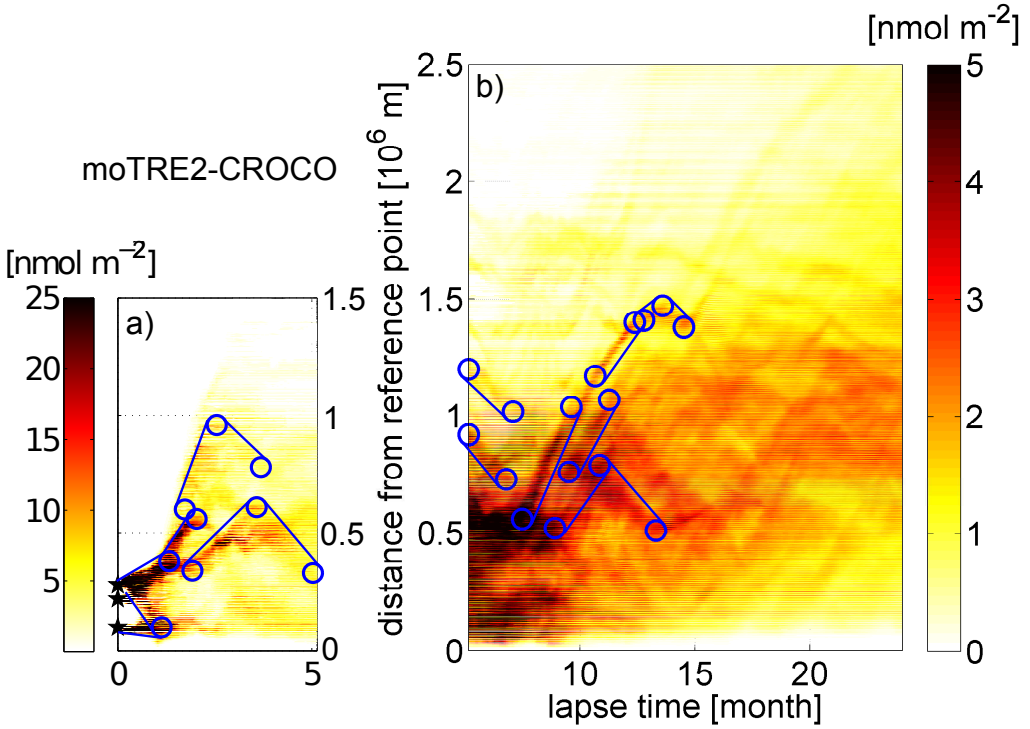

Figure 3.7: Hovmoeller diagram of moTRE2-CROCO with markers for points to derive the slopes indicating the tracer transport distances over time and thus the velocity.

between the lapse times of	covered distances of	and transport velocities of
0.41 to 1.13 months	$0.15{\cdot}10^6$ m	8 cm s^{-1}
0.41 to 1.33 to 2.03 months	$(0.13, 0.18){\cdot}10^6$ m	(5, 10) cm s^{-1}
1.93 to 3.58 to 5.03 months	$(0.27, 0.28){\cdot}10^6$ m	(6, 7) cm s^{-1}
1.73 to 2.55 to 3.69 months	$(0.36, 0.18){\cdot}10^6$ m	(17, 6) cm s^{-1} .

The values for the later stages of moTRE2-CROCO (Fig. 3.7b) are

between the lapse times of	with covered distances of	and transport velocities of
5.14 to 6.77 months	$0.19{\cdot}10^6$ m	5 cm s^{-1}
5.14 to 7.07 months	$0.18{\cdot}10^6$ m	4 cm s^{-1}
7.48 to 9.62 months	$0.48{\cdot}10^6$ m	9 cm s^{-1}
10.65 to 12.37 months	$0.23{\cdot}10^6$ m	5 cm s^{-1}
12.78 to 13.6 to 14.51 months	$(0.23, 0.09){\cdot}10^6$ m	(11, 4) cm s^{-1}
8.9 to 10.85 to 13.3 months	$(0.27, 0.28){\cdot}10^6$ m	(5, 4) cm s^{-1}
9.51 to 11.27 months	$0.31{\cdot}10^6$ m	7 cm s^{-1} .

In the first months of the experiment, the transport velocity (related to the coast parallel transport) is 5 to 17 cm s^{-1} and faster in moTRE2-CROCO than in moTRE1-ROMS. This increase in the transport velocity is reasonable as an effect of an El Niño appearance (e.g. Strub et al., 1998). The transport velocities in the later stages (related to mesoscale eddy activity) are very disperse, ranging from 4 to 11 cm s^{-1}. This is again faster than in moTRE1. Careful relations between the tracer pattern reveal a local tracer maxima path marked from 7.48 to 14.51 months

to be the "eddy channel". It is starting around Arica (18.5°S) and propagates tracer offshore towards and along 15°S. Its overall velocity is fast with 5 to 11 cm s^{-1} and slows down just far in the offshore ocean to 4 cm s^{-1}. Several paths shown by more local tracer maxima show velocities in the same range.

For both of the NEMO TREs it is hard to clearly identify local tracer maxima in the later months but the first three months are very clear. For moTRE3-NEMO (Fig. 3.8) the tracer transport in the early stages (Fig. 3.8a) is characterized by signals

between the lapse times of	covering distances of	and yielding transport velocities of
0 to 1.17 months	$0.33{\cdot}10^6$ m	11 cm s^{-1}
0 to 0.67 months	$0.06{\cdot}10^6$ m	3 cm s^{-1}
0.67 to 1.83 months	$0.37{\cdot}10^6$ m	12 cm s^{-1}
2 to 3 months	$0.14{\cdot}10^6$ m	5 cm s^{-1} .

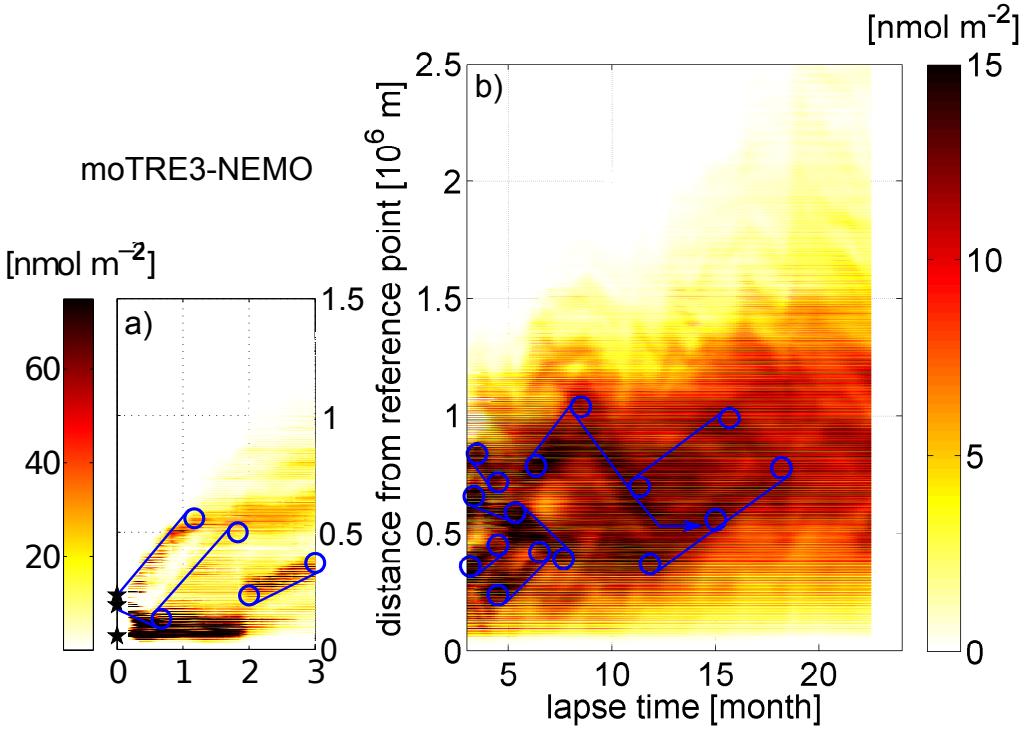

Figure 3.8: Hovmoeller diagram of moTRE3-NEMO with markers for points to derive the slopes indicating the tracer transport distances over time and thus the velocity.

And, in the later stages (Fig. 3.8b) by tracer signals

between the lapse times of	covering distances of	and yielding transport velocities of
6.33 to 8.5 to 11.33 to 15.67 months	$(0.25, 0.34, 0.29){\cdot}10^6$ m	(4, 4, 3) cm s^{-1}
11.83 to 15 to 18.17 months	$(0.19, 0.22){\cdot}10^6$ m	(2, 3) cm s^{-1}
3.5 to 4.5 months	$0.12{\cdot}10^6$ m	5 cm s^{-1}
3.33 to 5.33 to 7.67 months	$(0.07, 0.20){\cdot}10^6$ m	(1, 3) cm s^{-1}
3.17 to 4.5 months	$0.09{\cdot}10^6$ m	3 cm s^{-1}
4.5 to 6.5 months	$0.18{\cdot}10^6$ m	3 cm s^{-1} .

Around Callao (∼12°S) there is one tracer signal staying in this distance range (i.e. having zero velocity). A second signal is slow with a transport velocity of up to 3 cm s^{-1}. South of Callao moTRE3-NEMO shows a very fast propagation with 11 to 12 cm s^{-1} influencing the tracer signals for 1.17 months but quickly slows down thereafter. Afterwards the tracer is transported with 5 cm s^{-1} which is at this level very similar to the values found in moTRE1-ROMS. In the later stages of moTRE3-NEMO two quite persistent features (from 6.33 to 15.67 months and from 11.83 to 18.17 months) show eddy related velocities between 2 and 5 cm s^{-1}, slightly faster than moTRE1-ROMS and slower than moTRE2-CROCO. In the time span representative for the regime shift between the coast parallel and the offshoreward transport, the transport velocity slows down to at least 1 cm s^{-1}.

moTRE4-NEMO (Fig. 3.9) is slightly different to the experiments moTRE1 to moTRE3 as a remarkable tracer portion stays or recirculates in the near distance field of Callao (∼12°S) over at least 15 months after the injection. Some of this tracer move out of this blob with a velocity of 3 cm s^{-1} (covering a transport distance of $0.19 \cdot 10^6$ m in 2.17 months). In contrast to that, a tracer signal probably originating from the southern most injection site, south of Callao, propagates very fast with 9 cm s^{-1} while covering a distance of $0.57 \cdot 10^6$ m in 2.33 months (Fig. 3.9a). These values are similar to moTRE3-NEMO.

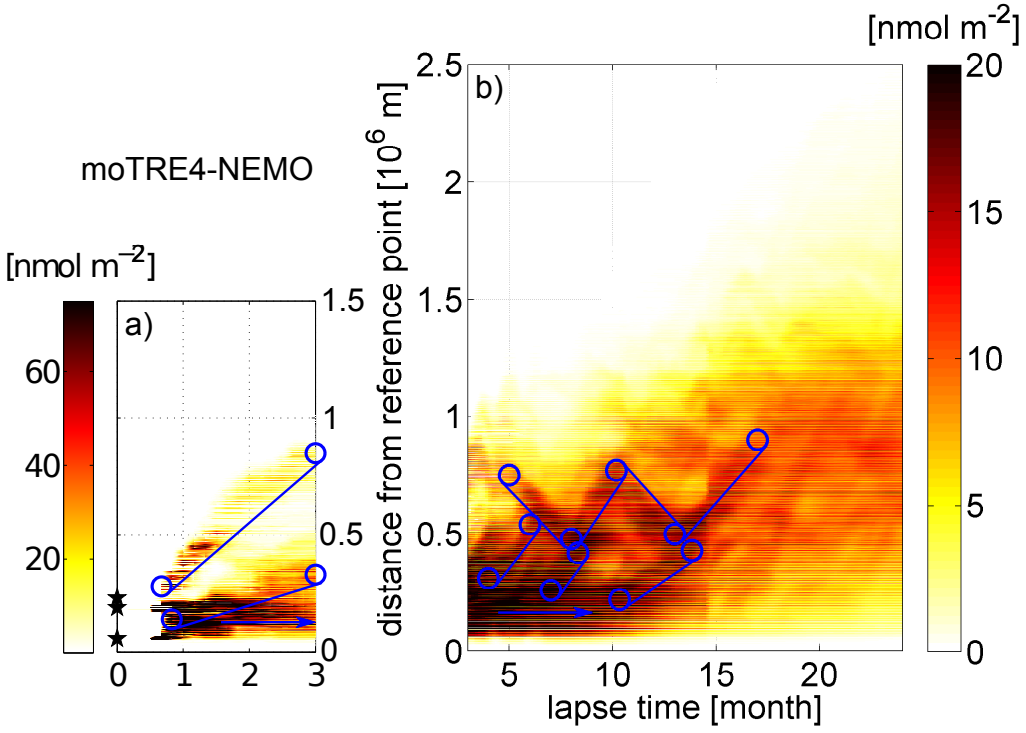

Figure 3.9: Hovmoeller diagram of moTRE4-NEMO with markers for points to derive the slopes indicating the tracer transport distances over time and thus the velocity.

In the experiment stages later than 3 months (Fig. 3.9b), there is a long lasting feature and several additional local tracer maxima:

Between lapse times of	the local tracer maxima cover distances of	and yielding transport velocities of
5 to 8 to 10.17 to 13 to 17 months	(0.27, 0.29, 0.27, 0.40)·10^6 m	(3, 5, 4, 4) cm s^{-1}
4 to 6 months	0.23·10^6 m	4 cm s^{-1}
7 to 8.33 months	0.16·10^6 m	5 cm s^{-1}
10.33 to 13.83 months	0.21·10^6 m	2 cm s^{-1} .

Thus the transport velocities in the later stages (related to eddy activity) are between 2 and 5 cm s^{-1}, similar to moTRE3-NEMO and slightly faster than moTRE1-ROMS.

3.4 Coast-Parallel Tracer Export by the PCUC

There is a strong advective pathway acting subsurface, coast-parallel along the shelf. In the ETSP this is the well known PCUC (e.g. Brink et al., 1983; Huyer et al., 1991; Silva and Neshyba, 1979; Hormazabal et al., 2013; Pizarro et al., 2002; Chaigneau et al., 2013; Penven et al., 2005; Thomsen et al., 2016; Montes et al., 2010).

To get an impression of the PCUC a velocity field is mapped and graphed as section over the shelf (Fig. 3.10). The velocities are exemplary these of the climatological driven ROMS configuration (ROMS-CLIM, used for moTRE1) averaged over three years. The PCUC acts coast parallel over the whole study area of ROMS-CLIM from 5°S to 30°S (Fig. 3.10a). North of Callao its velocity is up to 13 cm s^{-1}, slower near by Callao (with up to 9 cm s^{-1}) and decreases further (to max. 6 cm s^{-1}) toward about 14°S. After passing the Paracas headland (∼14°S) it is fastest with up to 22 cm s^{-1} but slows down again to max. 8 cm s^{-1} until reaching about 17.5°S. Minimum velocities appear around Arica (18.5 °S) with up to 5 cm s^{-1}. Just from around Antofagasta (23.6°S) onward the velocity increases to max. 8 cm s^{-1}. Regarding the section of the PCUC over the shelf, the three year mean velocity field (using the meridional component) of ROMS-CLIM gives a mean state along 15°S (Fig. 3.10b). The current is represented on the continental shelf with its core at about 150 m water depth.

Comparing this with the observations from the tracer survey cruise in March 2017 (Fig. 3.11), the cruise's snapshot denotes a very patchy velocity field with higher maximum values than in the ROMS-CLIM average. But, on the shelf there are southward velocities of up to 15-20 cm s^{-1}. As expected (by e.g. José et al., 2017; José et al., 2019; Czeschel et al., 2011; Chaigneau et al., 2013; Thomsen et al., 2016, and references therein) the PCUC seems to be very good represented in the models and in the observation related to POSTRE.

The mapped velocities, with the subsurface PCUC coast-parallel along the shelf, are highly related with the tracer dispersion pattern (cp. to Figs. 3.1, 3.3, SI-videos).

In addition to the velocity pattern, the denoted PCUC feature is supported by the hydrography and can be directly aligned with the tracer distribution. For instance, at 21°S it is well visible for moTRE2-CROCO (Fig. 3.12a) and for POSTRE (Fig. 3.12b). Most important, the relation to ESSW can be confirmed which gets south within the PCUC. It is characterized by a salinity

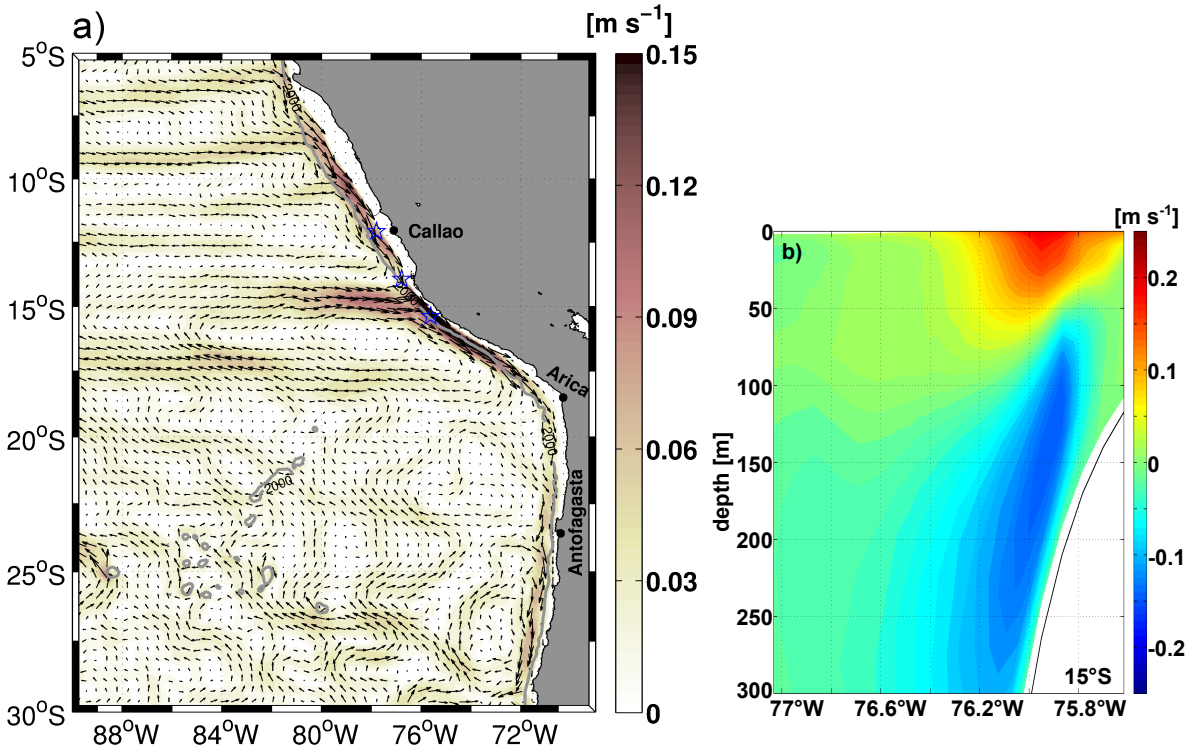

Figure 3.10: Averaged (over three years) velocity field from the ROMS-CLIM configuration. (a) Mean horizontal velocities over the depth range around 130±15 m with absolute velocity values in color and directions denoted by arrows. (b) Meridional velocity component along 15°S.

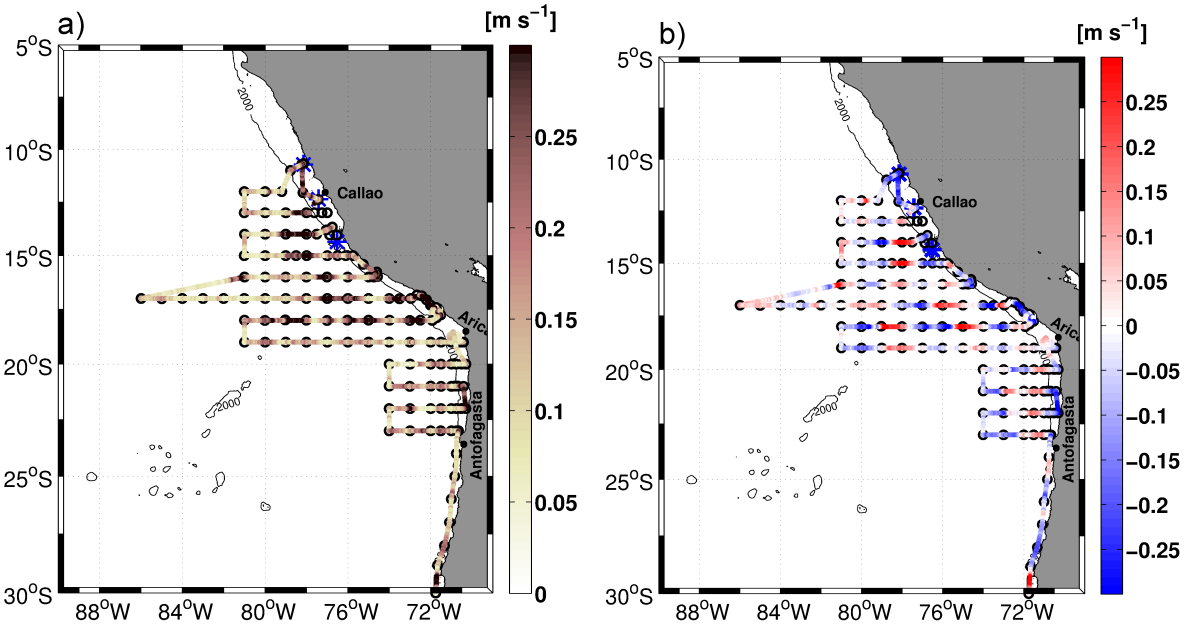

Figure 3.11: The velocity field as measured during the tracer survey in March 2017, averaged over 600s-bins in the depth range around 130±15 m. (a) The absolute value velocity. (b) The meridional velocity component.

maximum associated with a minimum in dissolved oxygen (Silva et al., 2009). Both, the velocity and salinity (and oxygen - not shown here) pattern are correlated to the tracer and identify its transport by the PCUC.

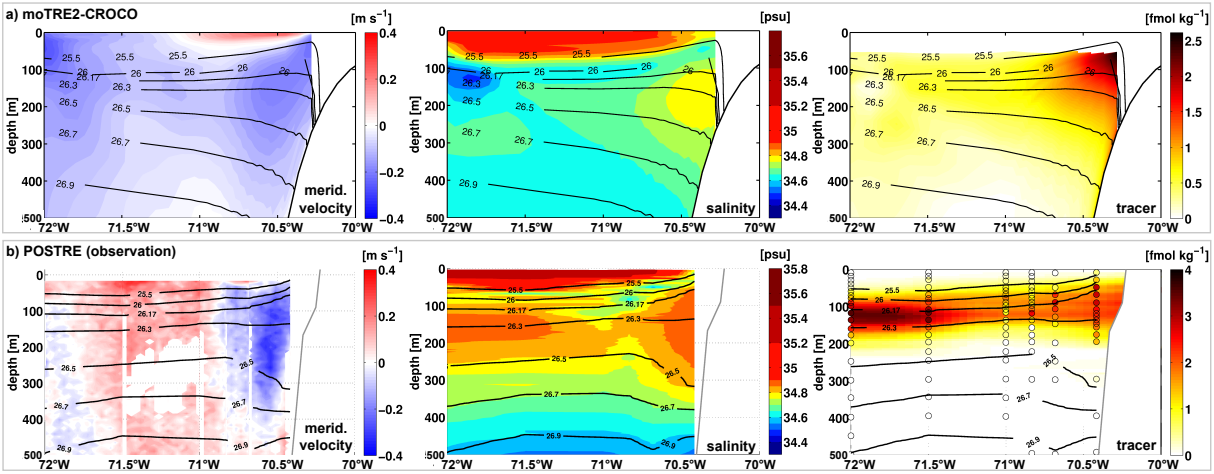

Figure 3.12: Aligning the tracer to the PCUC exemplary along 21°S 17 months after injection for (a) moTRE2-CROCO, and (b) POSTRE; via meridional velocity, salinity and tracer concentration. Please note the different color axis for the tracer concentration.

The tracer transport velocities (section 3.3) fit well with the mean PCUC current velocities. The tracer transport velocities also respect the different velocity segments within the current. Near by or slightly north of Callao (∼12°S) the tracer is transported with 4 cm s^{-1} (moTRE1-ROMS), 5 cm s^{-1} (moTRE2-CROCO), 3 cm s^{-1} (moTRE3-NEMO), and 3 cm s^{-1} (moTRE4-NEMO). After some time and distance, when reaching the PCUC segment around Paracas headland (∼14°S), the transport velocities get highest with 7 cm s^{-1} (moTRE1-ROMS), 17 cm s^{-1} (moTRE2-CROCO), up to 12 cm s^{-1} (moTRE3-NEMO), and 9 cm s^{-1} (moTRE4-NEMO). Finally, the decrease in velocity along the path is captured in moTRE1-ROMS and moTRE3-NEMO with tracer transport velocities reduced to 2 cm s^{-1} (moTRE1-ROMS), and 5 to 1 cm s^{-1} (moTRE3-NEMO), again consistent with the mean current velocities. The differences in the transport velocities of the moTREs most likely result from different forcings, slightly different injection sites and their location with respect to the representation of the PCUC in the various model configurations.

Out of the PCUC eddies are known to be generated and detaching from the shelf, highlighting the connection of the transport from this current to the eddy activity. Namely, the volume transport of anticyclonic mode-water eddies (AMWs) across the inshore-offshore boundary is about 0.5 Sv. This exports 30% of the PCUC transports, "leak a substantial fraction of low-oxygen, nutrient-rich undercurrent waters offshore", and "is accompanied by [...] stirring of [AMWs] along isopycnals" (Frenger et al., 2018, and references therein). The paths drawn by the eddy activity are strong and persistent enough to be visible in the mean velocity field as jets (Fig. 3.10a).

3.5 Offshore Tracer Export by Mesoscale Eddy Activity

3.5.1 POSTRE Tracer Captured in Anticyclonic (Mode-Water) Eddies

In the observation, with the deliberately regular sampling grid, there are only three eddy core stations. One at 19°S, 79°W, one at 21°S, 73°W, both in anticyclonic features and one at 23°S, 74°W in a cyclone. The eddy edges of eight more anticyclones (ANTs) and six more cyclones (CYCs) were sampled along 14°S at 78°W and 79°W; along 17°S at 76°W & 77°W, 74°W to 73°W; along 18°S at 75°W, 76°W and 80°W; as well as along 19°S at 78°W and 80°W.

To relate the tracer behavior to the sampled eddies a companion of timely sea level anomaly (SLA) satellite observations and the ship sections along 18°S, 19°S and 21°S is chosen. From that three eddies can be identified: Two anticyclonic mode-water eddies (AMWs - named A and C) and one regular ANT (named B). The SLA is shown in Fig. 3.13 for the area between 15 - 22°S at 17. March 2017. At this day, the ship operated along 18°S from 76 - 74°W. Its actual position is marked by 'x'. The two positive SLA anomalies in the center (A and B) could be tracked backward in time to their generation on the continental shelf (Schütte, F., 2017 - personal correspondence). At the beginning their propagation path was southwest, perpendicular to the coast, but became almost westward after passing 73°W.

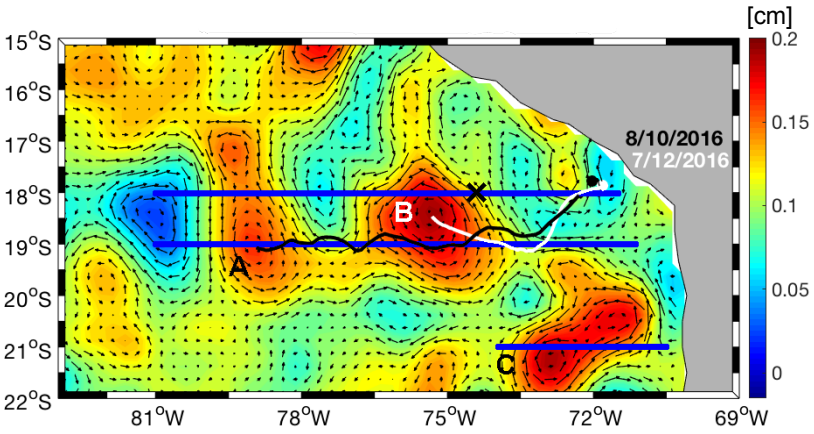

Figure 3.13: Eddies measured during the tracer survey with SLA (shaded) on 17. March 2017 with ship position (x) during survey cruise. Two eddies (A, B) tracked backward (white and black track) to their origin (dot). Sections of observed tracer and hydrography shown in Fig. 3.14 indicated. (Schütte, F., 2017 - personal correspondence)

The core of the left eddy A (black track) was passed and sampled at about 19°S, 79°W. It can be clearly identified in the meridional vmADCP velocity along 19°S (Fig. 3.14). In the core of this eddy A much higher tracer concentrations and a much higher vertical column integral of tracer could be detected compared to the stations at its edges or in the surrounding waters. In the hydrography this eddy core is well visible with a local salinity maximum and oxygen depletion. The overlaid isopycnals show a subsurface lens identifying this feature as AMW. The tracking revealed this eddy A to be generated on 08. October 2016. It was sampled after it traveled a distance of 750 km with an average westward velocity of about 4.3 cm s^{-1}. Similar to eddy A, eddy C is represented very well in the tracer, velocity and hydrography measurements (Fig. 3.14). Close to its core it could be sampled at station 21°S, 73°W and identified as an AMW with high tracer amount in its core. It points that the tracer is commonly captured in the core

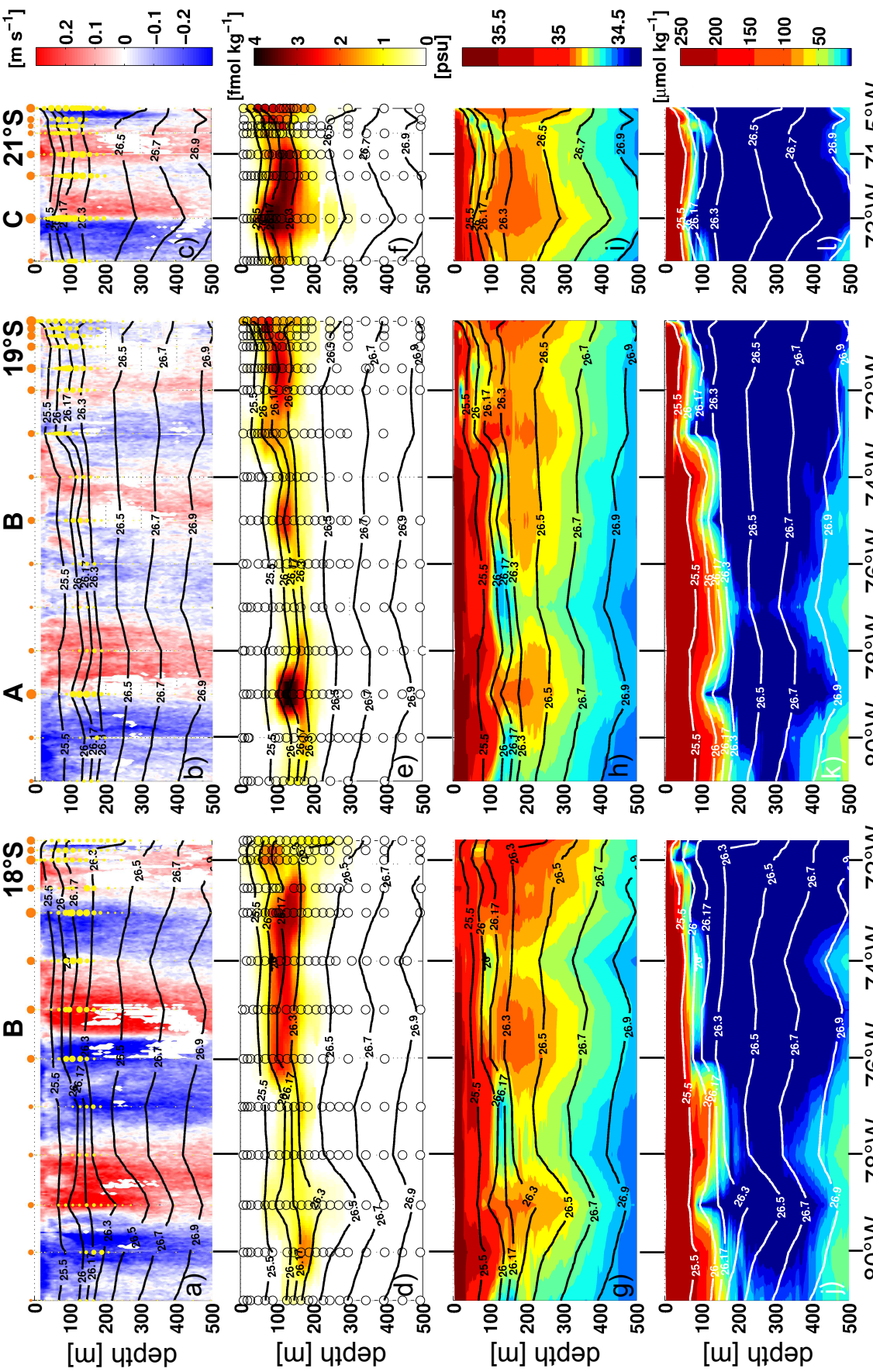

Figure 3.14: Eddy activity (and PCUC) found for POSTRE by observed meridional velocity, tracer, salinity, and oxygen along 18°S, 19°S, and 21°S. Please note the shelf to be at the right side of each section: at 18°S it is at about 70.4°W, at 19°S it is at about 71°W, and at 21° it is at about 70.3°W.

water of at least this eddy type, in AMWs.

For eddy B (white track in Fig. 3.13) the core is at about 18.5°S, 74.3°W and was not sampled nor passed. We could only cut the eddy edges along 19°S and especially along 18°S. The related isopycnals are deepened but do not form a subsurface lens. Thus eddy B is found to be a regular ANT (Fig. 3.14). The tracking identified the generation of eddy B on 07. December 2016. It was sampled after it traveled 380 km of distance with an average westward velocity of 5.2 cm s^{-1}. The related tracer samples show no clear peak in the vertical column integral. However, comparatively high concentrations are visible in the eddy regarding the tracer-depth distribution. This indicates that also regular ANTs capture the tracer.

At 23°S, 74°W a CYC was sampled right at the end of the tracer patch with a very low vertical tracer column integral. Unfortunately, there is insufficient information of the tracer amount surrounding this eddy. Thus no reliable indication can be gained from this station. Regarding the eddy generation of CYCs out of surface currents (Chaigneau et al., 2011; Colas et al., 2012; Johnson and McTaggart, 2010) and the tracer injection in intermediate depth, one could speculate with this finding at 23°S, 74°W that CYCs do not capture the tracer.

3.5.2 moTREs Tracer Relation to Mesoscale Eddies

When regarding the modeled eddy activity in relation to the tracer behavior only the ROMS/CROCO TREs (moTRE1 and moTRE2) are referred. The NEMO results will not be shown nor used for this purpose. As already stated (sections 3.1.2 & 3.2, Figs. 3.1, 3.5 c&d) the NEMO eddies merge into each other, their properties are hardly visible, and the isopycnals do not seem to react in relation to the tracer behavior due to data saved as 5 day averages. Thus it is not possible to clearly and reliable relate the tracer-indicated eddy features to the hydrography.

The ROMS/CROCO TREs support the observational results. The modeled AMWs and ANTs can be found to contain high tracer concentrations in their cores (e.g. Figs. 3.15 and 3.16a). Thus all anticyclonic eddies capture the tracer during their generation regardless if they are of the mode-water type or regular ones. CYCs can be identified in the moTREs to be almost free of tracer (e.g. Fig. 3.16b) as suggested from the observations.

Filaments are resolved in the moTREs and identified as features with tracer and salinity signatures of anticyclonic (mode-water) eddies, i.e. containing ESSW, but with eddy-untypical meridional velocities. A relation to the respective map of the vertical column integral clarifies their shape (e.g. Fig. 3.16c compared to Fig. 3.1b).

Beyond these clear results the moTREs show some more insights from the high temporal resolution. For instance, in Fig. 3.16c the tracer and salinity signature in the filament are somewhat before and in front of the offshore flank of a strong and clear AMW at 15°S, 80°W. The eddy itself is apparently but contradictory almost free of tracer, although not remarkable different to the tracer-trapping AMWs. 17 months after the injection, in this moTRE1-ROMS the shelf is almost tracer-free as far as about 17.5°S to the south (section 3.1.2). The eddy had to be formed when there was no tracer left in the eddy generation area. The filament get shaped

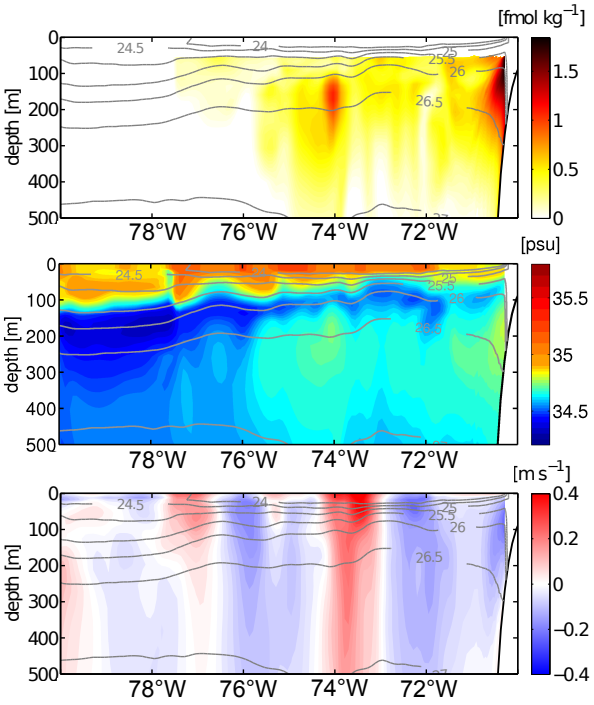

Figure 3.15: Representative examples of the eddy-tracer relation in the ROMS/CROCO experiments (continued in Fig. 3.16), shown here in moTRE2-CROCO. Namely, the tracer distribution is related to salinity and meridional velocity. This is section 21°S, 17 months after injection, showing the tracer captured in an AMW at 74-75°W just detached from the PCUC.

when the tracer-free eddy swirls through a high tracer concentration spot left behind from an already died eddy (SI-video). On the other hand, there are CYCs capturing the tracer (e.g. Fig. 3.16d) when they generate after the tracer got distributed nearly homogeneously in all waters of the generation area (SI-video). Both examples just show that the eddies capture whatever is available during their generation, propagate and swirl through every anomaly on their path and finally homogenize the tracer all over the area. When the homogenization proceeded far enough the tracer distribution cannot give conclusive insights into the governing processes anymore.

As another appealing point, the moTREs give insight in the northward tracer transport. This is after all just a northward component in the eddy motion, as already suggested by literature (e.g. Frenger et al., 2018, Fig. 1.4). Although, the tracer portion leaving to the north is very small in the ROMS/CROCO TREs, the eddies in there (and in the NEMO TREs) basically propagate north-west, with e.g. in moTRE1-ROMS a deviation angle from a pure westward motion of about 20° to the north (SI-videos).

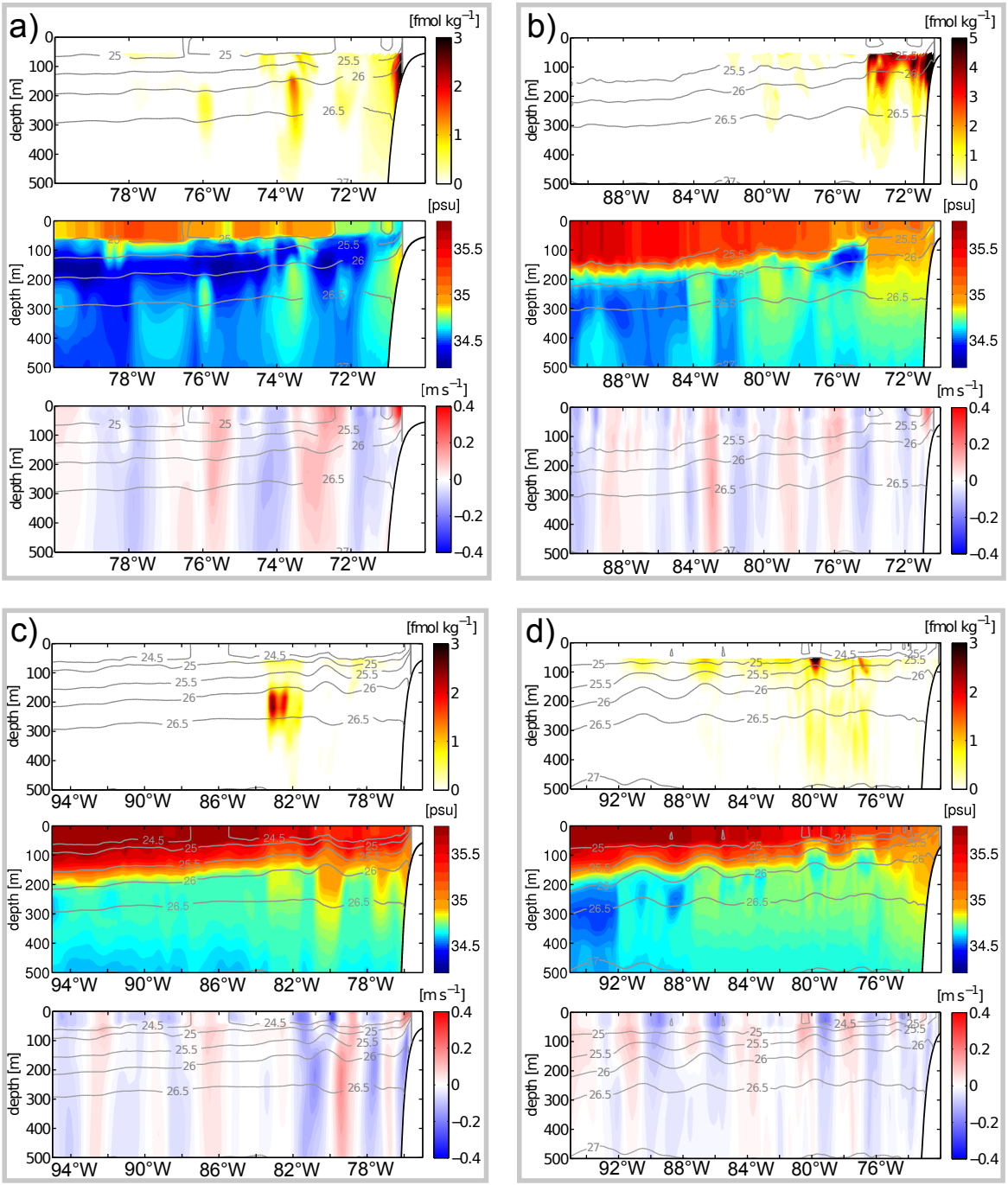

Figure 3.16: Continuing - Representative examples of the eddy-tracer relation in the ROMS/CROCO experiments, shown here in moTRE1-ROMS. Namely, the tracer distribution is related to salinity and meridional velocity. (a) 24°S, 17 months after injection, showing the tracer captured in an ANT at 73-74°W. (b) 19°S, 12 months after injection, showing the CYC at 74.5-76°W free of tracer. (c) 15°S, 17 months after injection, showing a tracer-tagged filament at 82-84°W, and a tracer free AMW at ∼80°W generated on an already tracer freed shelf. (d) 17°S, 17 months after injection, showing CYCs at ∼80°W capturing tracer after its distribution all over the place. Compare to the related lateral tracer distribution map Fig. 3.1 for e.g. the shape of filament and for the already tracer freed shelf.

3.6 Discussion

Two advective pathways are shown to clearly shape the tracer behavior and seem to dominate the lateral tracer distribution. These transport mechanisms, the PCUC and mesoscale eddy activity, are well known in the ETSP (e.g. for PCUC: Brink et al. (1983); Huyer et al. (1991); Hormazabal et al. (2013); Pizarro et al. (2002); Chaigneau et al. (2013); Penven et al. (2005); Thomsen et al. (2016); Montes et al. (2010) and e.g. for eddy activity: Chaigneau and Pizarro (2005); Chaigneau et al. (2008, 2011); Czeschel et al. (2018); Frenger et al. (2018)) and especially easy to identify in the moTREs. The coast-parallel tracer transport along the shelf is caused by the PCUC. South of about 18°S tracer is transferred out of the PCUC regime by eddy dynamics (in the periphery of eddies as well as by eddies trapped in the core that are leaving the region), i.e. the mesoscale eddy activity takes over and transports the tracer offshore to the west. The connectivity between both transport mechanisms is already known from e.g. Thomsen et al. (2016) or Frenger et al. (2018) (and references therein).

For the tracer distribution the chronological order of these both processes is of interest. First of all, near the injection sites in the northern part of the study area (∼10-14°S), the PCUC dominates the lateral tracer transport. One could have imagined an immediate capturing of all injected tracer in an eddy to get transported offshore. Such a perception might was based on a pilot study prior to POSTRE (Zocher, 2010) in which tracer maps show some offshore transport right in the area of the POSTRE injection sites. However, the tracer concentration apart from the shelf and thus the tracer amount actually leaving the shelf is very small but shown misleading in a logarithmic scale. Zocher (2010) states explicitly "most of the tracer is advected parallel to the coast, because of the current system of Peru and only a small part is advected cross shore." This is exactly what was found with POSTRE. And, this is also supported by the recent study of Frenger et al. (2018), showing (if any) only few eddies act in this region with a so called "cannonball effect" on dissolved properties. In later stages of the (mo)TRE(s) tracer containing eddy like features circling between 11-15°S but as the moTREs reveal they seem to get their tracer content from southern filaments (SI-videos).

The tracer is transported over a very large distance along the shelf, from ∼10-14°S (at the injection sites) to about 18°S and beyond. Although the PCUC is characterized as a current with a lot of recirculations and with a hard to measure mean velocity and mean transport properties (Chaigneau et al., 2013; Czeschel et al., 2011), it relentless pushes the tracer over a distance of several hundreds to thousands of kilometers within a narrow band on the continental shelf. The net along-shelf, i.e. tracer transport, velocities of about 4 cm s^{-1} (near by Callao at ∼12°S) is smaller than the values north of Callao denoted by previous studies to be e.g. 6-8 cm s^{-1} (at ∼6°S & ∼9°S, Penven et al., 2005), maximal ∼9 cm s^{-1} (6-9°S & 9-12°S, Chaigneau et al., 2013) or 10 cm s^{-1} (at 6°S, Feb. 2009, Czeschel et al., 2011), and even typically 10 cm s^{-1} (10°S, Huyer et al., 1991). However, these differences might arise from the slightly different latitudes investigated. The net along-shelf transport velocities of maximal 17 cm s^{-1} (around Paracas headland at ∼14°S) generally agree with literature velocities of at least 10-14

cm s^{-1} (12-15°S) and at least 7-8 cm s^{-1} (15-18°S) but with local means up to 20 cm s^{-1} (8-16°S) (Chaigneau et al., 2013, and references therein). Thus the results suggest mean current velocities of the PCUC applicable as transport velocities of dissolved constituents.

The unexpected fast and wide motion from the Peruvian shelf to the south is an interesting point when regarding actual nutrient distributions (e.g. Fig. 1.3). Along ∼12°S the pattern of substances released from the Peruvian sediments distributed over the shelf (e.g. in terms of nitrogen cycling: Scholz et al., 2016; Sommer et al., 2016, and references therein). Thus it was assumed previously that these pattern waft sluggish at its place or might recirculate locally. Contradicting to these previous assumptions, the tracer transports by the PCUC identified in this thesis indicate highly dynamic exchanges. Nutrients represented by the tracer would be "washed away" from their origin with the PCUC. As they are measured persistent in similar pattern along such a section these nutrients have to be replaced by newly released substances from the sediments to permanently reestablish their pattern. However as this thesis focus on the ocean physics, the interplay within the respective nutrient cycles or biological influences could add on top and thus could finally result in different net nutrient behavior.

Following the tracer in the PCUC until it reaches a comparable calm area south of 18°S, where the PCUC loses stability, get slower and meanders (e.g. Molemaker et al., 2015; Colas et al., 2012; Johnson and McTaggart, 2010), the tracer seems to accumulate and provide a reservoir to fill in eddies. Just at this point in time and space, the majority of the tracer leaves the shelf within the core of ANTs and AMWs consistent with literature (e.g. Frenger et al., 2018; Hormazabal et al., 2013; Johnson and McTaggart, 2010; Combes et al., 2015).

For a quantitative tracer transport by eddies a statistical approach would be ideal. However, this cannot be made from the observations and in the models it is beyond the time frame of this thesis. Thus an estimation based on literature values is given here: The tracer needs some time to reach the eddy generation areas south of 18°S, and need some more time until enough tracer arrived to fill almost every eddy. Regarding the moTREs results (Fig. 3.3) the second year of an experiment seems to be sufficient to be used. Statistically, 228-310 eddies are generated per year (Czeschel et al., 2018; Chaigneau et al., 2011) of which 51% are ANTs, and 25.7% reach the offshore area (Czeschel et al., 2018). The ANTs and AMWs are found to capture tracer, CYCs do not. Thus it can be estimated that there are 116-158 eddies in the second year of the TRE which contain tracer, and about 30-41 which contain tracer and reach the offshore ocean. Let's say an eddy core contain about 0.3 nmol m^{-2} of tracer (Fig. 3.1). The average eddy radius is 50-70 km (Frenger et al., 2018; Chaigneau et al., 2011; Czeschel et al., 2018) giving an average eddy area of about 7.9-15.4·10^9 m^2, and yielding a tracer content in an eddy of about 2.4-4.6 mol. This is 278.4-726.8 mol over all anticyclonic eddies of one year, and 72-189 mol transported into offshore ocean. As a reminder, the observational injected amount is 349 mol. The upper limit of the tracer amount affected by all eddies per year (based on the count of ∼310) exceed the total injection amount and is not applicable. The more recent and lower number of eddies counted by Czeschel et al. (2018) might be more realistic than the previous counts by Chaigneau et al. (2011). This is reasonable when assuming an evolution of the detection algorithms. Using

the values based on the eddy count by Czeschel et al. (2018) the following illustration gives an impression of the eddy effect: Using 228 eddies, i.e. 116 ANTs and AMWs per year, in total about 80% of the injected tracer amount is affected by eddies as captured by them (in the second year of the experiment), but not necessarily transported far offshore. 21-54% of the injected tracer amount gets in the offshore ocean within the core of ANTs and AMWs - the majority of this by AMWs (Frenger et al., 2018), i.e. up to 43%. This is consistent with the tracer portions found west of 80°W to be 20% (moTRE1-ROMS), 36% (moTRE2-CROCO), 18% (moTRE3-NEMO), 32% (moTRE4-NEMO), and 30±10% (POSTRE). And, it is consistent with the connection found by Frenger et al. (2018) that about 30% of the water transported in the PCUC are exported in the offshore areas by AMWs. Thus the entire westward transport is linked to the mesoscale eddy field. More detailed studies to identify and ideally track eddies back to their generation is recommended for the moTREs. This gives a more resilient value of how much tracer an eddy contains, and how many eddies actually capture the tracer in the duration of a TRE.

The tracer transport velocities related to the eddy activity are found to be about 2 cm s^{-1} (moTRE1-ROMS), 5-11 cm s^{-1} (moTRE2-CROCO), 2-5 cm s^{-1} (moTRE3-NEMO), 2-5 cm s^{-1} (moTRE4-NEMO). These agree well with the propagation velocities of the exemplary tracked eddies (A and B in Fig. 3.13) with 4.3 cm s^{-1} and 5.2 cm s^{-1}. Comparing the transport velocities with the eddy propagation velocity of about 3-6 cm s^{-1} identified by Chaigneau and Pizarro (2005), moTRE3-NEMO and moTRE4-NEMO are in the same range but with slightly slower minimal velocities. moTRE1-ROMS is generally slower and moTRE2-CROCO is at least in the maximal velocities much faster. Specifying the tracer content of the Hovmoeller diagrams to address this question further, probably would improve the velocities derived from it.

Linking the offshore tracer transport to real nutrients, there are indications that nutrients leave the shelf region and pass into the offshore ocean like the tracer. A model study by Frenger et al. (2018) and observations by e.g. Gruber et al. (2011); Czeschel et al. (2015); Karstensen et al. (2017); Hauss et al. (2016) already show nutrients to be captured and propagating in the cores of anticyclonic (mode-water) eddies. Especially, for iron an ongoing scientific discussion about its availability in the offshore ocean addresses the possible transport from shelf sediments in the offshore ocean (Conway et al., 2018). Future studies are needed to investigate iron, nitrate, nitrite, nitrogen fixation, phosphate and other nutrient measurements done during the tracer survey and to correlate their pattern to the tracer behavior. On the basis of ocean physics a qualitative connection between tracer and eddies could be proved and is potentially applicable to nutrients.

4 Upward Tracer Motion and the Connectivity from the Bottom Boundary to the Euphotic Zone

Abstract of the Chapter. The vertical tracer behavior revealed to be complex but can give important new insights in the related physical processes. As POSTRE was injected directly in the BBL of the Peruvian shelf, very dynamic features were expected to shape the tracer. However, water and tracer transport in the boundary regimes and especially in the BBL could not be shown before in such an observation. To disentangle the various aspects of the vertical tracer motion it is addressed in depth space, in density space, in θ-S space, and with regard to the density-depth relation of POSTRE. Here the vertical tracer behavior is described, its causes identified, and the governing processes indicated. The tracer is found to rise upward, even high enough to reach the surface waters. This happens mainly diapycnal, i.e. across density surfaces. Partly the upward motion occurs due to changes in the density-depth relation between injection and survey might caused by an El Niño event or short-term natural variabilities. The theoretical concepts by Ferrari et al. (2016) and Holmes et al. (2019) are applicable and provide a sufficient explanation of the tracer behavior. Recalling the tracer meant to represent nutrients, the upward motion is especially important as it shows a pathway into the euphotic surface waters provided by ocean physics. Thus nutrients released from the shelf sediments could potentially be used for primary production in these realms.

4.1 The Observational TRE - POSTRE

4.1.1 Tracer Distribution in Depth Space, and Upward Tracer Motion

The observed vertical tracer distribution over depth, 17 months after injection, (Figs. 4.1 & 4.8a) has an extend of about 350 m. The majority (76.5%) of the nonzero samples is between 50 to 200 m water depth but the existence of tracer shallower than 50 m is conspicuous. There are measurable high tracer concentrations in the upper water column regardless of the outgasing processes which would erase the tracer signal within a few weeks. Thus these signals show tracer brought up recently before the survey.

Interestingly, the tracer could be surveyed overall shallower than injected. Regarding the tracer weighted mean depth, the observed tracer was injected in 250 m but 17 months later found in 114 m depth. Thus the mean tracer depth reduced by 136 m (Tab. 4.1).

The POSTRE data enables only a regional separation between open ocean and coast. A focus on the coastal region in the early stages of the experiments cannot be derived. This is contrary to TREs in enclosed basins where a time dependent separation is common. For instance in the Baltic Sea, the Santa Monica or Santa Cruz Basin the tracer was injected in the interior of a basin. The observations last until the tracer experienced the effects of the boundaries. The time separation between the tracer patch in the basin interior and its spread influenced by the basin walls enables to quantify the two different processes from the same TRE (Holtermann et al., 2012; Ledwell and Hickey, 1995; Ledwell and Bratkovich, 1995, respectively). Based on the experimental setup, POSTRE would experience the influence of enhanced boundary mixing first and would spread throughout the ocean afterwards.

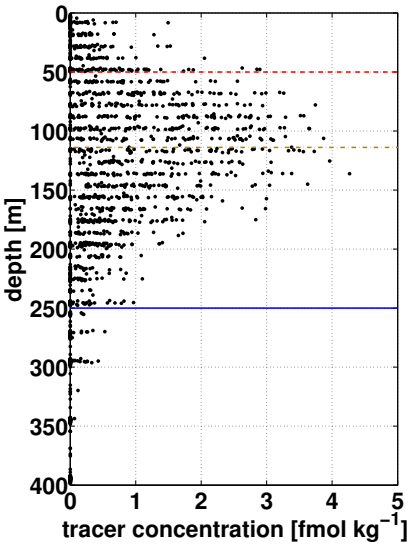

Figure 4.1: Surveyed tracer depth distribution. Injection depth indicated as blue line, the 50 m isobath dashed in red, the tracer weighted mean dash dotted in brown.

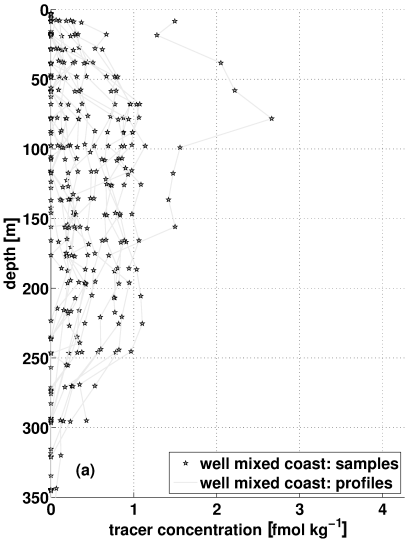

Figure 4.2: Well mixed coastal profiles as indication for enhanced mixing at the shelf.

The shape of some vertical profiles (Fig. 4.2) is typical for tracer behavior related to enhanced mixing processes at ocean boundaries. These are on the shelf at 23 stations located mainly north

of 18°S within about one degree longitude from the coast and coastward of the 2000 m isobath. They show equally high tracer concentrations throughout the water column and are comparable to the late stages of the Baltic Sea TRE (Holtermann et al., 2012).

4.1.2 Isopycnal Heave from Injection to Survey, El Niño Influence, and the Stratification Conditions of POSTRE

A straight forward explanation of the shoaling is caused by changing density-depth relations from injection to survey and a resulting heave of isopycnals. Therefore the hydrographic conditions of POSTRE's injection (in October) and survey (in March) are investigated in comparison to the climatology MIMOC (Monthly, Isopycnal/Mixed-layer Ocean Climatology - Schmidtko et al., 2013). The isopycnal heave is indicated as there seems to be a slight seasonal cycle in the density-depth distribution. For instance, the 26.3-isopycnal (as the tracer-weighted mean injection density) is in October a few deca-meter deeper than in March at several spots (Fig 4.3).

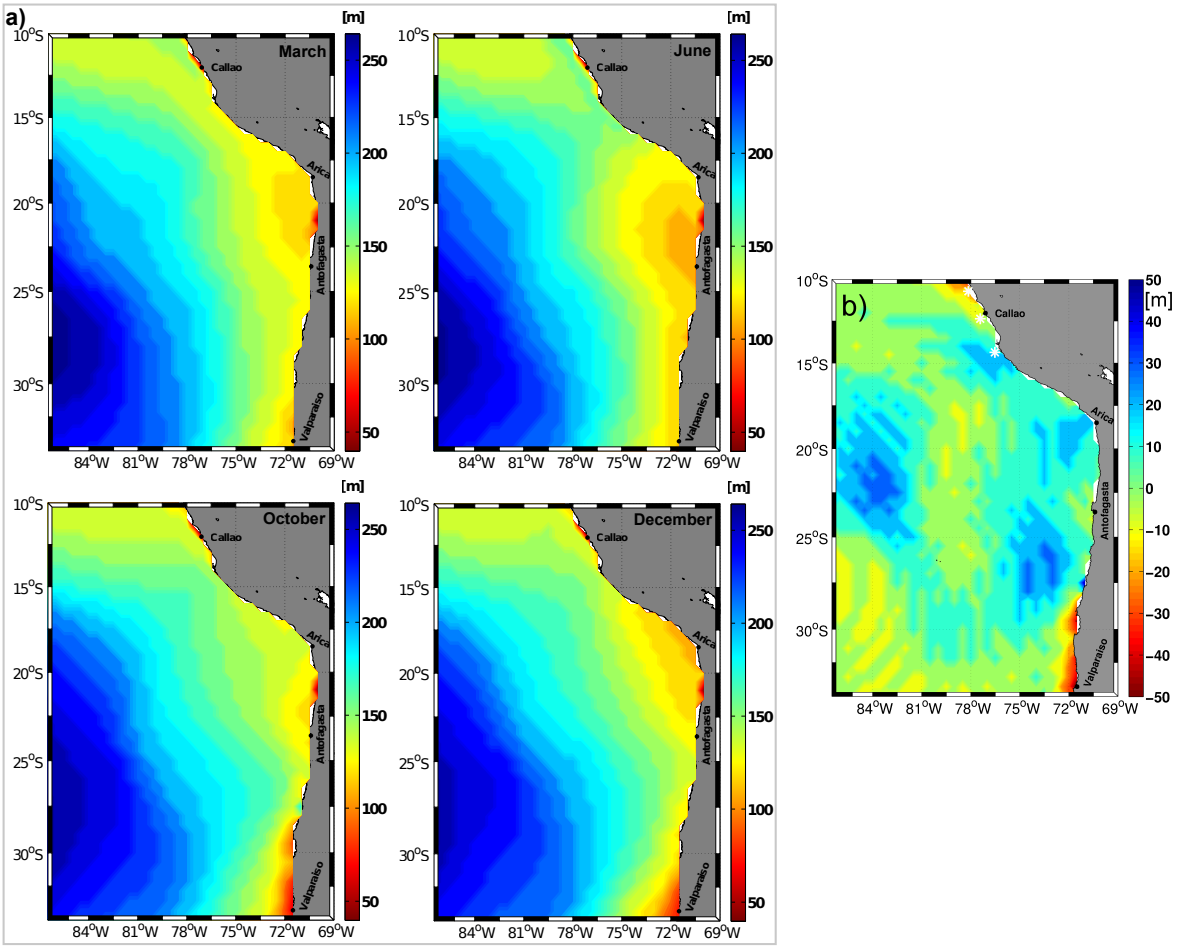

Figure 4.3: (a) The depth of 26.3-isopycnal in March, June, October, December. And (b) the depth difference of 26.3-isopycnal depth between October and March.

For March, when the tracer survey was conducted the observations and the climatology are

remarkably consistent, despite the appearance of an observed coastal El Niño which naturally is not dominant in the climatology. The depth of the tracer weighted mean survey density of 26.17 kg m^{-3} (in March - Fig 4.4b) appears mostly in a range of about 100-140 m. Although around the area of the injection sites, the observed density lays remarkable deeper than in the climatology.

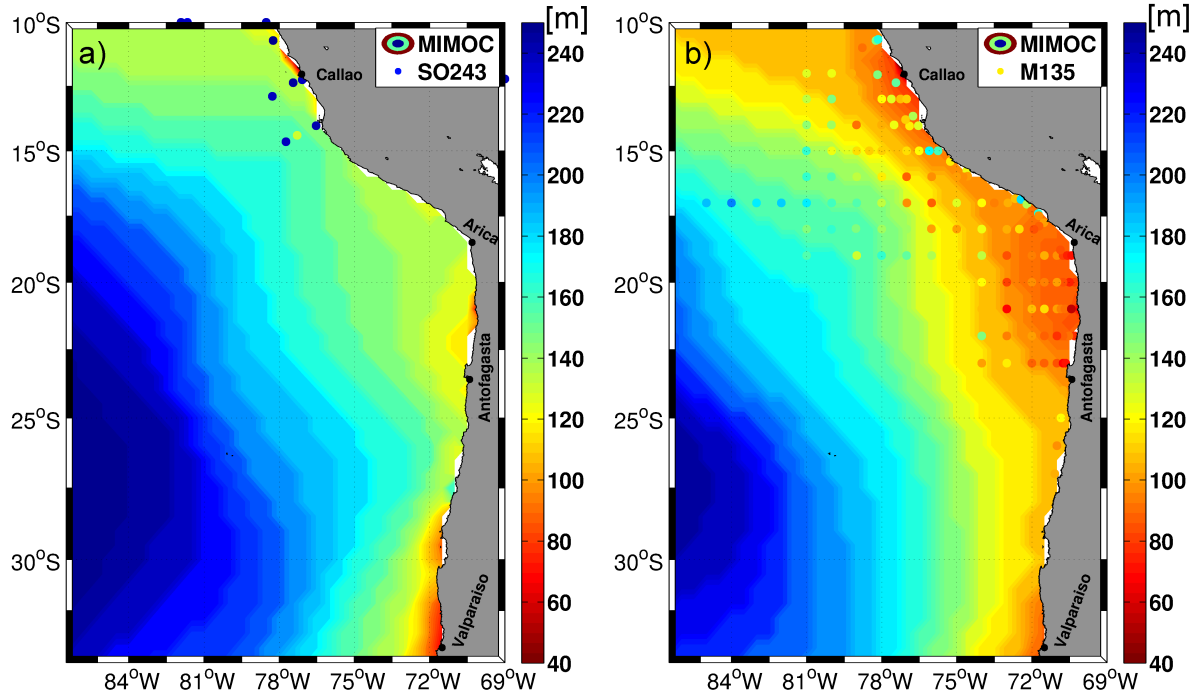

Figure 4.4: Comparing the observed and climatological (a) depth of 26.3-isopycnal in October and (b) the depth of the 26.17-isopycnal in March. The shades in the maps are derived from the MIMOC climatology (Schmidtko et al., 2013); the overlaid dots are the observed properties of the injection and survey cruises labeled with SO243 and M135, respectively.

In general and as to expect for an eastern boundary upwelling region, the (MIMOC) isopycnals get shallower towards the coast. In terms of tracer distribution this means, tracer propagating offshore along the isopycnals would descen in an order of 50 m, depending on latitude and covered distance into the offshore ocean. As this contradicts the observed upward motion, it cannot be the only factor to play a role.

Regarding the spatial density-depth relation under which POSTRE was injected, the observation is very different to MIMOC. The climatological depth of the tracer-weighted mean injection density of 26.3 kg m^{-3} (Fig 4.4a) in the area of the injection sites is at about 150 m depth or even shallower. Contrary, in the observations during the tracer injection cruise this isopycnal was measured in 250 m water depth. The climatological density at 250 m water depth of this area is 26.348±0.003 kg m^{-3} in March and October. Thus the POSTRE tracer was injected in waters lighter than expected from the climatology, i.e. in waters normally much shallower than measured during the injection cruise. Namely, it was expected to inject the tracer in the dense waters representative for bottom water on the continental shelf, but the tracer end up in

observational conditions different from climatology.

The difference between the unusual density-depth conditions of the observations and MIMOC could have a number of causes. On short-term there are to name: local wind stress curl variabilitiy (e.g. McCreary and Chao, 1985; Klenz et al., 2018), isopycnal displacements by along shore flow variabilities, or coastal trapped waves (e.g. Lüdke et al., 2019; Brink, 1982). On long-term the emergence of the El Niño event 2015/16 (during the injection cruise, Stramma et al., 2016) is a most likely explanation. The large scale isopycnal depth distribution of MIMOC should reflect the ocean adjustment to the large scale wind stress curl forcing (e.g. Albert et al., 2010), but MIMOC does not reflect intraseasonal variability. For the future, this is a point of interest to investigate. Variabilities in the magnitude of the PCUC are often linked to the passing of coastal trapped waves (e.g. Chaigneau et al., 2013; Pizarro et al., 2002, and references therein) which in turn appear more often during El Niños. Thus despite more detailed investigations of the effect by these variabilities are recommended, the El Niño and "its side effects" seems to provide a first order explanation. Especially, as El Niño comes along with additional on long-lasing changes: Due to El Niño conditions much more warm water fills the upper water column. Thus the isopycnals get pressed down. In depth the water is lighter than under normal conditions, since the light isopycnals are placed deeper. When the conditions return back to normal, the isopycnals rise due to the shrinking warm water reservoir on top of them. Cold and heavy water fills in from below. Thus based on the El Niño relaxation, an isopycnal heave on long time scales appears.

It is beyond the time frame of this thesis to conclusively settle the reasons for the density-depth conditions measured in the ETSP in October 2015. However, it can be summarized: The isopycnal heave could account for a local displacement of tracer-tagged water of up to $\sim$100 m in the vertical, according to the MIMOC climatology. This cannot account for the entire vertical distance covered by the tracer. A long lasting process contradicts the presence of tracer in surface waters during the survey as outgasing would have erased the tracer signal. That indicates a rather fast process for the upward tracer motion. The displacement of isopycnals does not change the density of the tracer-tagged water. Thus investigations of the tracer distribution in density space follow, to get insight if there is at least additionally a diapycnal process acting.

4.1.3 Tracer Distribution in Density Space, and Lightening of Tracer-Tagged Water

To investigate a diapycnal nature of the upward motion the tracer distribution in density space is referred (Figs. 4.5 & 4.10a). The tracer is distributed between 24.5-26.5 kg m^{-3} with one clear tracer peak at 26.17 kg m^{-3}.

Comparing the tracer weighted mean densities from injection and survey, it displays an overall lightening of tracer-tagged water to govern the upward tracer motion. The tracer-weighted mean survey density of 26.17 kg m^{-3} shifted 0.13 kg m^{-3} toward less dense waters compared to the injection tracer weighted mean potential density of 26.30 kg m^{-3} (Tab. 4.1).

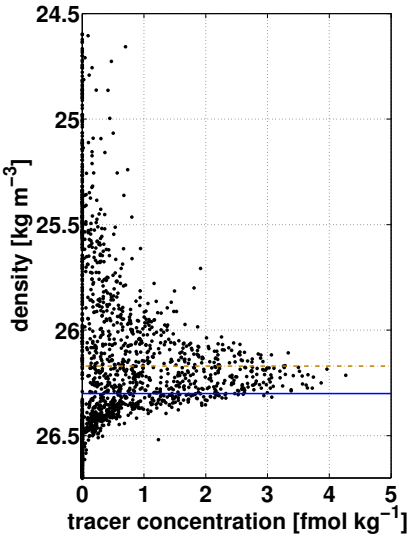

Figure 4.5: Surveyed tracer density distribution. Injection depth indicated as blue line, the tracer weighted mean dash dotted in brown.

4.1.4 Tracer Distribution in Temperature - Salinity Space, and Property Changes of the Lightening Tracer-Tagged Water

The water properties are investigated to understand how the diapycnal mixing acts. The tracer was surveyed in waters with a potential density between 26.51 and 25.46 kg m^{-3}, potential temperatures from 10.9 to 17.2°C and a salinity of 34.5 to 35.2. The oxygen values are between 0 and 197.5 μmol kg^{-1}, covering the whole range from anoxic to well oxygenated. The highest tracer concentrations coincide with potential densities of 26.03 to 26.32 kg m^{-3}, potential temperatures between about 12.9 and 14.3°C, a salinity of 34.8 to 35.0 and oxygen concentrations between 0 and 47.5 μmol kg^{-1} (Figs. 4.6, 4.7, 4.11 a&b). The surveyed tracer weighted means of these properties are a potential density of 26.17 kg m^{-3}, a potential temperature of 13.5°C, a salinity of 34.85 and an oxygen concentration of 15.6 μmol kg^{-1}.

Comparing the tracer-tagged water properties between injection and survey (Figs. 4.6, 4.7, 4.11 a&b, Tab. 4.1), there is a mean salinity reduction of 0.10 psu (from 34.95 at the injection to 34.85 during the survey), freshening the tracer-tagged water. Additional, the tracer spread into warmer and colder waters, showing just a slight mean warming of 0.28°C from injection (13.25°C) to survey (13.53°C). The mean potential density decrease is 0.13 kg m^{-3} from injection (26.3 kg m^{-3}) to survey (26.17 kg m^{-3}). With the comparison of the mean values but more important with regard to the tracer distribution over temperature and salinity, the salinity

decrease seems to dominate the reduction of density. Thus it appears that (1) a diapycnal effect took place, which made the tracer-tagged water lighter. (2) Although the temperature increase reduces the density, the lightening does not seem to be essentially driven by heating.

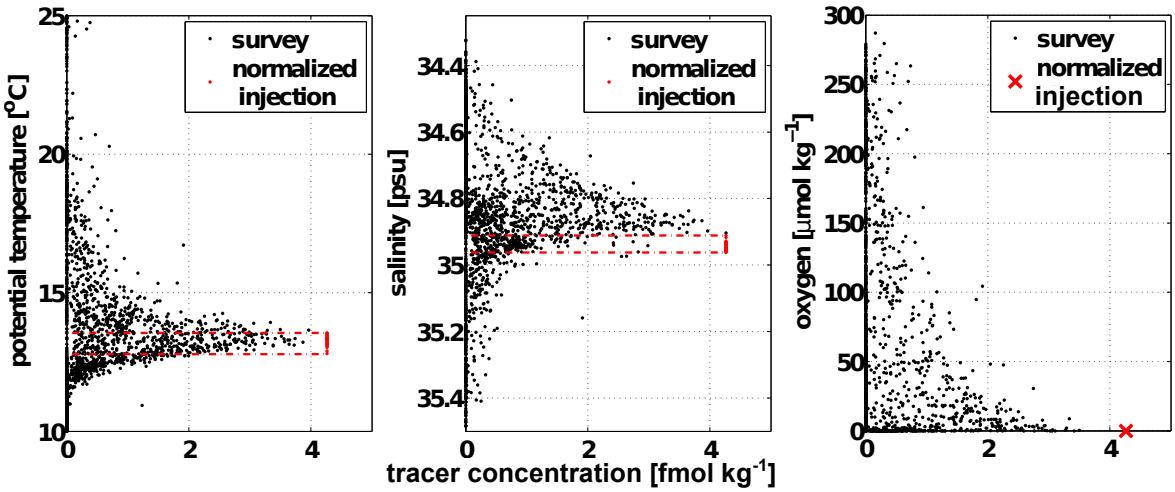

Figure 4.6: Properties (potential temperature, salinity, and oxygen) of POSTRE tracer-tagged water.

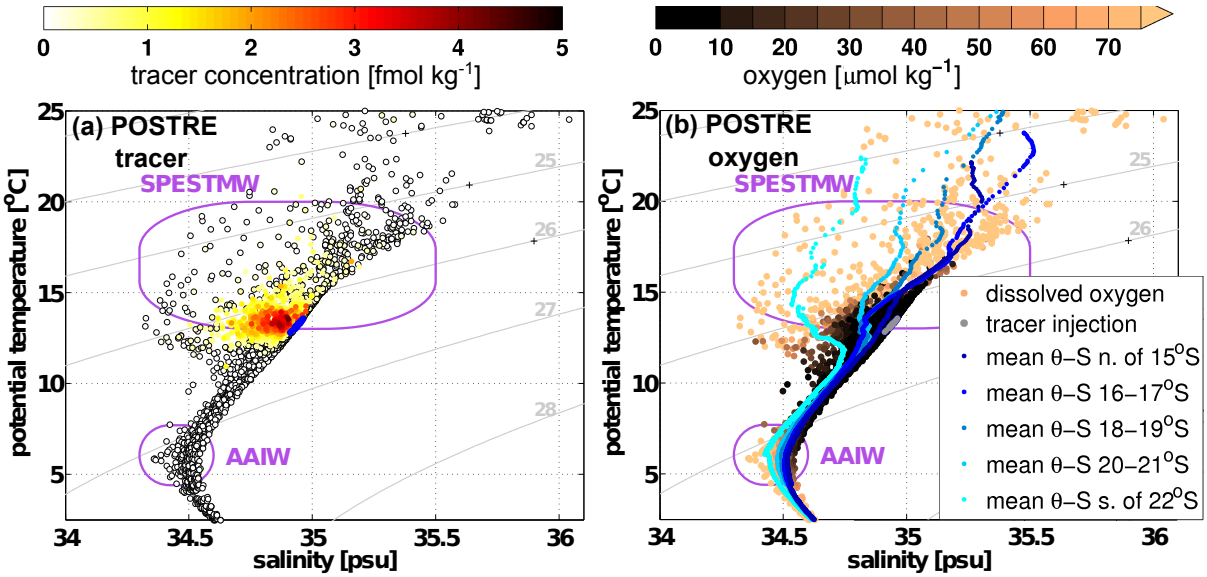

Figure 4.7: θ-S relation of (a) the surveyed tracer samples color coded by concentration and injection in blue; and of (b) the related oxygen content. Isopycnals in gray.
The bluish lines in (b) show the mean θ-S profiles averaged over five regions within the study area: (1) from the southernmost station up to including 22°S, (2) over 20°S to 21°S, (3) over 19°S to 18°S, (4) over 16°S to 17°S, and (5) from including 15°S to the northernmost station.

To understand the tracer spread through waters with these various properties it is worth to look into the water masses involved (Figs. 4.7, 4.11 a&b). First, the Antarctic Intermediate Water (AAIW) can be clearly identified as water masses below 500 m depth (e.g. Fiedler and Talley, 2006) and is of course free of tracer. The warmest and saltiest but lightest samples are related

to Subtropical (Surface) Water (e.g. Fiedler and Talley, 2006; Silva et al., 2009).

Second, intermediate waters appear to be most important for the tracer behavior and cover a wide range in the θ-S diagram. These are the South Pacific Eastern Sub-Tropical Mode Water (SPESTMW), ESSW (the Equatorial Subsurface Water), and decomposing Eastern South Pacific Intermediate Water (ESPIW). SPESTMW is a vertically near homogenous water without major signatures, known to be roughly located between 25.0 and 26.2 kg m^{-3}. Its generation occurs in the northern part of the subtropical gyre due to evaporation. The propagation is southward (Fiedler and Talley, 2006, and references therein).

ESSW was already introduced to be salty, oxygen depleted (Silva et al., 2009) and transported southward with the PCUC. When focusing on averaged θ-S relations in comparison to the concentration of dissolved oxygen related to the tracer samples (Figs. 4.7b & 4.11b), especially in the southernmost mean a subsurface salinity maximum is obvious. It can be found less pronounced for the means from 16°S to 21°S but disappears for the northernmost mean. The peak is located at a potential density of about 26.4 kg m^{-3} but covering also partly the density range of the tracer injection.

The decomposing ESPIW is the tracer-tagged mixture of ESSW and a mass characterized by a subsurface salinity minimum toward lighter water originating from ESPIW. ESPIW is generated in the southernmost parts of the Eastern South Pacific, subducted at 32.5°S and spreading north- and westward between the Subtropical (Surface) Water and ESSW. It appears at about 150-250 m water depth but deepening and thinning its vertical extend along its pathway. In its core region off central and northern Chile ESPIW is featured by its absolute salinity minimum of 34.2±0.08 and a temperature of 12.1±1.3°C (at 33.00°S and 73.53°W). ESPIW follows the isopycnal of 25.95±0.258 kg m^{-3}, whereas isopycnal mixing increases its salinity. North of 20°S only a relative salinity minimum (amplified by the ESSW salinity maximum) remains characteristic and between about 10-17°S the ESPIW signal disappears completely (Schneider et al., 2003).

Note the property changes from north to south of the study area, visualized by the mean θ-S relations. SPESTMW seem to contain a large amount of the tracer. Smaller portions are aligned to ESSW and decomposing ESPIW. As expected from the experimental setup the tracer was released in the PCUC characterized by (a mixture based on) ESSW and thus still can be found in this water during the survey. It is known that the ESSW in the PCUC get mixed more and more along the current pathway (e.g. Silva et al., 2009). Thus it is reasonable to assume that the tracer is mixed out of this water and out of the undercurrent on the way southward. The tracer ends up in the SPESTMW, and in the southern parts of the study region also in decomposed ESPIW.

4.2 The moTREs in Comparison to POSTRE

To compare the moTREs to POSTRE the graphics of the moTREs in this chapter are shown subsampled at the stations of the observation. However, the values stating results from the moTREs are naturally calculated by containing all relevant tracer of the moTREs, but not the surface tracer removed as bulk outgasing. This surface tracer amount is regarded separately. To give an impression about the entire tracer distribution in the moTREs there are appropriate graphics in appendix A. They highlight a lot of potential for further investigations of the tracer in the moTREs but this is beyond the time frame of this thesis.

4.2.1 Tracer Distribution in Depth Space, and Upward Tracer Motion

The modeled vertical tracer distribution over depth 17 months after injection is shown in Fig. 4.8b-e. The ROMS/CROCO tracers (moTRE1 and moTRE2) are in the upper 400 m with only small concentrations below. However, these two moTREs push so much tracer to the surface, that no subsurface tracer maximum remains, which contradicts the observation. Especially, in moTRE1-ROMS the majority of tracer is in the surface. In moTRE2-CROCO the tracer distribution seems to be unrealistic affected by the coordinate system. This should be addressed in the future. The NEMO tracers (moTRE3 and moTRE4) reach much deeper than the observation, down to about 800 m depth. This requires a large downward mixing. Subsurface maxima can be identified at about 228 m (moTRE3) and 270 m (moTRE4).

It is an important point to note that the vertical tracer behavior does not seem to interfere the advective mechanisms which govern the lateral distribution, or rather from the lateral distribution no conclusion can be made how the tracer behaves in the vertical. The vertical tracer behavior (in depth) is so different that none of the moTREs' vertical distributions is really comparable to the observation. This is unexpected as the lateral tracer distributions appear very similar for all moTREs and POSTRE (cp. Fig. 3.1).

Regarding the modeled tracer weighted mean depth over time, the tracer gets shallower right from the beginning of each experiment. An upward motion occur about within the first three months. Afterwards the tracer weighted mean depth stays in a certain level for each of the moTREs (Fig. 4.9) at about: 130-135 m for moTRE1-ROMS, 140-160 m for moTRE2-CROCO, 170-180 m for moTRE3-NEMO, and 200-220 m for moTRE4-NEMO. Thus all model results are deeper than the observation with its 114 m. 17 months after the injection the mean tracer depth reduced by 80.2 m (moTRE1-ROMS), 99.7 m (moTRE2-CROCO), 89.9 m (moTRE3-NEMO), and 121.9 m (moTRE4-NEMO) to 134.1 m (moTRE1-ROMS), 160.3 m (moTRE2-CROCO), 210.1 m (moTRE3-NEMO), 178.1 m (moTRE4-NEMO) (Tab. 4.1).

Considering the modeled tracer amount in the upper 50 m it quantifies the tracer portion entering into surface layers. This is (1) as a measure of how much tracer is brought upward so far toward the surface; and (2) a bulk tracer portion representative for the tracer loss if outgasing would appear. For a judge-able outgasing estimate that is comparable to the observations, the

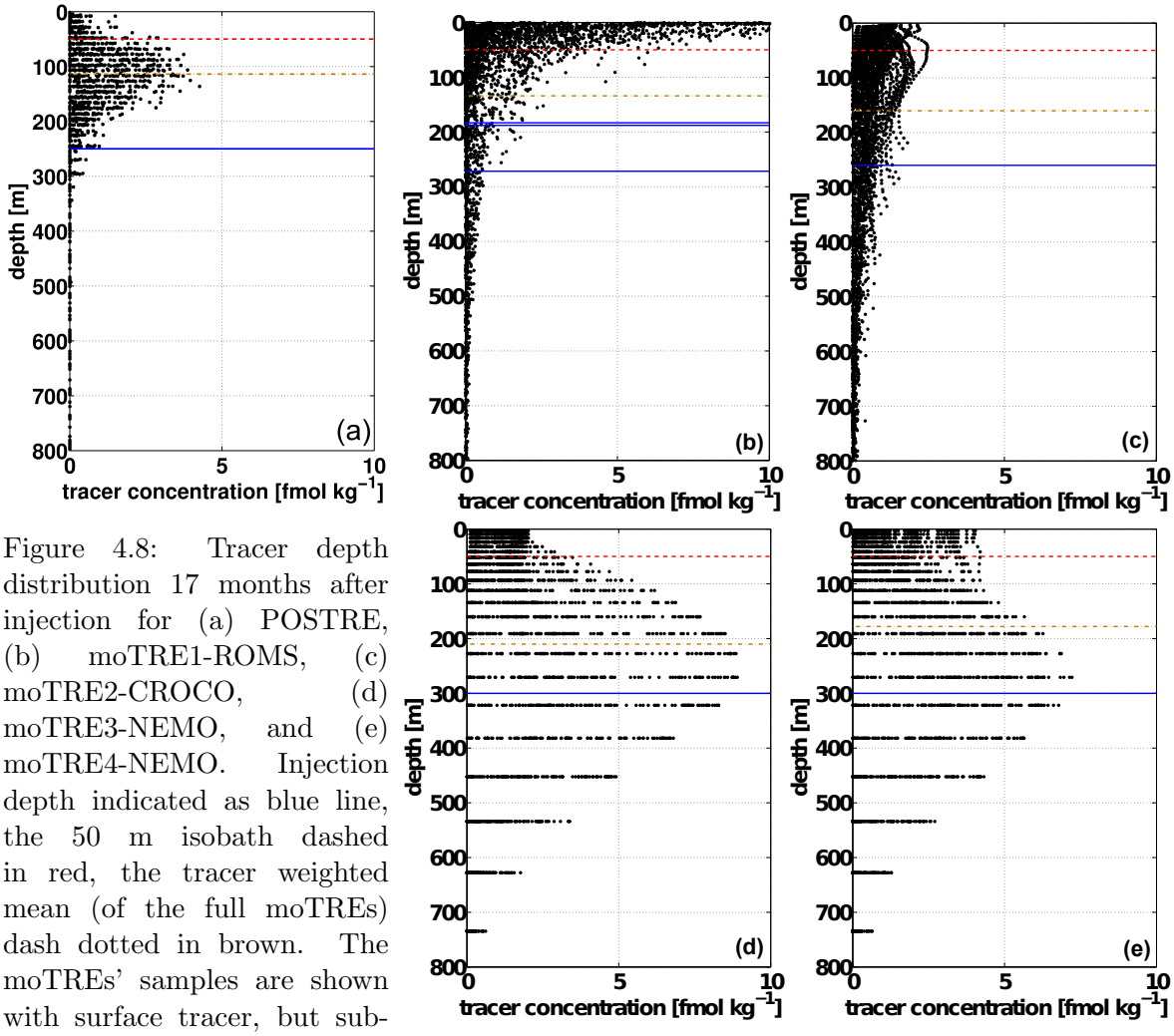

Figure 4.8: Tracer depth distribution 17 months after injection for (a) POSTRE, (b) moTRE1-ROMS, (c) moTRE2-CROCO, (d) moTRE3-NEMO, and (e) moTRE4-NEMO. Injection depth indicated as blue line, the 50 m isobath dashed in red, the tracer weighted mean (of the full moTREs) dash dotted in brown. The moTREs' samples are shown with surface tracer, but subsampled at the stations of the observation.

moTREs were subsampled 17 months after the injection at the survey stations and interpolated in the same way as POSTRE (Fig. 3.2).

The bulk outgasing as tracer portion within the upper 50 m for each of the subsampled moTREs is 47% (moTRE1-ROMS), 9% (moTRE2-CROCO), 16% (moTRE3-NEMO), and 15% (moTRE4-NEMO). moTRE1 is eye-catching high and probably not realistic with its strongly surface intensified tracer depth distribution incomparable to POSTRE (Fig. 4.8). As there is no observational value to compare, the process of elimination is applied for an estimate. The observational tracer inventory contains 40±10% of the tracer. Extrapolating the observed tracer beyond the survey grid, it is indicated that about 30±10% of the tracer got lost this way. The remaining tracer portion of another about 30% has to account for the amount which has gassed out. A possible tracer loss between the stations is assumed to affect the subsampled moTREs in the same way as the observations, and thus is neglected here. With that, a comparison to POSTRE show the moTREs (except moTRE1) to underestimate the tracer portion to be brought in the mixed layer, and thus possibly underestimate the efficiency of the upward tracer motion as well as the

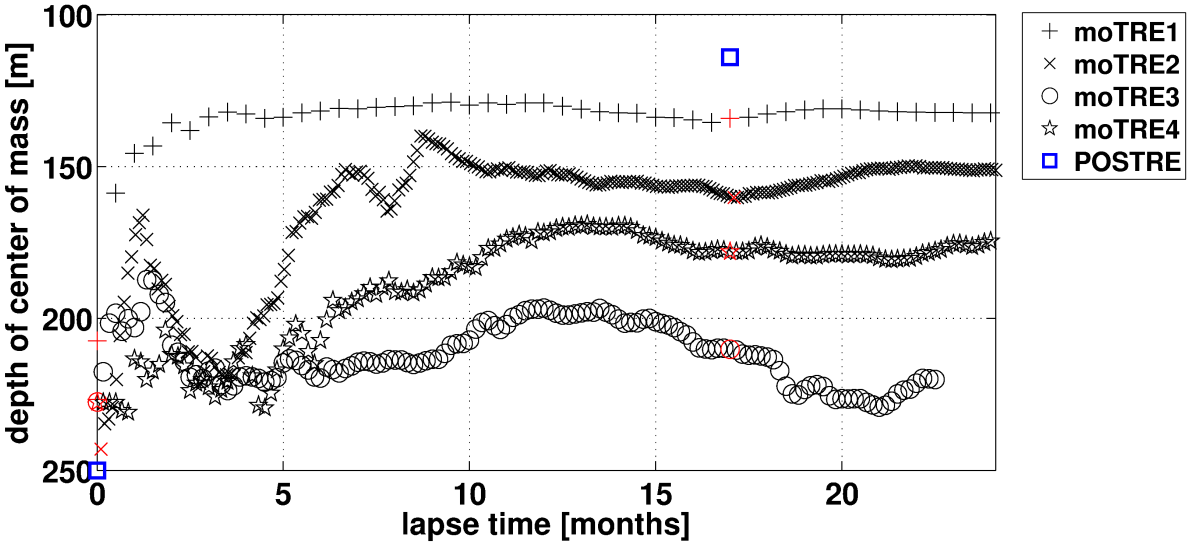

Figure 4.9: Tracer weighted mean depth over time.

tracer loss via outgasing.

Keeping in mind that the uncertainty of these bulk outgasing values is still at least ±10%, the bulk outgasing of the subsampled moTRE2, moTRE3, and moTRE4 suggest that outgasing is a significant but not the most important process in these experiments and smaller than expected from a single moTRE over the whole of each model domains (not shown) or from the observational data only. The best estimate of bulk outgasing that can be made within the scope of this thesis is 10-30±10%.

4.2.2 Tracer Distribution in Density Space, and Lightening of Tracer-Tagged Water

To investigate a diapycnal nature of the upward motion the tracer distribution in density space is analysed (Fig. 4.10). These distributions 17 months after injection are very different for POSTRE and the moTREs. The moTREs cover a much broader density range of 24.0-27.5 kg m^{-3} for the ROMS/CROCO experiments, and of 23.5-31.5 for the NEMO experiments. In the subsampled moTREs a peak can be identified but in the full resolution moTREs (appendix A) their overall peak is less clear. In detail, latitudinal dependent multiple peaks and ranges of high tracer content can be identified for the full moTREs. It would be interesting to go into the details of it, but without improved moTREs as indicated at several points of this thesis and without a possibility to compare the latitudinal different features of the full moTREs to observations, the value of such results cannot be captured at this moment. This is a project for future studies.

Comparing the tracer weighted mean densities from injection and survey (Tab. 4.1), it displays an overall lightening of tracer-tagged water to govern the upward tracer motion. The overall density shift in the moTREs is 0.54 kg m^{-3} (moTRE1-ROMS), 0.49 kg m^{-3} (moTRE2-CROCO),

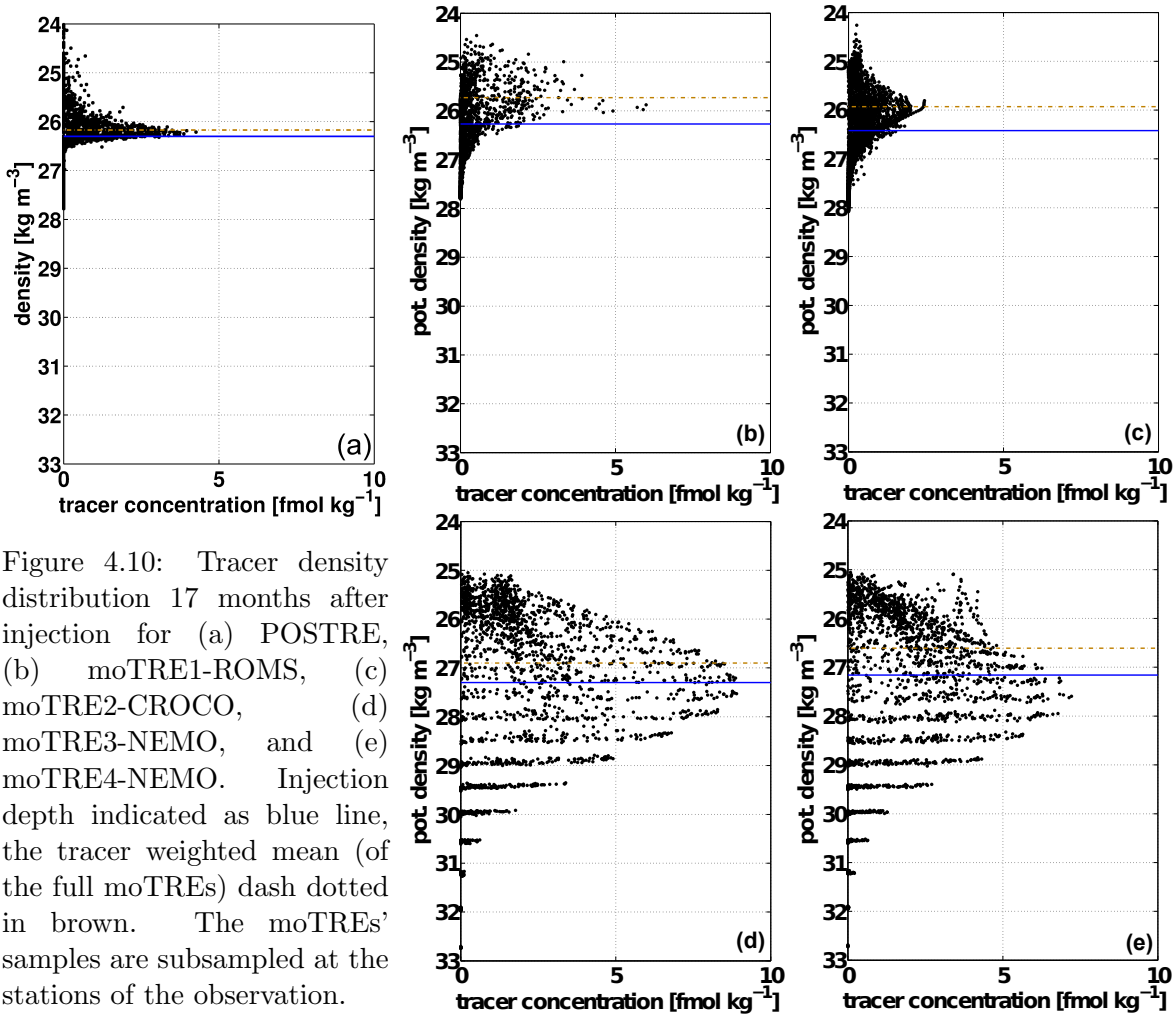

Figure 4.10: Tracer density distribution 17 months after injection for (a) POSTRE, (b) moTRE1-ROMS, (c) moTRE2-CROCO, (d) moTRE3-NEMO, and (e) moTRE4-NEMO. Injection depth indicated as blue line, the tracer weighted mean (of the full moTREs) dash dotted in brown. The moTREs' samples are subsampled at the stations of the observation.

0.40 kg m^{-3} (moTRE3-NEMO), 0.55 kg m^{-3} (moTRE4-NEMO). This is an even stronger lightening than in the observations.

Relating the tracer weighted means to the actual tracer-density distributions, the ROMS/CROCO TREs the overall tracer and the peak lighten clearly. For the NEMO TREs the tracer mainly spread around the injection density or even drop into slightly denser waters. The latitudinal dependencies show a more complex picture. As in the full moTREs (appendix A) the peak representing the northern part of the survey region lightens, whereas the peaks representing the southern and mid part keep the same density than the injection or get heavier.

4.2.3 Tracer Distribution in Temperature - Salinity Space, and Property Changes of the Lightening Tracer-Tagged Water

The tracer-tagged water properties are investigated to understand the diapycnal mixing in the moTREs. High concentrations of the model tracers spread much wider in θ-S-space (Fig. 4.11 c-f) compared to POSTRE. Comparing the subsampled to the full moTREs, this is not due to much more samples available but there are remarkable expansions of the tracer pattern. In contrast to the observation, all moTREs show high tracer concentrations in waters warmer than

18°C (and lighter than 25 kg m^{-3}), as well as waters colder than 11°C (more pronounced in the NEMO TREs as in the ROMS/CROCO TREs). The spread in salinity cover fresher and saltier waters. Especially, the tracer-tagged warm waters show high salinity, whereas the tracers (at strongest in NEMO) seems to spread along the isopycnals between 25-26 kg m^{-3} while getting much saltier. The tracer-tagged cold waters show low salinity. The overall tracer concentration of the NEMO TREs again largely exceeds these of the ROMS/CROCO TREs and POSTRE.

The tracer weighted mean temperature and salinity values 17 months after the injection (Tab. 4.1) are 15.44°C and 34.89 psu (moTRE1-ROMS), 14.13°C and 34.83 psu (moTRE2-CROCO), 15.24°C and 35.14 psu (moTRE3-NEMO), 16.50°C and 35.34 psu (moTRE4-NEMO).

Comparing the tracer-tagged water properties after 17 months to the injection (Tab. 4.1), their changes in the moTREs are very different to POSTRE. The temperature show a remarkable warming with increases by 2.12°C (moTRE1-ROMS), 2.18°C (moTRE2-CROCO), 1.55°C (moTRE3-NEMO), 1.73°C (moTRE4-NEMO). The salinity reduces only slightly for the ROMS/CROCO TREs by 0.04 psu (moTRE1) and 0.01 psu (moTRE2). For the NEMO TREs the tracer-tagged water got saltier by 0.10 psu (moTRE3) and 0.17 psu (moTRE4).

In the moTREs the tracer weighted mean density shift is mainly due to warming, strong enough to even compensate a salting in the NEMO TREs, indicating a different process for the lightening of the tracer-tagged water. The strong warming and the salinity increase contrast the observations. The salinity decrease in the ROMS/CROCO TREs is very small and is hardly responsible for the lightening. For the NEMO TREs the salinity change is strong enough to suggest a diapycnal mixing process involved but a salinity increase also cannot account for the lightening of tracer-tagged water. Rather the warming appears as the determining factor for this. Thus the question arose if and how the upward tracer motion of moTREs is represented realistic and related to diapycnal mixing in the BBL of the shelf region as to expect for POSTRE from theory (Ferrari et al., 2016; McDougall and Ferrari, 2017; Holmes et al., 2019, and references therein - section 4.2.4).

Regarding the water masses in the models 17 months after injection, a good portion of the tracer is in the property range of SPESTMW for all moTREs, similar to POSTRE. All moTREs show an unrealistic mixing into deeper waters with NEMO tracers getting into the AAIW, contrary to the observations. Regional means (not shown) denote no clear salinity peaks or dips, and oxygen cannot be regarded as it was not implemented in the models. Thus no clear connection to ESSW and ESPIW is possible. Although the modeled tracer shown in Fig 4.11 appears below 50 m water depth, the high tracer concentrations indicate an unreasonable high tracer amount in surface waters, probably the Subtropical (Surface) Water, strongest in moTRE4-NEMO.

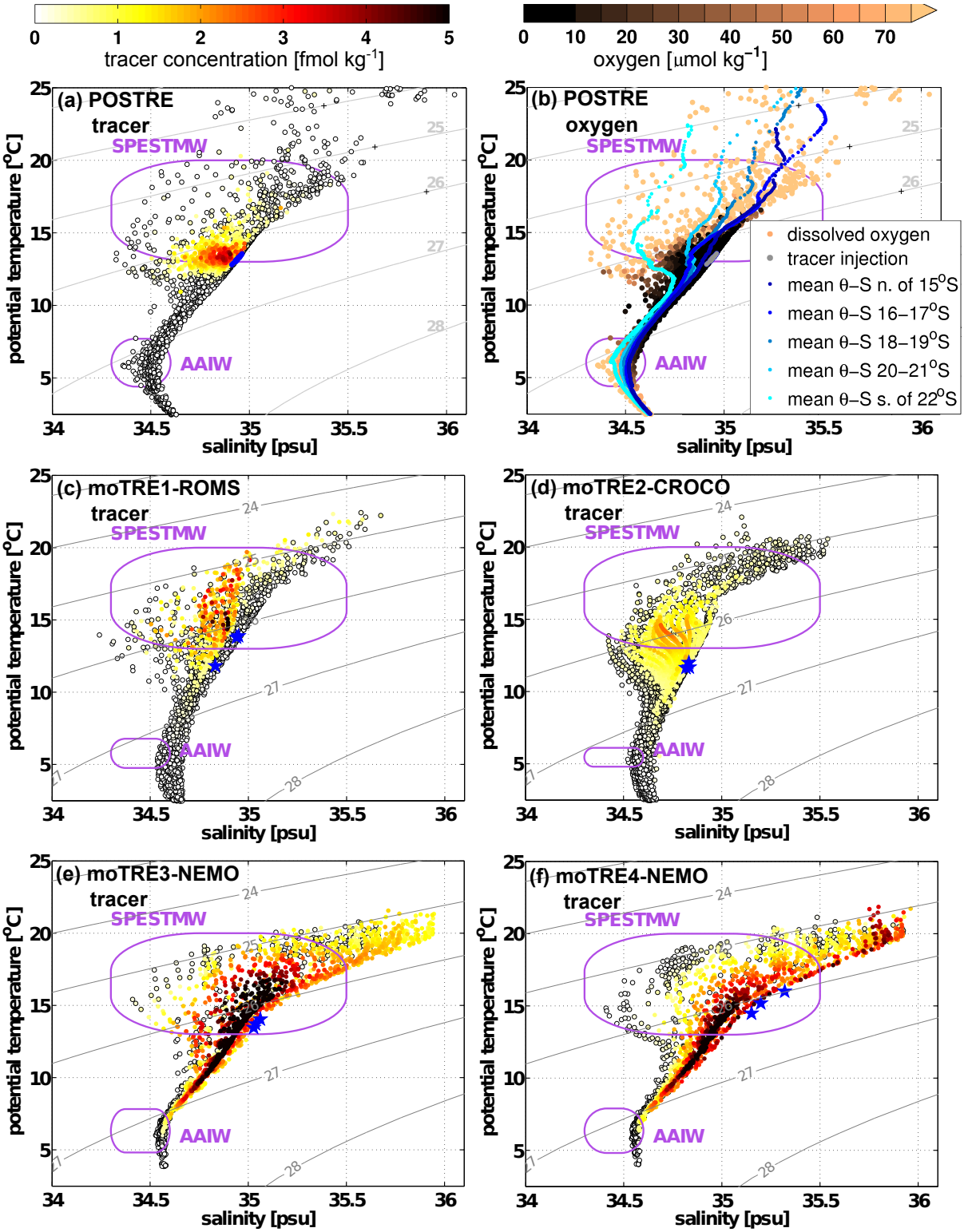

Figure 4.11: θ-S relation of POSTRE (a & b) as in Fig. 4.7. θ-S relation of the tracer concentration after 17 months for (c) moTRE1-ROMS, (d) moTRE2-CROCO, (e) moTRE3-NEMO, (f) moTRE4-NEMO; subsampled on the observational stations. The injection is shown in blue. Isopycnals in gray.

4.2.4 moTREs' Focus on the Coastal Region and the Early Stages of the Experiments

The theoretical tracer behavior with shelf related diapycnal mixing and BBL related dynamics (e.g. Ferrari et al., 2016) is indicated for POSTRE. Using the moTREs to focus on the coastal region and the early stages of the experiments, the ROMS/CROCO TREs show the tracer "crawling up" the shelf along the continental slope (Fig. 4.12). This is similar to Holmes et al. (2019) for the near boundary point injection as both show the tracer-tagged water lighten and the centroid gets shallower. Although, the ROMS/CROCO tracer particles do not react on diffusion, the BBL related dynamics as some kind of diapycnal advection are implemented. This most likely explains the better performance of ROMS/CROCO on the lightening of tracer-tagged water. As NEMO represents the tracer as a dissolved quantity, the tracer got affected by diffusion. However, probably due to the resolution (spatial comparable coarse on the shelf and temporal averaged on 5 days) the BBL dynamics are not represented and the effect of diffusion only cannot reproduce the POSTRE tracer behavior in lightening of tracer-tagged water. Thus the theory by Ferrari et al. (2016) seems to sufficiently explain the observed behavior.

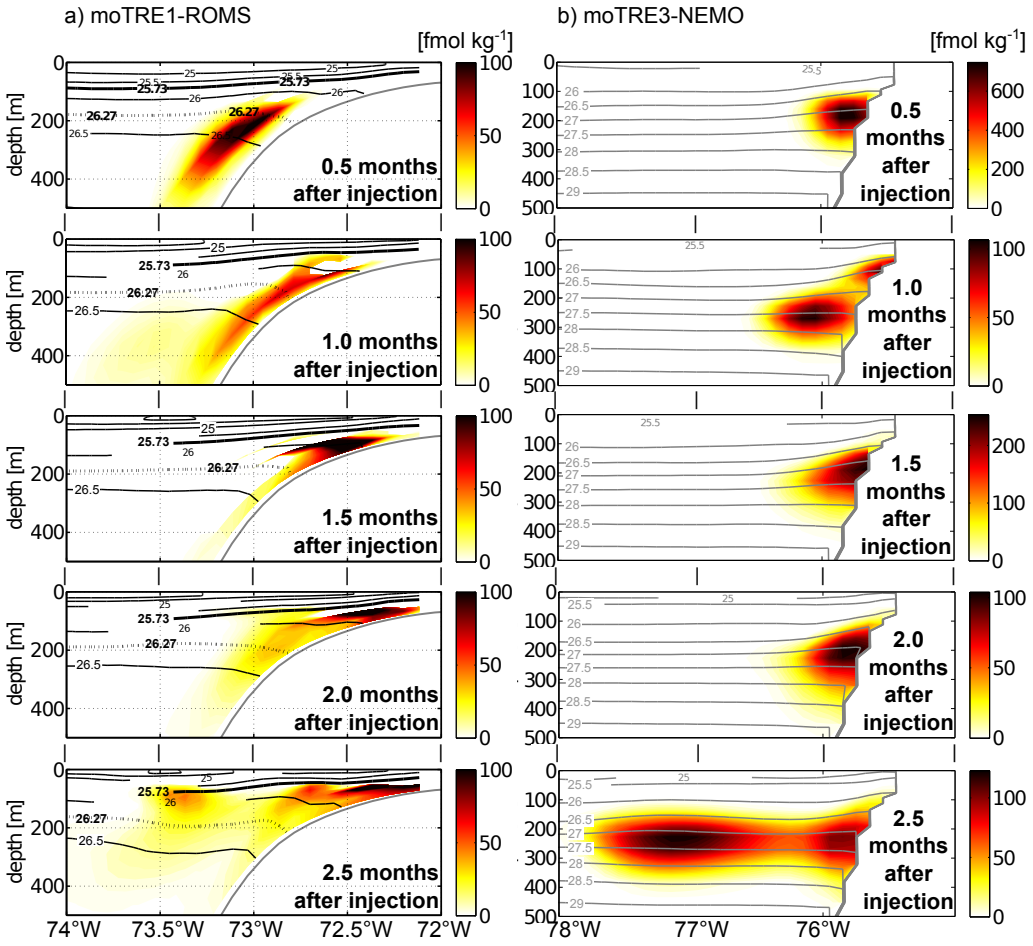

Figure 4.12: Tracer at the shelf in the early stages of the experiment, exemplary for (a) moTRE1-ROMS at 17°S and (b) moTRE3-NEMO at 15°S, i.e. in both cases about 1-1.5° of latitude south of the southern most injection site.

4.3 Summary and Discussion

An upward tracer motion is found. It partly seems to be caused by regionally changing density-depth relations between injection and survey. The development of a strong El Niño event during the injection cruise (Stramma et al., 2016) could be an explanation for that but also coastal trapped waves or other variabilities might account for it. Though, the change in density-depth relation cannot account for all of the upward motion. Namely, the local rise of isopycnals by up to 100 m is compensated by the descenting of tracer-tagged water of about 50 m when it propagats offshore along an isopycnal. The related net upward motion is not even half of the observed mean shoaling of 136 m and is only a small contribution to get the tracer from the sea floor in 250 m water depth to the sea surface. Additional, there is a clear lightening of tracer-tagged water pointing on a diapycnal process related to the upward motion. Thus the isopycnal displacements strengthen the upward transport but basically do not cause it.

Table 4.1: Tracer weighted mean values of depth, density, salinity and temperature compared between injection and 17 months after and the differences in these properties.

	depth [m]	density [kg m^{-3}]	salinity [psu]	temperature [°C]
POSTRE (observed) injection	250.0	26.30±0.03	34.95±0.05	13.25±0.53
POSTRE after 17 months	114.0	26.17±0.34	34.85±0.18	13.53±1.17
difference for POSTRE	-136.0	-0.13	-0.10	+0.28
moTRE1-ROMS injection	214.3	26.27±0.14	34.92±0.05	13.32±0.88
moTRE1 after 17 months	134.1	25.73±0.60	34.88±0.28	15.44±3.45
difference for moTRE1	- 80.2	-0.54	-0.04	+2.12
moTRE2-CROCO injection	260.0	26.42±0.15	34.84±0.04	11.95±0.98
moTRE2 after 17 months	160.3	25.93±0.63	34.83±0.30	14.13±3.70
difference for moTRE2	- 99.7	-0.49	-0.01	+2.18
moTRE3-NEMO injection	300.0	27.30±0.02	35.04±0.01	13.69±0.13
moTRE3 after 17 months	210.1	26.90±1.13	35.14±0.42	15.24±3.80
difference for moTRE3	- 89.9	-0.40	+0.10	+1.55
moTRE4-NEMO injection	300.0	27.16±0.04	35.16±0.03	14.77±0.25
moTRE4 after 17 months	178.1	26.61±1.11	35.34±0.45	16.50±3.91
difference for moTRE4	-121.9	-0.55	+0.18	+1.73

The upward tracer motion is related to an observational freshening of the tracer-tagged water which results in a density reduction. In the models the θ-S relations reveal a warming rather than a freshening. This indicates a different behavior of the models; it is questionable if the right process is represented. The ROMS/CROCO TREs overestimate the upward motion of the tracer-tagged water but reproduce the lightening. The NEMO TREs are hardly comparable to the observation although they have indications of the observed features. Generally, there is a lot more to investigate in all moTREs and improvements to make. Nevertheless, it is of special interest that POSTRE shows the lightening of tracer-tagged water due to different reasons than the moTREs. In POSTRE it is mainly due to freshening (and additional but minor warming) but in the moTREs it is due to warming (accompanied with a salting). This issue is not re-

stricted to one moTRE or one model but seems to be a consistent bias.

The enhanced mixing due to boundary influences is very complex, in the case depicted by POSTRE. Based on the experimental setup, POSTRE (and the moTREs) experienced the influence of enhanced boundary mixing first and spread throughout the ocean afterwards. This means strong vertical (diapycnal) mixing occurs first, shapes the tracer accordingly, and afterwards the redistributed tracer get influenced by weak mixing as typical for dynamical calm regimes apart from the basin boundaries. To get to know the respective processes and to distinguish between their effects, the shelf must be separated from the offshore ocean and both regimes need to be investigated by their own.

The higher time resolution of the models allows to focus on the shelf in about the first three months of the experiments. The ROMS/CROCO TREs show the tracer "crawling" up the shelf along the continental slope. Thus both, observational and model data, restrict this process to the shelf. There are vertical tracer profiles related to the shelf indicating enhanced diapycnal diffusivity (Fig. 4.2) comparable to e.g. the Baltic Sea TRE (Holtermann et al., 2012). Although, on the Peruvian shelf the circumstances of POSTRE stand to reason that the upward mixing appears due to an active upslope transport of tracer-tagged water within the BBL on the shelf (cp. Ferrari et al., 2016). That means there is not only a larger diffusive diapycnal spreading near the shelf. The ROMS/CROCO TREs show the upslope tracer motion as to expect from theory and idealized model experiments (Holmes et al., 2019). Albeit the BBL-theory (Ferrari et al., 2016; McDougall and Ferrari, 2017; Holmes et al., 2019) was constructed for the abyssal, it seems to be applicable. Investigations on the details will be continued as subject of future studies. Whereas, the open ocean diapycnal mixing of the offshore advected tracer is found to be common for such calm mixing regimes (chapter 5) and does not seem to play a major role.

For the shelf related processes which shape the tracer, a consolidation with Micro-Structure measurements is part of an ongoing study to evaluate the diapycnal velocity and density fluxes at the continental slope off Peru. The Micro-Structure measurements were obtained directly after the tracer survey (Thomsen and Lüdke, 2018; Sommer and Dengler, 2019) and are comparable to a previous campaign (Dengler, 2016). However, the sampling grid of the Micro-Structure measurements is restricted to shelf normal sections between 11°S and 15°S. This comprises only the northern part of the tracer survey area; and it need to be proved if the regional difference is essential when regarding the shelf mixing. Though, the findings in this thesis show the low salinity water mass ESPIW to appear only in the southern parts of the study region consistent with literature (Schneider et al., 2003). It is indicated that southerly ESPIW mix in and lighten the tracer-tagged waters where the PCUC slows down due to instabilities. This suggests the upward motion to happen probably around Arica (18.5°S) but cannot be proven by POSTRE (and moTREs') data only.

With respect to the nutrient based motivation of POSTRE, there was already a very interesting series of six dye releases with similar purposes. Although the environmental conditions captured

by POSTRE are unique for a TRE, these dye releases are interesting to compare with POSTRE. The dye experiments were conducted between 1996 and 2002 at the New England continental shelfbreak front (further called New England Dye Experiments - NEDEs[1]). The NEDEs were coastal experiments using the (short-term lasting) dye tracers Rhodamine-WT and Fluorescein. The last three injections (2001-2002) were accompanied by drifter floats, nutrient chemistry and bio-optical measurements, and all NEDEs profit from the context by research of decades investigating the area and the related thermohaline front (Houghton et al. (2006), and references therein, especially Houghton (1997); Houghton and Visbeck (1998)).

Like POSTRE the NEDEs were motivated by the need to answer the question about nutrient transport from the shelf bottom to the euphotic zone, if and how the reveled upward motion can account for it. Both, POSTRE and the NEDEs, investigated a very dynamic coastal regime and were injected in or related to the BBL. Rather than getting different results from repeating experiments during the NEDEs the variety of observations support several aspects of the observed system.

Different to POSTRE, the NEDEs where conducted at the western boundary of the North Atlantic whereas POSTRE represents the oceanic conditions at the eastern boundary of the South Pacific. Further, due to the use of flouorometers, dye tracers are generally more easy to measure and detect than SF_6 or SF_5CF_3 but quickly drop below the detection limit and thus are only short-term lasting (Watson and Ledwell, 2000). POSTRE was conducted on much longer time scales (possible due to using the long-term lasting tracer SF_5CF_3) and rather than having tracer results for about 100 hours, POSTRE capture about 17 months of tracer motion. Also, POSTRE was conducted for a much broader oceanic area, spanning over the regions of the continental shelf, along the shelf for many deca-kilometers, and over a huge offshore open ocean regime. This puts the results of POSTRE in a different context than those of the NEDEs.

The NEDEs found especially "the notion of BBL separation and upwelling along the shelfbreak front" (Houghton et al., 2006). An upward motion, an advection dominated regime, and water detaching from the shelf in mesoscale features are results very similar for the NEDEs and for POSTRE.

The vertical diffusivity values of the NEDEs are derived "from the vertical distribution of the dye patch variance" by the use of Fick's law. In the less stratified pelagic water above the shelf closest to the coast the vertical diffusivity is about $3 \cdot 10^{-5}$ m^2 s^{-1}. It even decreases towards the offshoreward stratified frontal boundary to about $4 \cdot 10^{-6}$ m^2 s^{-1} (Houghton et al., 2006). These NEDEs results are unexpected small compared to the enhanced boundary mixing in an order of 10^{-4} m^2 s^{-1} as reported in the frame of e.g. the Brazil Basin TRE or DIMES (Polzin et al., 1997; Watson et al., 2013). Although, Holtermann et al. (2012) showed for the Baltic Sea TRE that a boundary related increase in diffusivity by one order of magnitude is a more

[1]Note that two series of dye experiments were conducted at the New England shelf at the same temporal and spatial scales in the same region. For the purpose of the discussion in this thesis only the results by Houghton et al. (1997-2006) are of interest. The dye series done by Ledwell et al. (2004) pursued different objectives and thus should not be mismatched.

persistent observation than values in an special order of magnitude. The NEDEs results are contra intuitive as the diffusivity close to the coast is an order of magnitude smaller than in the frontal boundary, not vise versa. Comparable values of the offshore ocean probably could not be derived from the NEDEs' experimental frame.

In contrast, for POSTRE a comparable vertical diffusivity value was found just in the far offshore ocean. Near coast a classical diapycnal diffusivity coefficient could not be derived as the approach based on Fick's law was not applicable at all. Instead, the diapycnal transport in the BBL (Ferrari et al., 2016) accounts for the upward motion of the POSTRE tracer. Thus it stand to reason that also for the NEDEs the same theoretical concept of BBL motion provide better results than estimating a classical diapycnal diffusivity coefficient. This means the reported NEDEs' values of diffusivity would be misleading small as the used methodological approach did not capture the actual but only the net tracer spread. A reinterpretation of the NEDEs' diffusivities with respect to the recent findings of BBL tracer transport is recommended. However, this suggests that the NEDEs' diffusivities cannot support the findings in this thesis by filling in where POSTRE lacks of details when it comes to the shelf region.

Thus, performing observational TREs turns out to be critical. Even if some aspects seem to be already known or previous TREs let expect similar outcomes, they provide new evidences. They importantly highlight new insights with respect to more recent theories. As modeled TREs support the observations but do not yet reproduce all aspects correctly, the observations are still key, at least until the models improve.

Final, the (diapycnal) upward motion implicate that nutrients released from anoxic sediments (represented by the tracer) reach the euphotic zone. There is a physical pathway, proximately near the coast, available to the nutrients. Namely, it is estimated that about 10-30$\pm$10% of the released amount end up in these realms and are in principle usable for primary production.

Further, one could speculate if the appearance of El Niño events and their side effects (e.g. more frequent appearance of coastal trapped waves) support higher nutrient transports to the surface as the appearance of such an event accompanies with an isopycnal heave of tracer-tagged water. For conclusive results the effects of several long- and short-term natural variabilities on the tracer behavior would need to be investigated.

5 Eastern Tropical South Pacific Diapycnal Diffusivity within the Offshore Oxygen Minimum Zone

Abstract of the Chapter. Diapycnal mixing is an important process for the vertical redistribution of heat, salt and dissolved chemical constituents. Yet it is difficult to measure directly. In this chapter a new estimate of diapycnal turbulent diffusion is presented. It is obtained from the large-scale POSTRE. The open ocean diapycnal diffusivity coefficient is $(1.4 \pm 0.4) \cdot 10^{-5}$ m^2 s^{-1} . This rate of vertical mixing is similar to those found from open ocean mixing tracer release experiments in the Eastern Tropical North Atlantic and the Southern Ocean. Through this experiment could fill a geographic gap in estimates of diapycnal diffusivity in the ETSP. The value based on observations is necessary to understand ocean ventilation, calculate oxygen and nutrient budgets and to parameterize mixing in ocean models.

5.1 Preamble

As it is a well-established method, POSTRE was utilized to determine the diapycnal diffusivity. It is advantageous compared to temporal and spatial sparse microstructure measurements, and gives an (integral) estimate with relatively low uncertainty (Watson and Ledwell, 2000). However, as an integral, the TRE estimate of diapycnal diffusivity is only comparable to time and space averaged estimates of microstructure measurements, but not to single diffusivity profiles or vertical averages (Fischer et al., 2013).

As already shown (chapter 3, Fig. 3.1a) the tracer could be surveyed all over the sampling area. In particular, the majority of tracer entered into the dynamically calm open ocean regime. The tracer spread far away from the injection sites. It crossed the shelf break and left the coastal regime.

It is also already discussed that the tracer got affected in the coastal areas before leaving the shelf. On the one hand there are the advections. However, here it is assumed that neither the PCUC transport nor the eddy transport change the density of tracer-tagged water remarkably while regarding them as geostrophic current, isopycnal eddy diffusion, and so on. On the other hand, there is the upward motion. This is an issue discussed below, while stating its effect on the diapycnal diffusivity coefficient. At the end the time the tracer spend on the shelf, and the effect of shelf related processes cannot be quantified in a way to disentangle it from the offshore diffusivity estimate. The other way round, such an estimate is important to infer how much the tracer contact into the coastal areas could affect the value.

5.2 Data Analysis and Result

Since we are interested in the diapycnal mixing of the open ocean regime, in this chapter only survey stations are considered where the water depth was larger than 2000 m, i.e. 83 vertical profiles (Figs. 5.1a & 5.3a). The 2000 m isobath separates the regimes based on the shape of all survey profiles.

A separation of the survey samples by stratification regimes is not indicated. This is implemented here, as different stratification regimes would affect the diffusivity estimate (Banyte et al., 2012). The buoyancy frequency as a measure of stratification is calculated from the hydrographic profiles using TEOS-10 for the depth layers of the isopycnals - between the depth of the 26.17-isopycnal and the depth of the 26.348-isopycnal (Fig. 5.2). It changes between the northern and the southern part of the study area from about $4.5{\cdot}10^{-3}$ s^{-1} to about $8{\cdot}10^{-3}$ s^{-1}, respectively. One could separate the two regimes as shown by the line in Fig. 4.4 . However, almost all survey stations refer to the northern regime. Overall their buoyancy frequency values fit quite well with the climatology. But in the southern region the frequencies of the survey stations are a bit lower than in the climatology, more representative for the northern part.

A diapycnal diffusivity estimate (D) can be calculated with the time dependent (dt) increase of

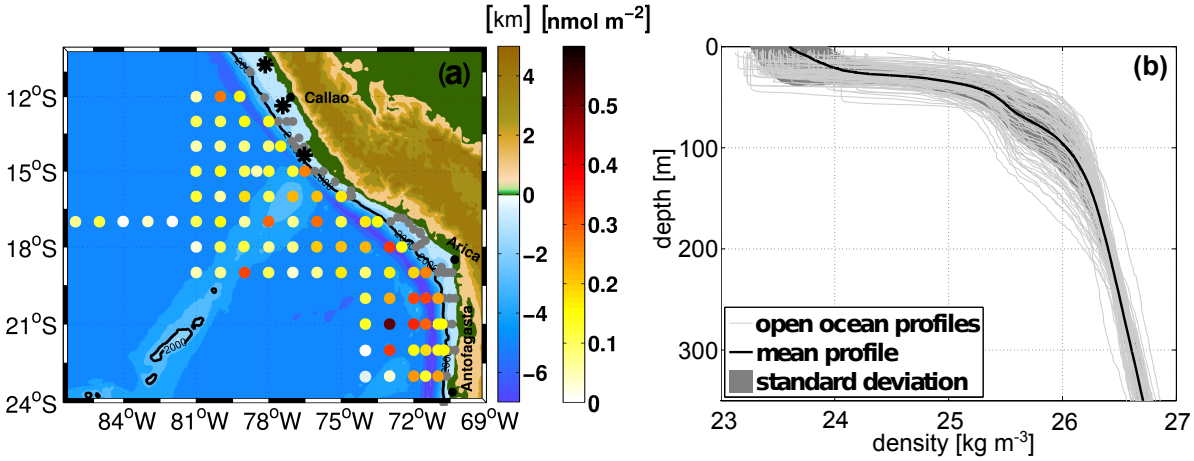

Figure 5.1: (a) Vertical column integral to show the stations used here; with injection sites (asterisks), and the 2000 m isobath (black line). Stations not used are in gray. Bathymetry and topography are shown in blue, green, and brown.
(b) Vertical profiles of the density-depth conditions for the open ocean stations of the survey cruise (gray) and its mean (black).

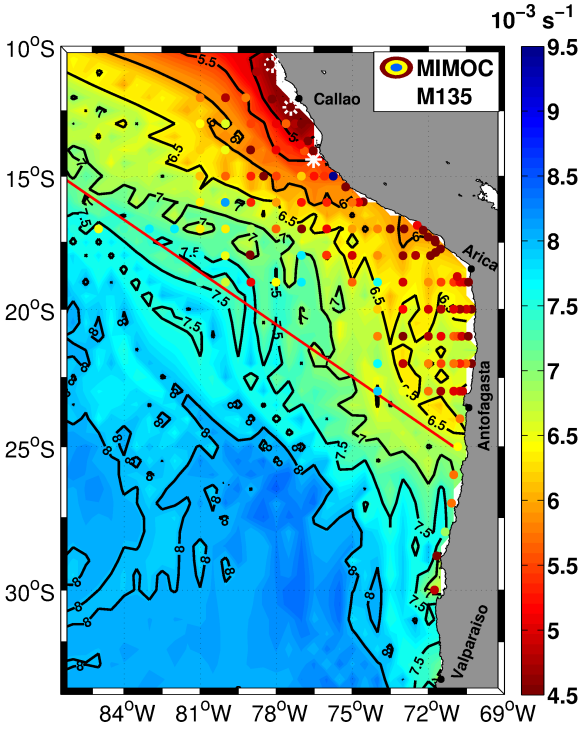

Figure 5.2: Buoyancy frequency (N) in March, whereas N is calculated for the depths layers between the 26.17 and 26.348 - isopycnals, from hydrographic profiles using the toolbox by McDougall and Barker (2011). The shades in the maps are derived from the MIMOC climatology (Schmidtko et al., 2013); the overlaid dots are the observed properties of the survey cruises labeled with M135. The injection sites are indicated by asterisks.

the second moment (dM), in accordance to Fick's law of diffusion (D=0.5·dM/dt). This is the only approach used since the Gaussian fit approach and a numerical solution of the advection-diffusion equation lead to similar results within the uncertainties (Banyte et al., 2012). For the calculation we implicitly assume (in accordance to the shape of the profiles) that the second moment of the tracer found at the open ocean stations was only less influenced before leaving the shelf regions. Thus it was primary influenced by the offshore diapycnal diffusivity and reasonably represents these open ocean conditions. Since the diapycnal diffusivity likely is significantly

higher on the shelf, any time the tracer spends on the shelf would tend to bias our estimate high.

To calculate the change in the second moment (dM) from the initial to the survey conditions, we oriented our analysis based on previous mixing TRE studies (Banyte et al., 2012; Köllner et al., 2016). First the surveyed open ocean tracer profiles were cubic interpolated onto 0.001 kg m^{-3} density bins and averaged along these bins to derive a mean *survey* tracer-density profile and its standard deviation (Fig. 5.3a). For the injection, the amount of tracer released in potential density intervals (Fig. 2.2b) is fitted Gaussian to provide a mean *injection* tracer-density profile and its standard deviation.

The next step is to project the mean tracer-density profiles into depth coordinates. For that the CTD sensor profiles of the open ocean stations were also cubic interpolated onto 0.001 kg m^{-3} density bins. A mean density-depth lookup table (Fig. 5.1b) is derived by averaging the interpolated CTD profiles along density bins. Investigations of the buoyancy frequency, as a measure of stratification, and the lateral density-depth distribution (not shown) did not give any indications that using any regional density-depth relation would be sensible and would reduce the uncertainty. Further, it is essential to note that every single as well as the mean density-depth profile are significantly curved with a rapid decrease towards the mixed layer (Fig. 5.1b) showing a clear influence of the sea surface on our experiment.

The entire mean density-depth profile is used to transpose both mean tracer-density profiles into depth space: For each density value of the tracer profile the corresponding depth value of the density-depth lookup table is used to reach mean tracer-depth profiles. This is because the depicted shape of the density-depth profiles cannot be represented by a single value relation of a linear regression. Although, between 200-300 m (in the depth range of the injection) the mean density-depth profile could be linearly approximated, this would not be suitable for the depth range of the surveyed tracer profiles. It is necessary to use only one relation. Otherwise wrong diapycnal diffusivity would be gained.

The Gaussian fitted mean tracer-depth profiles provide the second moments. Whereas, the injection was already Gaussian fitted before the transformation and keeps its Gaussian shape, giving a width of 17.7 ± 4.5 m. The surveyed mean tracer-depth profile is fitted to a Gaussian after the transformation, yielding a width of 71.2 ± 8.3 m.

Finally, the change in the second moment (dM) is calculated by the difference between that of the survey and that of the injection. For better illustration the survey profiles are shown in comparison to the injection profile normalized and graphed as a function of distance from their respective peak densities (Fig. 5.3b).

Applying Fick's law of diffusion, we calculate the diapycnal diffusivity to be D= $(1.4 \pm 0.4) \cdot 10^{-5}$ m^2 s^{-1}.

The overall uncertainty of the diapycnal diffusivity estimate arise from an error calculation of three contributions (similar to e.g. Schafstall et al., 2010, and references therein), with

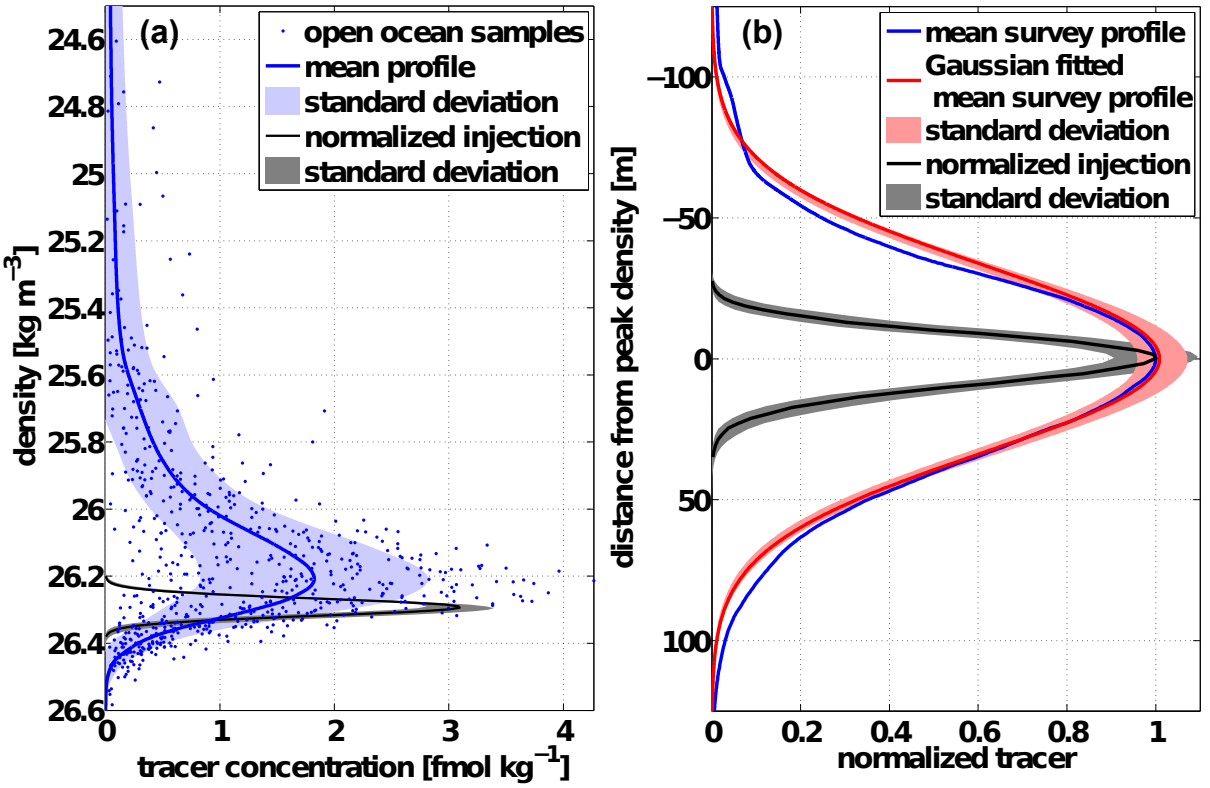

Figure 5.3: Vertical tracer profiles as a function of density (a) and distance from their respective peak density (b); with the mean surveyed profile in blue, its Gaussian fit in red, and the Gaussian fitted injection profile (cp. Fig. 2.2b) in black.

$$\Delta D = D \left[\left(\frac{\Delta M_{inj}}{M_{inj}} \right)^2 + \left(\frac{\Delta M_{sur}}{M_{sur}} \right)^2 + \left(\frac{\Delta dt}{dt} \right)^2 \right]^{1/2} = 0.4 \cdot 10^{-5} \text{ m}^2 \text{ s}^{-1}.$$

The standard deviation of the second moment of the *injection* (ΔM_{inj}) is derived with common statistic approach. This is the same for the standard deviations shown graphically, i.e. these of the Gaussian fitted tracer *injection* profiles (Figs. 2.2b, 5.3a & 5.3b), the mean density-depth profile (Fig. 5.1b), and the *surveyed* mean tracer-density profile (Fig 5.3a).

For the standard deviation of the second moment of the *survey* (ΔM_{sur}) a bootstrap procedure turned out to yield most realistic values. It is shown as standard deviation of the *surveyed* Gaussian fitted mean tracer-depth profile (Fig. 5.3b). We used 1000 subsets with random samples containing 50% of the open ocean stations (following Köllner et al., 2016, and references therein). The bootstrap procedure is most realistic, because it represents all conceivable sources of uncertainty. Especially, influences from the lateral tracer distribution with its interference from advection are included, and it accounts for variances in the shape of the vertical profiles.

The uncertainty of the time interval between the injection and the survey (Δdt) is due to its approximation. The injection took place within 5 days and it is reasonable to regard this as a starting point without noteworthy time variation. In contrast, the survey cruise spanned 39 days. Thus, actually the time difference from the injection to the survey is 16.7-18 months. For the diffusivity calculation the time interval (dt) is approximated with 17 months. The devia-

tion between the approximated value and the actual time span is a minor but still important uncertainty.

5.3 Discussion

Directly continuing from the data analysis and results section, the usage of the injection peak width is discussable as an important uncertainty of the diapycnal diffusivity calculation. The used width results from the initial conditions during the injection. However, between the injection and the vertical tracer spread occurring in the open ocean, coastal processes likely act on the tracer and change its vertical distribution. Thus a peak width for the beginning of the experiment needed in the diffusivity calculation has to represent the vertical tracer dispersion at the time the tracer leave the shelfbreak and enters the offshore ocean. Just after its entrance in the calm open ocean regime the offshore diapycnal diffusivity would dominate the tracer behavior. So, technically not the injection peak width but a tracer peak width after some instantaneous diapycnal mixing on the shelf, i.e. an *initial* peak width, would be needed. In this study, the injection peak width was treated as initial peak width because the initial conditions already account for the highly dynamic shelf region and show the peak width expanded by one order of magnitude, compared to regular open ocean mixing TREs. Some bulk investigations below support this choice, whereas the details of the tracer behavior on the shelf and the shelf mixing processes are beyond the scope of this study and will be investigated in the future.

To get an impression of how strong such initial mixing could affect the result, we exemplary presume an initial tracer spread causing a doubling of the injection peak width. We further presume this doubling in peak width occurs within one to four weeks, in agreement with the basic assumption that the tracer left the shelf regions shortly after injection. Therefore, the diffusivity in this initial phase on the shelf is in order of 10^{-4} m^2 s^{-1} (Toole et al., 1994; Polzin et al., 1997; Watson et al., 2013, Tab. 5.1, in agreement with e.g.). In contrast, the open ocean diapycnal diffusivity based on the *initial* peak width (instead of the *injection* peak width) decreases to about $1.1{\cdot}10^{-5}$ m^2 s^{-1} (Tab. 5.1). A variety of reliable values is given in Tab. 5.1.

Interestingly, most values in Tab. 5.1 show the resulting open ocean diapycnal diffusivity in the order of 10^{-5} m^2 s^{-1}. Just very strong shelf mixing larger than 10^{-4} m^2 s^{-1} and / or time spans of more than 4 weeks, reduce the open ocean value strongly. However, the largest as well as the smallest resulting open ocean diapycnal diffusivities set the scene of possibilities. Thus, there is especially no supportive indication to speculate for a diapycnal diffusivity estimate in order of 10^{-6} m^2 s^{-1} to be more realistic than our result, as might be indicated when consulting the eastern South Pacific diffusivities from the ARGO data by Whalen et al. (2012). Thus we postulate that the diapycnal diffusivity coefficient of $(1.4 \pm 0.4) \cdot 10^{-5}$ m^2 s^{-1} is representative as a temporal mean for the overall region of the ETSP, although temporal and local diffusivities indeed can show a variety of values with orders of 10^{-6} to 10^{-4} m^2 s^{-1} (Whalen et al., 2012). On the one hand, this is a matter of methods and simultaneously on the other hand a matter of needs and aims. That means, when a long-term and large-scale diffusivity estimate represen-

Table 5.1: Bulk investigations to get an impression of how strong the initial mixing could affect the open ocean diapycnal diffusivity. Presumed values are written in red, the bulk results from it are black.

time over which the initial diffusivity on the shelf acts on the tracer	order of magnitude of the initial diffusivity on the shelf	initial peak width at the shelf break	open ocean diapycnal diffusivity based on the changed initial peak width
assuming an initial mixing that is suitable to cause the given initial peak widths		3 m i.e. an injection peak width of regular open ocean mixing TREs	$1.44{\cdot}10^{-5}$ m^2 s^{-1}
		7 m i.e. more than a doubling of injection peak width of regular open ocean mixing TREs	$1.43{\cdot}10^{-5}$ m^2 s^{-1}
		12 m	$1.40{\cdot}10^{-5}$ m^2 s^{-1}
		27 m	$1.36{\cdot}10^{-5}$ m^2 s^{-1}
		22 m	$1.30{\cdot}10^{-5}$ m^2 s^{-1}
		27 m	$1.23{\cdot}10^{-5}$ m^2 s^{-1}
4 weeks	$0.59{\cdot}10^{-4}$ m^2 s^{-1}	35.39 m,	$1.15{\cdot}10^{-5}$ m^2 s^{-1}
3 weeks	$0.65{\cdot}10^{-4}$ m^2 s^{-1}	i.e. doubling of the	$1.13{\cdot}10^{-5}$ m^2 s^{-1}
2 weeks	$0.97{\cdot}10^{-4}$ m^2 s^{-1}	injection peak	$1.11{\cdot}10^{-5}$ m^2 s^{-1}
1 week	$1.94{\cdot}10^{-4}$ m^2 s^{-1}	width	$1.10{\cdot}10^{-5}$ m^2 s^{-1}
2 weeks	10^{-4} m^2 s^{-1}, i.e.	35.79 m	$1.11{\cdot}10^{-5}$ m^2 s^{-1}
4 weeks	enhanced by one	47.42 m	$0.85{\cdot}10^{-5}$ m^2 s^{-1}
6 weeks	order compared to	56.71 m	$0.57{\cdot}10^{-5}$ m^2 s^{-1}
8 weeks	offshore diffusivity	64.68 m	$0.28{\cdot}10^{-5}$ m^2 s^{-1}
2 weeks	10^{-3} m^2 s^{-1}	99.95 m	initial peak width
4 weeks		140.24 m	exceeds that of the survey

tative for the overarching region of the ETSP is needed, as in the case of budget calculations, than a TRE based value is suitable. When studies investigate the underlying processes and aim to account for temporal and spatial variability, than the tracer estimate can give no insight as it is an integral over every process acting. Naturally, local measurements would be preferable in such a case.

Further, there is another very recent argument in this discussion. Holmes et al. (2019) investigated idealized model experiments with several scenarios for tracer releases similar to our injection setup. Their tracer injection is near a sloping boundary and within a flow based on the theory of the one-dimensional boundary layer. They found bulk diffusivity values for isolated near-boundary tracer releases much smaller than to expect. This is due to opposite tracer dispersion in the changing stratification regimes related to the boundary dynamics (Holmes et al., 2019). Thus the expectations about the initial peak width easily assume misleading large values. In absence of a clear evidence to give an indisputable answer on this point, using the *injection*

tracer peak width as a starting point is more resilient than an approximation of the *initial* peak width, which would be arbitrary in any case.

Having said that, another eye-catching point in the tracer-density profiles is the difference between the tracer weighted mean injection and survey densities. Namely, the tracer peaks move into lighter densities from injection to survey (Fig. 5.3a). This motion can be set in context also with the recent study by Holmes et al. (2019). Similar to the findings from our observational samples, Holmes et al. (2019) found the tracer moving upslope, and specify the buoyancy tending to drive the tracer upslope toward less dense fluid when along isopycnal diffusion is weak. It highlights the complexity, which is beyond the scope of this study. Thus again, the related vertical tracer behavior, a quantification of the lightening and a related upward tracer motion was clarified in chapter 4. The processes causing the lightening on the Peruvian shelf are identified from a consolidation of the tracer data and microstructure measurements in a different study . As a brief teaser, an upward mixing of chemical constituents (e.g. nutrients) from the bottom water of the Peruvian shelf would implicate that these constituents enter the pelagic water column or even the euphotic zone, where they are potentially usable in biological processes.

In this study, we found the open ocean diapycnal diffusivity in generally good agreement with the few other large-scale, time integrated open ocean values, world-wide. In the offshore regime over smooth topography only breaking internal waves cause the diapycnal diffusion (e.g. Alford et al., 2016), which gives all of these regimes the same physical basis. Nevertheless, the derived diapycnal diffusivity values show small differences of probably regional origin. The DIMES ('Diapycnal and Isopycnal Mixing Experiment in the Southern Ocean') estimate for the Pacific sector of the Southern Ocean (over smooth topography) after one year is $(1.3\pm0.2)\cdot10^{-5}$ m^2 s^{-1} (Ledwell et al., 2011), and at this state very close to the POSTRE result. However, the DIMES best estimate over the whole experiment duration of 26 months increased to $(1.78\pm0.06)\cdot10^{-5}$ m^2 s^{-1} (Watson et al., 2013). This longer integrated value is in better agreement with the North Atlantic TRE estimate of $(1.7 \pm 0.2) \cdot 10^{-5}$ m^2 s^{-1} (Ledwell et al., 1998). Both are a bit higher than the POSTRE diffusivity.

High conformity between the diffusivity estimates appears for POSTRE, the Guinea Upwelling TRE, and the Oxygen Supply TRE. The latter both were conducted in the Eastern Tropical North Atlantic. Their mean diapycnal diffusivities are $(1.11 \pm 0.22) \cdot 10^{-5}$ m^2 s^{-1} and $(1.06 \pm 0.24) \cdot 10^{-5}$ m^2 s^{-1}, respectively (Köllner et al., 2016; Banyte et al., 2012). These values are slightly smaller than the POSTRE estimate but very close within the range of uncertainty. In the Eastern Tropical North Atlantic also Fischer et al. (2013) found the diffusivity to be $1 \cdot 10^{-5}$ m^2 s^{-1} from a combination of the Guinea Upwelling TRE, microstructure profiles and ship-board acoustic current measurements. It is noteworthy that the POSTRE diffusivity estimate is in good agreement with this value notwithstanding of the differences in study area and methods.

The good agreement between the diffusivity values highlights dynamic similarities between the

ETSP and the Eastern Tropical North Atlantic in relation to their OMZs. For the OMZ of the South Pacific, our result supports the oxygen budget calculation of Llanillo et al. (2018). The new POSTRE value of diapycnal diffusivity is close to the assumption made by Llanillo et al. (2018) when using the diffusivity of 10^{-5} m^2 s^{-1} (referring to the North Atlantic value by Fischer et al., 2013). By that the POSTRE value also supports the state of the art knowledge about deep OMZ ventilation: The oxygen is supplied by advection but to an important extend also by diapycnal diffusion (Brandt et al., 2015; Llanillo et al., 2018). Thus diapycnal diffusivity is again confirmed to be essential in the offshore OMZ regions where advection is characterized to be sluggish (e.g. Luyten et al., 1983).

Concluding, the diapycnal diffusivity estimate from the POSTRE experiment fills a geographic gap in the ETSP, maintaining the global view of mixing in calm open ocean regimes. It is found to be $(1.4 \pm 0.4) \cdot 10^{-5}$ m^2 s^{-1}, serving as an empirical basis for future research.

6 Summary and Outlook

In the last decades a lot of research has been done to understand the ocean physics and biogeochemistry of the ETSP. Nevertheless, the ETSP is a highly dynamic regime. Estimating a mean state and how the physical processes affect overall biogeochemical tracers is still an important subject of research. Especially, the fate of nutrients released by anoxic marine sediments on the continental shelf is not well understood, yet. This thesis summarizes the studies about a TRE that was performed in the ocean and in models to investigate integral aspects of the physical processes which affect nutrient transports from the BBL. The along-shelf and offshore advections as well as shelf related diapycnal transport in the BBL are found to be essential.

In detail, chemical constituents originating from sediments of the continental shelf are affected by ocean circulation. Right away, the PCUC transports them coast parallel along the shelf to the south. The PCUC transport velocity near by Callao is 3-5 cm s^{-1} and 7-17 cm s^{-1} southward from Paracas headland (14-17.5°S). South of about 18°S the mesoscale eddy activity takes over and acts as a carrier providing the dispersion pathway across the shelf break into the open ocean. Dissolved constituents get captured in the cores of surface and mainly subsurface anticyclones. This way 21-54% of the tracer reaches the offshore ocean as the eddies transport their content westward. On top, a diapycnal upward motion is detected. It provides a physical connection, a pathway, from the sea floor to the sea surface. This way 10-30±10% of the tracer reaches into the surface water layers. First investigations show this motion explainable by BBL dynamics. That means the process governing the upward motion is related to the shelf region. Somewhat surprising, it turned out that, with some restrictions, an open ocean diapycnal diffusivity within the offshore OMZ of the ETSP can be derived similar to usual mixing TREs. It is representative for calm open ocean regimes with a best estimate of $(1.4 \pm 0.4) \cdot 10^{-5}$ m^2 s^{-1}. This supports again the relation of the upward motion to the shelf, as the offshore diffusivity cannot account for it.

On the basis of these pathways provided by ocean physics, nutrients mimicked by the tracer are potentially transported along the shelf to the south, might enter the offshore ocean, and possibly reach the euphotic zone to be used for primary production. However, as nutrient dynamics are not only affected by ocean physics, it is an important task of ongoing research to identify which nutrients behave like the tracer and what are possible restrictions. As an example, it can be assumed that nutrients under some conditions are used by biology while following the ocean physics' pathway which naturally changes their overall behavior compared to the tracer. Thus

the next step on this issue is to link the artificial tracer to real nutrients and relate their behavior for further insights.

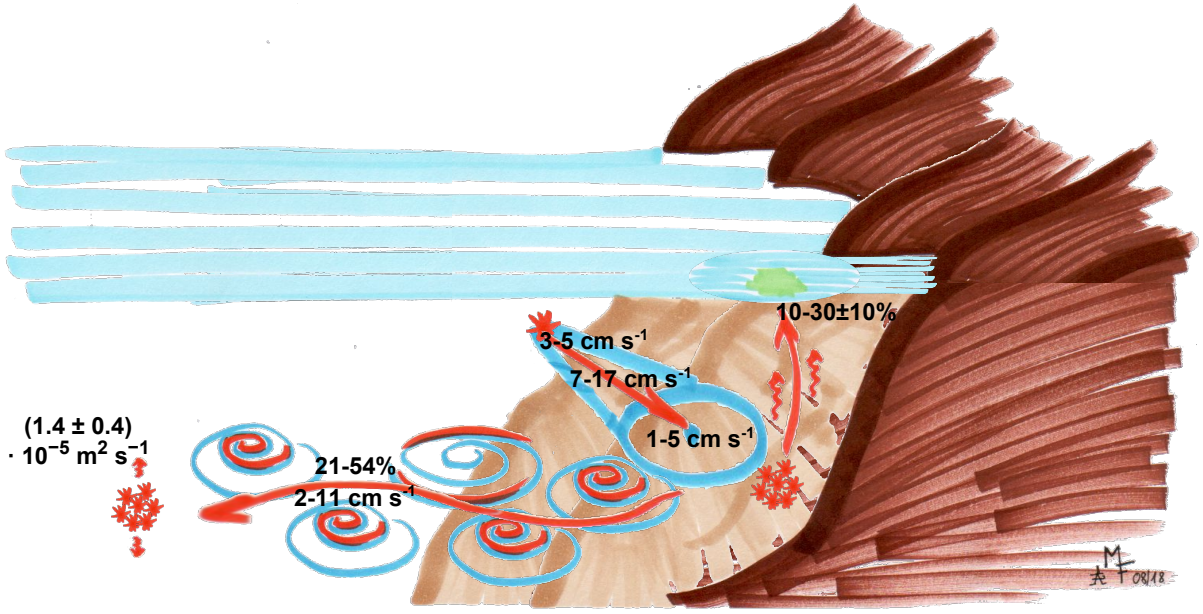

Figure 6.1: Summarizing the relevant processes governing the tracer distribution and their quantified effect on the tracer in the ETSP. The tracer and its behavior is indicated in red; shelf/land in brown, the water (including its motions: PCUC, and eddies) in blue.

The upward tracer motion was quite unexpected at the beginning, when planning, injecting and surveying the tracer in the ocean, and also when performing the first moTRE. By now, serveral theoretical studies are published which can explain this point. However, in this thesis only a first step is done on the way to prove the theory in the observation (or the moTREs). Ongoing investigations are recommended to better understand the observations by e.g. relating the tracer behavior to micro-structure measurements on the Peruvian shelf and investigating the turbulent diffusion and diapycnal motions related to it.

Also several other investigations could not be made within the time frame of this thesis but provide promising approaches for future evidence. In this course the moTREs are to name. Based on the moTREs, both models (and all four configurations) generally perform very well in terms of advective regimes. The lateral dispersion provides a promising high degree of realism. However, investigations about their isopycnal heave, a possible El Niño influence, and the stratification conditions could be used to identify long- and short-term variabilities acting additional to the diapycnal upward motion. This would give, for instance, insight if more nutrients could reach the surface in times of more frequent passings of coastal trapped waves or during the emergence of El Niño events and so on. For the PCUC transport and in general the tracer transport velocities, the moTREs could be investigated more deeply to potentially improve the values found here. Moreover, a statistical approach on the mesoscale eddy activity can be addressed in the moTREs for more resilient values of how much tracer an eddy contains, and how many eddies capture the tracer in the duration of such a TRE. Thus the moTREs

contain more potential (at least on the lateral tracer dispersion) for several further insights.

For the vertical tracer transport the models capture some features comparable to the observation. Namely, all of them show an upward motion. However, the changes of properties causing the rise of tracer-tagged water are remarkably different between the models and the observation. This is a point to go into in the future. ROMS/CROCO shows the representation of the shelf related BBL motion which is probably possible due to the high resolution over the shelf resulting from the 's-coordinate'. Nevertheless, the 's-coordinates' have also an important bias which counteract the represented physical motion by bringing tracer in unrealistic depths. Thus further investigations are recommended to better model a reliable vertical transport of chemical constituents; might accompanied with future investigations about the observational upward motion. Then the moTREs with their high horizontal resolution are promising to look for local details related to the vertical tracer behavior.

The results shown in this thesis contributes to the understanding of the physical processes and pathways in the ETSP as basis for nutrient distributions and model improvements. It is an important step forward on the way to capture the coupled ocean physics and biogeochemistry of the ETSP in the ocean and numerical simulations.

Appendices

A moTREs in Depth-, Density-, and θ-S-Space at Full Horizontal Resolution

To give an impression about the full resolution tracer distribution in the moTREs selected graphics are included here. The tracer is shown between 5-30°S, and execpt for the tracer depth distribution shown below 50 m water depth. These figures highlight a lot of potential for further investigations of the tracer in the moTREs but this is beyond the time frame of this thesis.

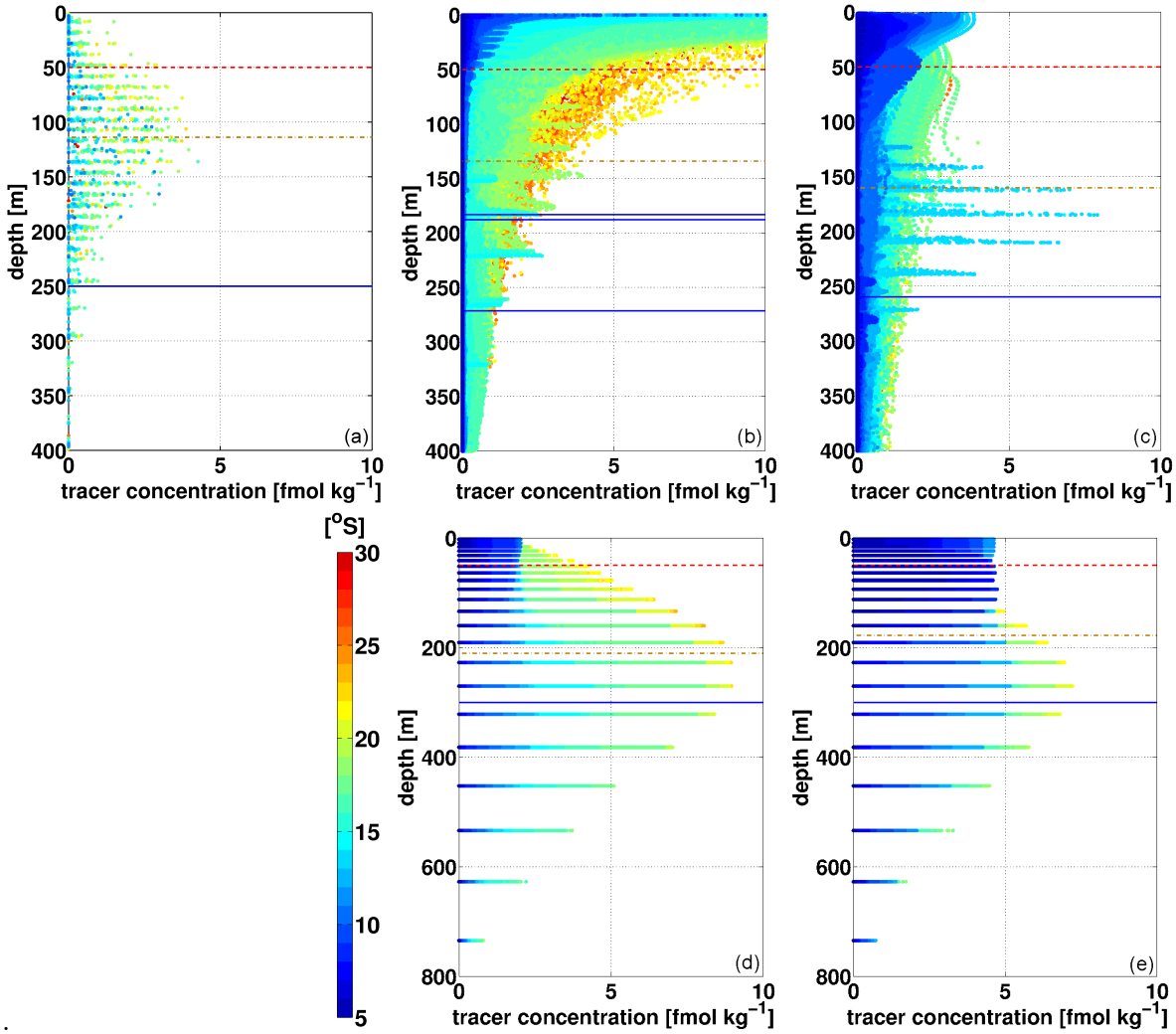

Figure A.1: Tracer depth distribution 17 months after injection for (a) POSTRE, (b) moTRE1-ROMS, (c) moTRE2-CROCO, (d) moTRE3-NEMO, and (e) moTRE4-NEMO. Injection depth indicated as blue line, the 50 m isobath dashed in red, the tracer weigthed mean dash dotted in brown. The moTREs are shown with surface tracer. Note the different y-axis for NEMO.

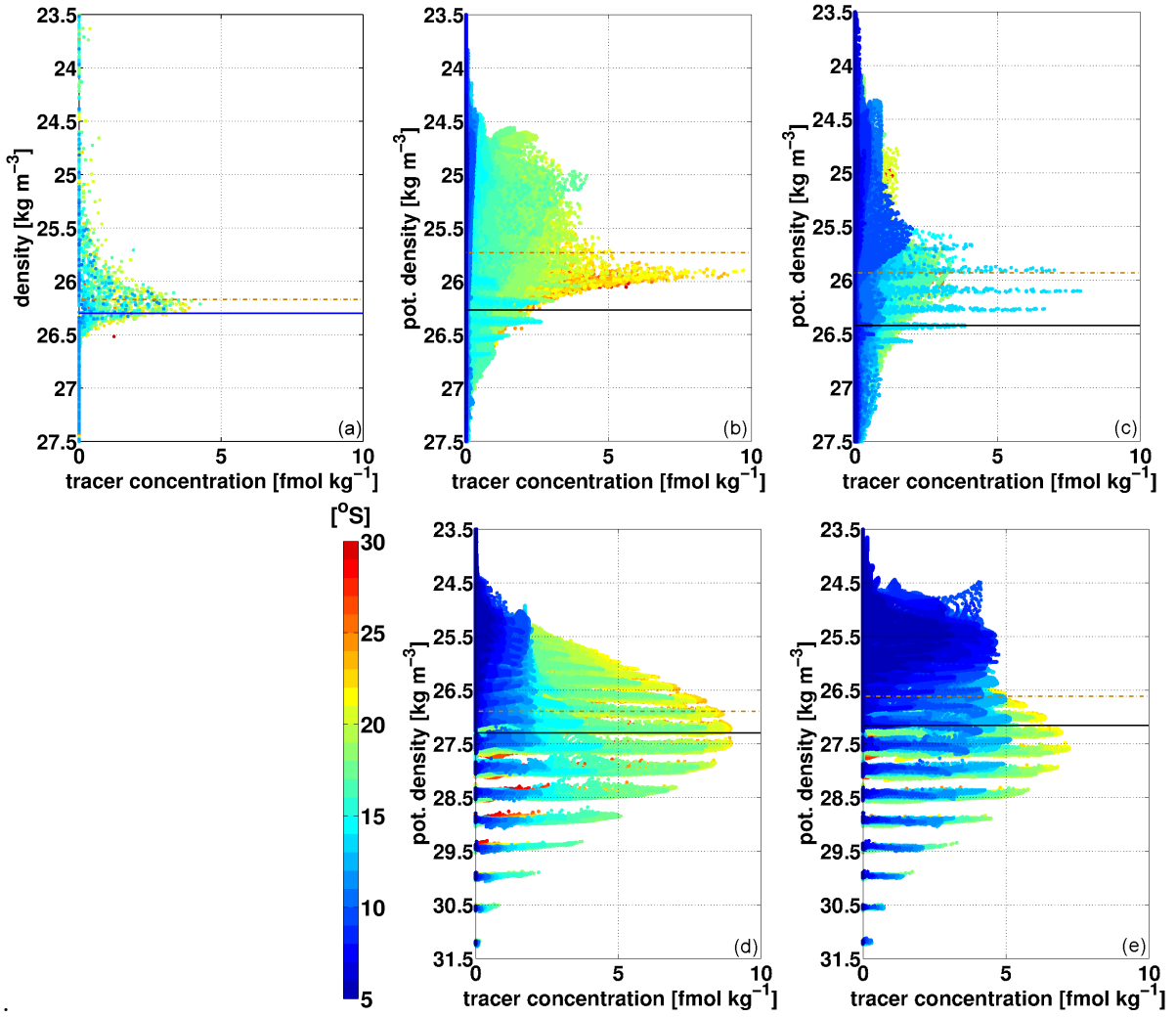

.

Figure A.2: Tracer density distribution for (a) POSTRE, (b) moTRE1-ROMS, (c) moTRE2-CROCO, (d) moTRE3-NEMO, (e) moTRE4-NEMO. Injection depth indicated as blue/black line, the tracer weigthed mean dash dotted in brown. Note the different y-axis for NEMO.

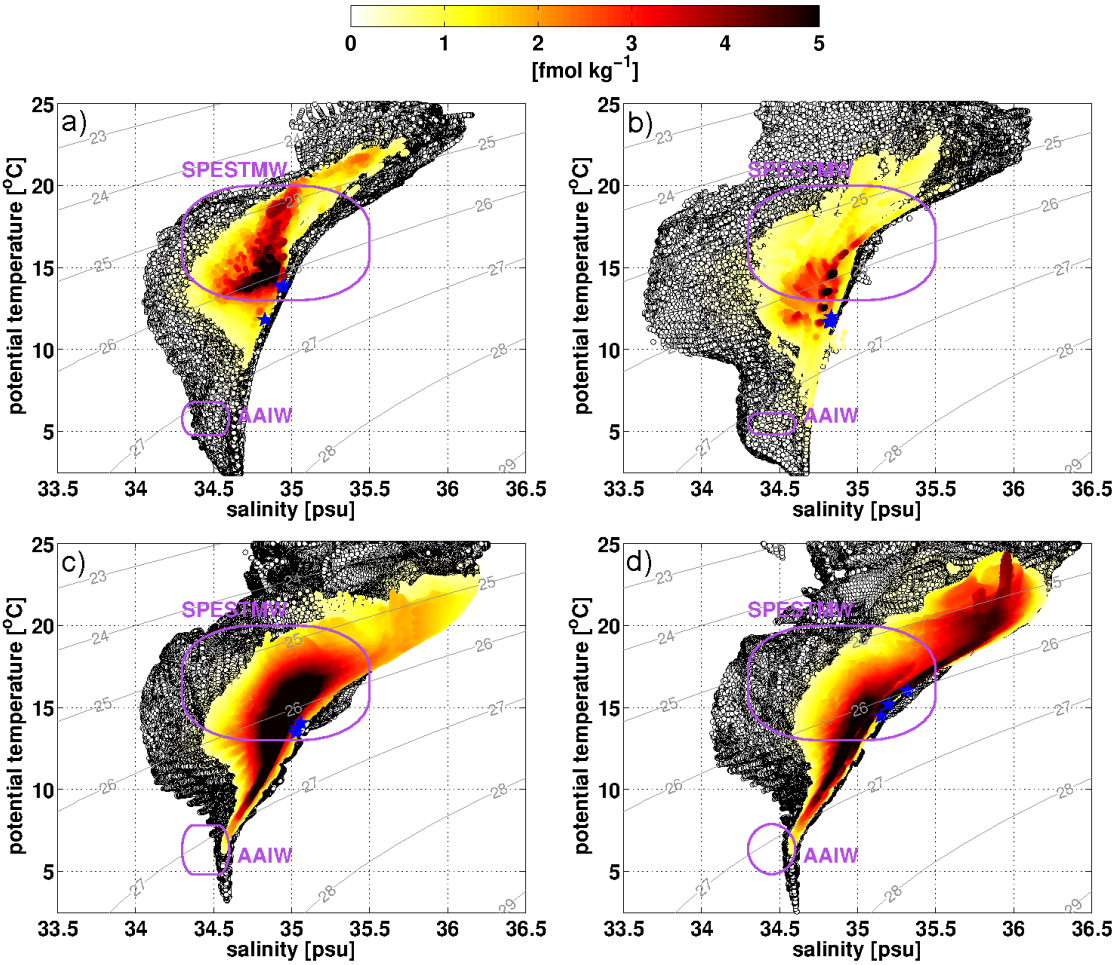

Figure A.3: θ-S relation of (a) moTRE1-ROMS, (b) moTRE2-CROCO, (c) moTRE3-NEMO, (d) moTRE4-NEMO. The injection is shown in blue. The tracer concentration 17 months after the injection is color coded. Isopycnals in gray.

B Supporting Information - Data Set: The Processed Tracer Injection Data

This supporting information provides a processed data set of the tracer injection to make the study reproducible. The tracer injection took place during the research cruise SO243 with RV Sonne II between 13 and 18 October 2015 using the OTIS. A total of 68.5kg SF_5CF_3 was injected at three locations (25kg at 10°42.9'S and 78°14.1'W, 28kg at 12°21.87'S and 77°26.25'W, and 15.5kg at 14°02.16'S and 76°31.67'W - asterisks in Fig. 2.1a) into the anoxic BBL over the Peruvian shelf at about 250m depth. First plots were shown in (Marandino, 2016) as preliminary results. The full log of the tracer release is available on request[1].

For this study we calibrated the data as described in the main text. To derive a tracer-density function 550 time and 30 potential density intervals were chosen while the tracer pump worked. The tracer is summed over the time intervals yielding the injected tracer amount as a function of density.

[1]Madeleine Freund, mfreund@geomar.de, GEOMAR Helmholtz Centre of Ocean Research Kiel, Duesternbrooker Weg 20, D-24105 Kiel, Germany
Toste Tanhua, ttanhua@geomar.de, GEOMAR Helmholtz Centre of Ocean Research Kiel, Duesternbrooker Weg 20, D-24105 Kiel, Germany

Table B.1: Processed tracer injection data, which is used to infer the initial conditions as shown in Fig. 2.2 (a and b) of the main text.

Potential density anomaly (kg m^{-3})	tracer amount of injection site at $\sim 10°S$ (mol)	tracer amount of injection site at $\sim 12°S$ (mol)	tracer amount of injection site at $\sim 14°S$ (mol)	total tracer amount injected (mol)
26.2401	0.00	0.00	0.00	0.00
26.2446	0.00	0.00	0.00	0.00
26.2491	0.00	0.00	0.00	0.00
26.2536	7.99	0.00	0.00	7.99
26.2581	6.50	0.00	0.00	6.50
26.2626	24.45	0.00	0.00	24.45
26.2671	12.25	0.00	0.00	12.25
26.2716	18.44	0.00	0.00	18.44
26.2761	15.54	0.24	0.00	15.79
26.2806	17.40	2.06	3.32	22.78
26.2851	17.14	12.07	4.18	33.39
26.2896	1.20	18.60	4.77	24.56
26.2941	2.75	27.78	4.05	34.58
26.2986	2.25	16.49	3.89	22.63
26.3031	0.89	6.44	3.89	11.22
26.3076	0.00	5.71	3.52	9.23
26.3121	0.00	3.98	10.61	14.58
26.3166	0.00	16.10	8.83	24.93
26.3211	0.00	16.02	8.35	24.38
26.3256	0.00	5.05	1.85	6.90
26.3301	0.00	7.28	2.27	9.54
26.3346	0.00	6.48	3.26	9.74
26.3391	0.00	1.62	1.83	3.45
26.3436	0.00	0.00	0.74	0.74
26.3481	0.00	0.00	2.27	2.27
26.3526	0.00	0.00	5.29	5.29
26.3571	0.00	0.00	3.13	3.13
26.3616	0.00	0.00	1.32	1.32
26.3661	0.00	0.00	1.36	1.36
26.3706	0.00	0.00	1.30	1.30

References

Albert, A., Echevin, V., L´evy, M., , and Aumont, O.: Impact of nearshore wind stress curl on coastal circulation and primary productivity in the Peru upwelling system, J. Geophys. Res.: Oceans, 115, C12, 2010.

Alford, M. H., MacKinnon, J. A., Simmons, H. L., and Nash, J. D.: Near-inertial internal gravity waves in the ocean, Annual review of marine science, 8, 95–123, 2016.

Atlas, R., Hoffman, R., Bloom, S., Jusem, J., and Ardizzone, J.: A multiyear global surface wind velocity dataset using SSM/I wind observations, Bulletin of the American Meteorological Society, 77, 869–882, 1996.

Banyte, D., Tanhua, T., Visbeck, M., Wallace, D. W. R., Karstensen, J., Krahmann, G., Schneider, A., Stramma, L., and Dengler, M.: Diapycnal diffusivity at the upper boundary of the tropical North Atlantic oxygen minimum zone, J. Geophys. Res.: Oceans, 117, C09 016, https://doi.org/10.1029/2011JC007762, 2012.

Banyte, D., Visbeck, M., Tanhua, T., Fischer, T., Krahmann, G., and Karstensen, J.: Lateral diffusivity from tracer release experiments in the tropical North Atlantic thermocline, J. Geophys. Res.: Oceans, 118, 1–15, https://doi.org/10.1002/jgrc.20211, 2013.

Beckmann, A.: The representation of bottom boundary layer processes in numerical ocean circulation models, in: Ocean Modeling and Parameterization, pp. 135–154, Springer, 1998.

Bohlen, L., Dale, A. W., Sommer, S., Mosch, T., Hensen, C., Noffke, A., Scholz, F., and Wallmann, K.: Benthic Nitrogen Cycling Traversing the Peruvian Oxygen Minimum Zone, Geochimica et Cosmochimica Acta, 75, 6094–6111, https://doi.org/10.1016/j.gca.2011.08.010, 2011.

Brandt, P., Bange, H. W., Banyte, D., Dengler, M., Didwischus, S. H., Fischer, T., Greatbatch, R. J., Hahn, J., Kanzow, T., Karstensen, J., Körtzinger, A., Krahmann, G., Schmidtko, S., Stramma, L., Tanhua, T., and Visbeck, M.: On the role of circulation and mixing in the ventilation of oxygen minimum zones with a focus on the eastern tropical North Atlantic, Biogeosciences, 12, 489–512, https://doi.org/10.5194/bg-12-489-2015, 2015.

Brink, K.: A comparison of long coastal trapped wave theory with observations off Peru, J. Phys. Oceanogr., 12, 897–913, 1982.

Brink, K. H., Halpern, D., Huyer, A., and Smith, R. L.: The physical environment of the Peruvian upwelling system, Progress in Oceanogr., 12, 285–305, 1983.

Carton, J. A. and Giese, B. S.: A reanalysis of ocean climate using Simple Ocean Data Assimilation (SODA), Monthly Weather Review, 136, 2999–3017, 2008.

Carton, J. A., Chepurin, G. A., and Chen, L.: SODA3: A new ocean climate reanalysis, Journal of Climate, 31, 6967–6983, 2018.

Chaigneau, A. and Pizarro, O.: Surface circulation and fronts of the South Pacific Ocean, east of 120°W, Geophys. Res. Lett., 32, 2005.

Chaigneau, A., Gizolme, A., and Grados, C.: Mesoscale eddies off Peru in altimeter records: Identification algorithms and eddy spatio-temporal patterns, Progress in Oceanogr., 79, 106–119, 2008.

Chaigneau, A., Eldin, G., and Dewitte, B.: Eddy activity in the four major upwelling systems from satellite altimetry (1992–2007), Progress in Oceanogr., 83, 117–123, 2009.

Chaigneau, A., Le Texier, M., Eldin, G., Grados, C., and Pizarro, O.: Vertical structure of mesoscale eddies in the eastern South Pacific Ocean: A composite analysis from altimetry and Argo profiling floats, J. Geophys. Res.: Oceans, 116, 2011.

Chaigneau, A., Dominguez, N., Eldin, G., Vasquez, L., Flores, R., Grados, C., and Echevin, V.: Near-coastal circulation in the Northern Humboldt Current System from shipboard ADCP data, J. Geophys. Res.: Oceans, 118, 5251–5266, 2013.

Chavez, F. P. and Messié, M.: A comparison of eastern boundary upwelling ecosystems, Progress in Oceanogr., 83, 80–96, 2009.

Chelton, D. B., Schlax, M. G., Samelson, R. M., and de Szoeke, R. A.: Global observations of large oceanic eddies, Geophys. Res. Lett., 34, 2007.

Colas, F., McWilliams, J. C., Capet, X., and Kurian, J.: Heat balance and eddies in the Peru-Chile current system, Climate Dyn., 39, 509–529, 2012.

Colling, A.: Ocean circulation, vol. 3, Butterworth-Heinemann, 2001.

Combes, V., Hormazabal, S., and Di Lorenzo, E.: Interannual variability of the subsurface eddy field in the Southeast Pacific, Journal of Geophysical Research: Oceans, 120, 4907–4924, 2015.

Conway, T. M., Palter, J. B., and de Souza, G. F.: Gulf Stream rings as a source of iron to the North Atlantic subtropical gyre, Nature Geoscience, 11, 594, 2018.

Czeschel, R., Stramma, L., Schwarzkopf, F. U., Giese, B. S., Funk, A., and Karstensen, J.: Middepth circulation of the eastern tropical South Pacific and its link to the oxygen minimum zone, J. Geophys. Res.: Oceans, 116, C01 015, https://doi.org/10.1029/2010JC006565, 2011.

Czeschel, R., Stramma, L., and Johnson, G. C.: Oxygen decreases and variability in the eastern equatorial Pacific, J. Geophys. Res.: Oceans, 117, https://doi.org/10.1029/2012JC008043, 2012.

Czeschel, R., Stramma, L., Weller, R. A., and Fischer, T.: Circulation, eddies, oxygen, and nutrient changes in the eastern tropical South Pacific Ocean, Ocean Science, 11, 455–470, https://doi.org/10.5194/os-11-455-2015, 2015.

Czeschel, R., Schütte, F., Weller, R. A., and Stramma, L.: Transport, properties, and life cycles of mesoscale eddies in the eastern tropical South Pacific, Ocean Science, 14, 731–750, https://doi.org/10.5194/os-14-731-2018, 2018.

Debreu, L., Vouland, C., and Blayo, E.: AGRIF: Adaptive grid refinement in Fortran, Computers & Geosciences, 34, 8–13, https://doi.org/10.1016/j.cageo.2007.01.009, 2008.

Debreu, L., Marchesiello, P., Penven, P., and Cambon, G.: Two-way nesting in split-explicit ocean models: algorithms, implementation and validation, Ocean Modelling, 49, 1–21, 2012.

Dengler, M.: Microstructure Measurements during METEOR cruise M92, https://doi.org/10.1594/PANGAEA.858896, 2016.

Dewitte, B., Ramos, M., Echevin, V., Pizarro, O., et al.: Vertical structure variability in a seasonal simulation of a medium-resolution regional model of the Eastern South Pacific, Progress in Oceanogr., 79, 120–137, 2008.

Duteil, O. and Oschlies, A.: Sensitivity of simulated extent and future evolution of marine suboxia to mixing intensity, Geophys. Res. Lett., 38, 2011.

Echevin, V., Albert, A., Lévy, M., Graco, M., Aumont, O., Piétri, A., and Garric, G.: Intraseasonal variability of nearshore productivity in the Northern Humboldt Current System: The role of coastal trapped waves, Cont. Shelf Res., 73, 14–30, 2014.

Ferrari, R., Mashayek, A., McDougall, T. J., Nikurashin, M., and Campin, J.-M.: Turning ocean mixing upside down, J. Phys. Oceanogr., 46, 2239–2261, 2016.

Fiedler, P. C. and Talley, L. D.: Hydrography of the eastern tropical Pacific: a review, Progress in Oceanogr., 69, 143–180, 2006.

Fischer, T., Banyte, D., Brandt, P., Dengler, M., Krahmann, G., Tanhua, T., and Visbeck, M.: Diapycnal oxygen supply to the tropical North Atlantic oxygen minimum zone, Biogeosciences, 10, 5079–5093, 2013.

Frenger, I., Bianchi, D., Stührenberg, C., Oschlies, A., Dunne, J., Deutsch, C., Galbraith, E., and Schütte, F.: Biogeochemical role of subsurface coherent eddies in the ocean: Tracer cannonballs, hypoxic storms, and microbial stewpots?, Global Biogeochemical Cycles, 32, 226–249, 2018.

Fuenzalida, R., Schneider, W., Garcés-Vargas, J., Bravo, L., and Lange, C.: Vertical and horizontal extension of the oxygen minimum zone in the eastern South Pacific Ocean, Deep Sea Research Part II: Topical Studies in Oceanography, 56, 992–1003, 2009.

Gent, P. R. and McWilliams, J. C.: Isopycnal mixing in ocean circulation models, J. Phys. Oceanogr., 20, 150–155, 1990.

Gruber, N., Lachkar, Z., Frenzel, H., Marchesiello, P., Münnich, M., McWilliams, J. C., Nagai, T., and Plattner, G.-K.: Eddy-induced reduction of biological production in eastern boundary upwelling systems, Nature Geoscience, 4, 787–792, 2011.

Haine, T. W. and Hall, T. M.: A generalized transport theory: Water-mass composition and age, J. Phys. Oceanogr., 32, 1932–1946, 2002.

Hauss, H., Christiansen, S., Schütte, F., Kiko, R., Lima, M. E., Rodrigues, E., Karstensen, J., Löscher, C. R., Körtzinger, A., and Fiedler, B.: Dead zone or oasis in the open ocean? Zooplankton distribution and migration in low-oxygen modewater eddies, Biogeosciences, 13, 1977–1989, https://doi.org/doi:10.5194/bg-13-1977-2016, wOS:000377274100016, 2016.

Ho, D. T.: Deep Ocean Tracer Release Experiment Information, Retrieved from http://sf6.soest.hawaii.edu, 2019.

Ho, D. T., Ledwell, J. R., and Smethie, W. M.: Use of SF_5CF_3 for ocean tracer release experiments, Geophys. Res. Lett., 35, 2008.

Holmes, R., de Lavergne, C., and McDougall, T. J.: Tracer transport within abyssal mixing layers, Journal of Physical Oceanography, https://doi.org/10.1175/JPO-D-19-0006.1, 2019.

Holtermann, P. L., Umlauf, L., Tanhua, T., Schmale, O., Rehder, G., and Waniek, J. J.: The Baltic Sea tracer release experiment: 1. Mixing rates, J. Geophys. Res.: Oceans, 117, C01 021, https://doi.org/10.1029/2011JC007439, 2012.

Hormazabal, S., Combes, V., Morales, C. E., Correa-Ramirez, M. A., Di Lorenzo, E., and Nuñez, S.: Intrathermocline eddies in the coastal transition zone off central Chile (31–41°S), J. Geophys. Res.: Oceans, 118, 4811–4821, 2013.

Houghton, R. W.: Lagrangian flow at the foot of a shelfbreak front using a dye tracer injected into the bottom boundary layer, Geophys. Res. Lett., 24, 2035–2038, 1997.

Houghton, R. W. and Visbeck, M.: Upwelling and convergence in the Middle Atlantic Bight shelfbreak front, Geophys. Res. Lett., 25, 2765–2768, 1998.

Houghton, R. W., Hebert, D., and Prater, M.: Circulation and mixing at the New England shelfbreak front: Results of purposeful tracer experiments, Progress in Oceanography, 70, 289–312, 2006.

Huyer, A., Knoll, M., Paluszkiewicz, T., and Smith, R. L.: The Peru Undercurrent: a study in variability, Deep Sea Res. Part I: Oceanogr. Res. Papers, 38, S247–S271, 1991.

Ingall, E. and Jahnke, R.: "Evidence for enhanced phosphorus regeneration from marine sediments overlain by oxygen depleted waters", Geochimica et Cosmochimica Acta, 58, 2571 – 2575, https://doi.org/https://doi.org/10.1016/0016-7037(94)90033-7, 1994.

IOC, IHO, and BODC: Centenary Edition of the GEBCO Digital Atlas, published on CD-ROM on behalf of the Intergovernmental Oceanographic Commission and the International Hydrographic Organization as part of the General Bathymetric Chart of the Oceans, British Oceanographic Data Centre, Liverpool, UK, 2003.

Jackson, P. R., Ledwell, J. R., and Thurnherr, A. M.: Dispersion of a tracer on the East Pacific Rise (9°N to 10°N), including the influence of hydrothermal plumes, Deep Sea Res. Part I: Oceanogr. Res. Papers, 57, 37–52, 2010.

Johnson, G. C. and McTaggart, K. E.: Equatorial Pacific 13C Water Eddies in the Eastern Subtropical South Pacific Ocean, J. Phys. Oceanogr., 40, 226–236, https://doi.org/10.1175/2009JPO4287.1, 2010.

José, Y. S., Dietze, H., and Oschlies, A.: Linking diverse nutrient patterns to different water masses within anticyclonic eddies in the upwelling system off Peru, Biogeosciences, 14, 1349, 2017.

José, Y. S., Stramma, L., Schmidtko, S., and Oschlies, A.: ENSO-driven fluctuations in oxygen supply and vertical extent of oxygen-poor waters in the oxygen minimum zone of the Eastern Tropical South Pacific, Biogeosciences Discussions, 2019, 1–20, https://doi.org/10.5194/bg-2019-155, URL `https://www.biogeosciences-discuss.net/bg-2019-155/`, 2019.

Kalvelage, T., Lavik, G., Lam, P., Contreras, S., Arteaga, L., Löscher, C. R., Oschlies, A., Paulmier, A., Stramma, L., and Kuypers, M. M.: Nitrogen cycling driven by organic matter export in the South Pacific oxygen minimum zone, Nature Geoscience, 6, 228–234, https://doi.org/10.1038/ngeo1739, 2013.

Karstensen, J., Stramma, L., and Visbeck, M.: Oxygen minimum zones in the eastern tropical Atlantic and Pacific oceans, Progress in Oceanogr., 77, 331–350, https://doi.org/10.1016/j.pocean.2007.05.009, 2008.

Karstensen, J., Schütte, F., Pietri, A., Krahmann, G., Fiedler, B., Grundle, D., Hauss, H., Körtzinger, A., Löscher, C. R., Testor, P., Vieira, N., and Visbeck, M.: Upwelling and isolation in oxygen-depleted anticyclonic modewater eddies and implications for nitrate cycling, Biogeosciences, 14, 2167–2181, https://doi.org/doi:10.5194/bg-2016-34, 2017.

Klein, P. and Lapeyre, G.: The oceanic vertical pump induced by mesoscale and submesoscale turbulence, Annual review of marine science, 1, 351–375, 2009.

Klenz, T., Dengler, M., and Brandt, P.: Seasonal variability of the Mauritania Current and hydrography at 18 N, J. Geophys. Res.: Oceans, 123, 8122–8137, 2018.

Köllner, M., Visbeck, M., Tanhua, T., and Fischer, T.: Diapycnal diffusivity in the core and oxycline of the tropical North Atlantic oxygen minimum zone, J. Mar. Syst., 160, 54–63, https://doi.org/10.1016/j.jmarsys.2016.03.012, 2016.

Large, W. G. and Yeager, S.: The global climatology of an interannually varying air–sea flux data set, Climate Dyn., 33, 341–364, 2009.

Ledwell, J. R.: Comment on "Abyssal Upwelling and Downwelling Driven by Near-Boundary Mixing", J. Phys. Oceanogr., 48, 739–748, 2018.

Ledwell, J. R. and Bratkovich, A.: A tracer study of mixing in the Santa Cruz Basin, J. Geophys. Res.: Oceans, 100, 20 681–20 704, 1995.

Ledwell, J. R. and Hickey, B. M.: Evidence for enhanced boundary mixing in the Santa Monica Basin, J. Geophys. Res.: Oceans, 100, 20 665–20 679, 1995.

Ledwell, J. R. and Watson, A. J.: The Santa Monica Basin tracer experiment: A study of diapycnal and isopycnal mixing, J. Geophys. Res.: Oceans, 96, 8695–8718, 1991.

Ledwell, J. R., Watson, A. J., and Law, C. S.: Evidence for slow mixing across the pycnocline from an open-ocean tracer-release experiment, Nature, 364, 701–703, 1993.

Ledwell, J. R., Watson, A. J., and Law, C. S.: Mixing of a tracer in the pycnocline, J. Geophys. Res.: Oceans, 103, 21 499–21 529, 1998.

Ledwell, J. R., Montgomery, E. T., Polzin, K. L., Laurent, L. S., Schmitt, R. W., and Toole, J. M.: Evidence for enhanced mixing over rough topography in the abyssal ocean, Nature, 403, 179–182, 2000.

Ledwell, J. R., Duda, T. F., Sundermeyer, M. A., and Seim, H. E.: Mixing in a coastal environment: 1. A view from dye dispersion, J. Geophys. Res.: Oceans, 109, 2004.

Ledwell, J. R., St. Laurent, L. C., Girton, J. B., and Toole, J. M.: Diapycnal mixing in the Antarctic circumpolar current, J. Phys. Oceanogr., 41, 241–246, 2011.

L'Heureux, M. L., Takahashi, K., Watkins, A. B., Barnston, A. G., Becker, E. J., Di Liberto, T. E., Gamble, F., Gottschalck, J., Halpert, M. S., Huang, B., et al.: Observing and predicting the 2015/16 El Niño, Bulletin of the American Meteorological Society, 98, 1363–1382, 2017.

Liu, W. T., Tang, W., and Polito, P. S.: NASA scatterometer provides global ocean-surface wind fields with more structures than numerical weather prediction, Geophys. Res. Lett., 25, 761–764, 1998.

Llanillo, P., Pelegrí, J., Talley, L., Peña-Izquierdo, J., and Cordero, R.: Oxygen Pathways and Budget for the Eastern South Pacific Oxygen Minimum Zone, J. Geophys. Res.: Oceans, 2018.

Loginova, A. N., Thomsen, S., Dengler, M., Lüdke, J., and Engel, A.: Diapycnal dissolved organic matter supply into the upper Peruvian oxycline, Biogeosciences, 16, 2033–2047, https://doi.org/10.5194/bg-16-2033-2019, 2019.

Lomnitz, U., Sommer, S., Dale, A. W., Löscher, C. R., Noffke, A., Wallmann, K., and Hensen, C.: Benthic phosphorus cycling in the Peruvian oxygen minimum zone, Biogeosciences, 13, 1367–1386, https://doi.org/doi:10.5194/bg-13-1367-2016, 2016.

Lüdke, J., Dengler, M., Sommer, S., Clemens, D., Thomsen, S., Krahmann, G., Dale, A. W., Achterberg, E. P., and Visbeck, M.: Influence of intraseasonal eastern boundary circulation variability on hydrography and biogeochemistry off Peru, Ocean Science Discussions, 2019.

Lukas, R.: The termination of the equatorial undercurrent in the eastern Pacific, Progress in Oceanogr., 16, 63–90, 1986.

Luyten, J. R., Pedlosky, J., and Stommel, H.: The ventilated thermocline, J. Phys. Oceanogr., 13, 292–309, 1983.

Madec, G. et al.: NEMO ocean engine version 3.1, Note pole modelisation, 27, 2008.

Marandino, C. A.: RV SONNE SO243 Cruise Report/Fahrtbericht Guayaquil, Ecuador: 05. October 2015 Antofagasta, Chile: 22. October 2015 SO243 ASTRA-OMZ: AIR SEA INTERACTION OF TRACE ELEMENTS IN OXYGEN MINIMUM ZONES, 81 pp., https://doi.org/10.3289/CR_SO243, 2016.

Mashayek, A., Ferrari, R., Merrifield, S., Ledwell, J. R., St Laurent, L., and Garabato, A. N.: Topographic enhancement of vertical turbulent mixing in the Southern Ocean, Nature communications, 8, 14 197, 2017.

McCreary, J. P. and Chao, S.-Y.: Three-dimensional shelf circulation along an eastern ocean boundary, Journal of marine research, 43, 13–36, 1985.

McDougall, T. J. and Barker, P. M.: Getting started with TEOS-10 and the Gibbs Seawater (GSW) Oceanographic Toolbox, Rep. SCOR/IAPSO WG127, 28 pp., https://doi.org/10.1002/2014JC010066, available at www.TEOS-10.org, 2011.

McDougall, T. J. and Ferrari, R.: Abyssal Upwelling and Downwelling Driven by Near-Boundary Mixing, J. Phys. Oceanogr., 47, 261–283, https://doi.org/10.1175/JPO-D-16-0082.1, 2017.

McPhaden, M.: Playing hide and seek with El Niño, Nature Climate Change, 5, 791, 2015.

McPhaden, M. J.: Evolution of the 2002/03 El Niño, Bull. Amer. Meteor. Soc., 85, 677–696, 2004.

McPhaden, M. J.: Understanding and predicting El Niño and the Southern Oscillation, New Frontiers in Operational Oceanography, pp. 653–662, https://doi.org/10.17125/gov2018.ch23, 2018.

Molemaker, M. J., McWilliams, J. C., and Dewar, W. K.: Submesoscale instability and generation of mesoscale anticyclones near a separation of the California Undercurrent, J. Phys. Oceanogr., 45, 613–629, 2015.

Montes, I., Colas, F., Capet, X., and Schneider, W.: On the pathways of the equatorial subsurface currents in the eastern equatorial Pacific and their contributions to the Peru-Chile Undercurrent, J. Geophys. Res.: Oceans, 115, 2010.

Montes, I., Dewitte, B., Gutknecht, E., Paulmier, A., Dadou, I., Oschlies, A., and Garçon, V.: High-resolution modeling of the Eastern Tropical Pacific oxygen minimum zone: Sensitivity to the tropical oceanic circulation, J. Geophys. Res.: Oceans, 119, 5515–5532, https://doi.org/10.1002/2014JC009858, 2014.

Munk, W. H.: Abyssal recipes, in: Deep Sea Research and Oceanographic Abstracts, vol. 13-4, pp. 707–730, Elsevier, 1966.

Noffke, A., Hensen, C., Sommer, S., Scholz, F., Bohlen, L., Mosch, T., Graco, M., and Wallmann, K.: Benthic iron and phosphorus fluxes across the Peruvian oxygen minimum zone, Limnol. & Oceanogr., 57, 851–867, https://doi.org/0.4319/lo.2012.57.3.0851, 2012.

Penven, P. and Tan, T.-A.: ROMSTOOLS user's guide, Rapport techn., IRD and LPO/UBO, Laboratoire de Physique des Oceans, Universite de Bretagne Occidentale/UFR Sciences, updated versions from 2007; online version 2012 created and modified 2015: http://www.romsagrif.org/index.php/documentation/ROMSTOOLS-Documentation, 2003.

Penven, P., Echevin, V., Pasapera, J., Colas, F., and Tam, J.: Average circulation, seasonal cycle, and mesoscale dynamics of the Peru Current System: A modeling approach, J. Geophys. Res.: Oceans, 110, 2005.

Penven, P., Marchesiello, P., Debreu, L., and Lefèvre, J.: Software tools for pre-and post-processing of oceanic regional simulations, Environmental Modelling & Software, 23, 660–662, 2008.

Pizarro, O., Shaffer, G., Dewitte, B., and Ramos, M.: Dynamics of seasonal and interannual variability of the Peru-Chile Undercurrent, Geophys. Res. Lett., 29, 22–1, 2002.

Polzin, K., Toole, J., Ledwell, J., and Schmitt, R.: Spatial variability of turbulent mixing in the abyssal ocean, Science, 276, 93–96, 1997.

Ramírez, I. J. and Briones, F.: Understanding the El Niño costero of 2017: The definition problem and challenges of climate forecasting and disaster responses, International Journal of Disaster Risk Science, 8, 489–492, 2017.

Rodríguez-Morata, C., Díaz, H., Ballesteros-Canovas, J., Rohrer, M., and Stoffel, M.: The anomalous 2017 coastal El Niño event in Peru, Climate Dynamics, pp. 1–18, 2018.

Saha, S., Moorthi, S., Pan, H.-L., Wu, X., Wang, J., Nadiga, S., Tripp, P., Kistler, R., Woollen, J., Behringer, D., et al.: NCEP climate forecast system reanalysis (CFSR) 6-hourly products, January 1979 to December 2010, Research Data Archive at the National Center for Atmospheric Research, Computational and Information Systems Laboratory, Boulder, CO, 2010.

Schafstall, J., Dengler, M., Brandt, P., and Bange, H.: Tidal-induced mixing and diapycnal nutrient fluxes in the Mauritanian upwelling region, J. Geophys. Res.: Oceans, 115, https://doi.org/10.1029/2009JC005940, 2010.

Schlosser, C., Streu, P., Frank, M., Lavik, G., Croot, P. L., Dengler, M., and Achterberg, E. P.: H_2S events in the Peruvian oxygen minimum zone facilitate enhanced dissolved Fe concentrations, Scientific reports, 8, 12 642, 2018.

Schmidtko, S., Johnson, G. C., and Lyman, J. M.: MIMOC: A global monthly isopycnal upper-ocean climatology with mixed layers, J. Geophys. Res.: Oceans, 118, 1658–1672, 2013.

Schmidtko, S., Visbeck, M., and Krahmann, G.: Physical oceanography (CTD) during METEOR cruise M135, URL `https://doi.pangaea.de/10.1594/PANGAEA.904009`, 2019.

Schneider, W., Fuenzalida, R., Rodríguez-Rubio, E., Garcés-Vargas, J., and Bravo, L.: Characteristics and formation of eastern South Pacific intermediate water, Geophys. Res. Lett., 30, 2003.

Scholz, F., Löscher, C. R., Fiskal, A., Sommer, S., Hensen, C., Lomnitz, U., Wuttig, K., Göttlicher, J., Kossel, E., Steininger, R., and Canfield, D. E.: Nitrate-dependent iron oxidation limits iron transport in anoxic ocean regions, Earth and Planetary Science Letters, 454, 272–281, https://doi.org/doi:10.1016/j.epsl.2016.09.025, wOS:000386645700027, 2016.

Shchepetkin, A. F. and McWilliams, J. C.: A method for computing horizontal pressure-gradient force in an oceanic model with a nonaligned vertical coordinate, J. Geophys. Res., 108, https://doi.org/10.1029/2001JC001047, 2003.

Shchepetkin, A. F. and McWilliams, J. C.: The regional oceanic modeling system (ROMS): a split-explicit, free-surface, topography-following-coordinate oceanic model, Ocean Modelling, 9, 347–404, 2005.

Silva, N. and Neshyba, S.: On the southernmost extension of the Peru-Chile undercurrent, Deep Sea Res. Part I: Oceanogr. Res. Papers, 26, 1387 – 1393, https://doi.org/10.1016/0198-0149(79)90006-2, 1979.

Silva, N., Rojas, N., and Fedele, A.: Water masses in the Humboldt Current System: Properties, distribution, and the nitrate deficit as a chemical water mass tracer for Equatorial Subsurface Water off Chile, Deep Sea Res. Part II: Topical Studies in Oceanogr., 56, 1004–1020, https://doi.org/https://doi.org/10.1016/j.dsr2.2008.12.013, 2009.

Sommer, S. and Dengler, M.: Benthic element cycling, fluxes and transport of nutrients and trace metals across the benthic boundary layer in the Peruvian oxygen minimum zone (SFB 754), Cruise No. 137, 06.05. - 29.05.2017 Callao (Peru) - Callao, Cruise report, DFG-Senatskommission für Ozeanographie, Bremen, Germany, https://doi.org/doi: 10.2312/cr_m137, 2019.

Sommer, S., Gier, J., Treude, T., Lomnitz, U., Dengler, M., Cardich, J., and Dale, A. W.: Depletion of oxygen, nitrate and nitrite in the Peruvian oxygen minimum zone cause an imbalance of benthic nitrogen fluxes, Deep Sea Res. Part I: Oceanogr. Res. Papers, 112, 113–122, https://doi.org/10.1016/j.dsr.2016.03.001, 2016.

Song, Y. and Haidvogel, D.: A semi-implicit ocean circulation model using a generalized topography-following coordinate system, Journal of Computational Physics, 115, 228–244, https://doi.org/10.1006/jcph.1994.1189, 1994.

St. Laurent, L., Naveira Garabato, A. C., Ledwell, J. R., Thurnherr, A. M., Toole, J. M., and Watson, A. J.: Turbulence and diapycnal mixing in Drake Passage, J. Phys. Oceanogr., 42, 2143–2152, 2012.

Steinfeldt, R., Sültenfuß, J., Dengler, M., Fischer, T., and Rhein, M.: Coastal upwelling off Peru and Mauritania inferred from helium isotope disequilibrium, Biogeosciences, 12, 7519–7533, 2015.

Stramma, L., Bange, H. W., Czeschel, R., Lorenzo, A., and Frank, M.: On the role of mesoscale eddies for the biological productivity and biogeochemistry in the eastern tropical Pacific Ocean off Peru, Biogeosciences, 10, 7293–7306, 2013.

Stramma, L., Fischer, T., Grundle, D. S., Krahmann, G., Bange, H. W., and Marandino, C. A.: Transition to El Niño conditions in the eastern tropical Pacific in October 2015, Ocean Science Discussions, pp. 1–30, https://doi.org/10.5194/os-2016-14, 2016.

Strub, P. T., Mesias, J. M., Montecino, V., Rutllant, J., and Salinas, S.: Coastal ocean circulation off western South America, in The Sea: The Global Coastal Ocean, vol. 11, John Wiley, N. Y., 11 edn., 1998.

Takahashi, K. and Martínez, A. G.: The very strong coastal El Niño in 1925 in the far-eastern Pacific, Climate Dynamics, https://doi.org/10.1007/s00382-017-3702-1, 2017.

Talley, L.: Hydrographic Atlas of the World Ocean Circulation Experiment (WOCE). Volume 2: Pacific Ocean, International WOCE Project Office, Southampton, U.K., https://doi.org/10.21976/C6WC77, 2007.

Tanhua, T. and Visbeck, M.: Hydrochemistry of water samples during METEOR cruise M135, https://doi.org/10.1594/PANGAEA.890441, URL https://doi.org/10.1594/PANGAEA.890441, 2018.

Thomsen, S. and Lüdke, J.: Microstructure measurements during METEOR cruise M136, https://doi.org/10.1594/PANGAEA.890121, 2018.

Thomsen, S., Kanzow, T., Krahmann, G., Greatbatch, R. J., Dengler, M., and Lavik, G.: The formation of a subsurface anticyclonic eddy in the Peru-Chile Undercurrent and its impact on the near-coastal salinity, oxygen, and nutrient distributions, J. Geophys. Res.: Oceans, 121, 476–501, https://doi.org/10.1002/2015JC010878, 2016.

Timmermann, A., An, S.-I., Kug, J.-S., Jin, F.-F., Cai, W., Capotondi, A., Cobb, K., Lengaigne, M., McPhaden, M. J., Stuecker, M. F., et al.: El Niño–Southern Oscillation complexity, Nature, 559, 535, 2018.

Toole, J. M., Polzin, K. L., and Schmitt, R. W.: Estimates of diapycnal mixing in the abyssal ocean, Science, 264, 1120–1124, 1994.

Visbeck, M.: Oxygen in the Tropical Pacific POSTRE II First Tracer Survey, Cruise No. M135, 01 March – 08 April 2017, Valparaiso (Chile), Callao (Peru), METEOR-Berichte, under review.

Visbeck, M., Czeschel, R., and Krahmann, G.: ADCP current measurements (38 and 75 kHz) during METEOR cruise M135, https://doi.org/10.1594/PANGAEA.887131, 2018.

Waterhouse, A. F., MacKinnon, J. A., Nash, J. D., Alford, M. H., Kunze, E., Simmons, H. L., Polzin, K. L., St. Laurent, L. C., Sun, O. M., Pinkel, R., et al.: Global patterns of diapycnal mixing from measurements of the turbulent dissipation rate, J. Phys. Oceanogr., 44, 1854–1872, 2014.

Watson, A. J. and Ledwell, J. R.: Oceanographic tracer release experiments using sulphur hexafluoride, J. Geophys. Res.: Oceans, 105, 14 325–14 337, 2000.

Watson, A. J., Ledwell, J. R., Messias, M.-J., King, B. A., Mackay, N., Meredith, Michael P.and Mills, B., and Naveira Garabato, A. C.: Rapid cross-density ocean mixing at mid-depths in the Drake Passage measured by tracer release, Nature, 501, 408–411, https://doi.org/10.1038/nature12432, 2013.

Whalen, C., Talley, L., and MacKinnon, J.: Spatial and temporal variability of global ocean mixing inferred from Argo profiles, Geophys. Res. Lett., 39, https://doi.org/10.1029/2012GL053196, 2012.

Willebrand, J., Barnier, B., Böning, C., Dieterich, C., Killworth, P. D., Le Provost, C., Jia, Y., Molines, J.-M., and New, A. L.: Circulation characteristics in three eddy-permitting models of the North Atlantic, Progress in Oceanogr., 48, 123–161, 2001.

Worley, S. J., Woodruff, S. D., Reynolds, R. W., Lubker, S. J., and Lott, N.: ICOADS release 2.1 data and products, International Journal of Climatology, 25, 823–842, 2005.

Xie, R. and Fang, X.: The unusual 2014–2016 El Niño events: Dynamics, prediction and enlightenments, Science China Earth Sciences, pp. 1–8, 2019.

Zocher, J.: Simulation of a Tracer Release Experiment on the continental shelf off Peru, Diploma thesis, Christian-Albrechts-Universität, URL `http://oceanrep.geomar.de/10957/`, 2010.

Acknowledgements

The studies shown in this thesis were financially supported, and performed within the frame of the Collaborative Research Center 754 "Climate - Biogeochemistry Interactions in the Tropical Ocean" (SFB754) as part of subproject A3 ("A tracer release experiment (POSTRE) to quantify benthic-pelagic exchanges in the Peruvian oxygen minimum zone (OMZ) and constraining the age-spectrum of the OMZ with transient tracers").

Acknowledgements for Chapter 1. Introduction

Thanks to Jan Lüdke and Daniela Niemeyer for their helpful feedbacks on an early draft of the Introduction.

Acknowledgements for Chapter 2. Data and Methods

I appreciate the sustained efforts of the captains and crews of *RV Sonne* and *RV Meteor* as well as the scientific and technical group involved in the release and survey of the tracer.

The model runs and the implemented moTREs were performed by Yonss José (for ROMS/ CROCO) and Olaf Duteil (for NEMO). They provided the model output and summarized the methodological important points in short paragraphs. The content of the related sections profited from their helpful discussions at early stages.

Observational Data Availability

- The injected tracer amount as a function of density is provided as Supporting Information in Appendix B.
- The surveyed tracer experiment data set, the CTD and vmADCP data related to the tracer injection and survey are publicly available at the data base PANGAEA
  - **tracer survey data:** Tanhua, T., and Visbeck, M. (2018): Hydrochemistry of water samples during METEOR cruise M135, data set, doi: 10.1594/PANGAEA.890441.
  - **CTD data related to tracer injection:** Stramma, L., and G. Krahmann (2016): Physical oceanography during SONNE cruise SO243, PANGAEA, doi: 10.1594/PANGAEA.861388 (supplement to: Stramma et al., 2016).

- **CTD data related to tracer survey:** Schmidtko, S., Visbeck, M., and Krahmann, G. (2019): Physical oceanography (CTD) during METEOR cruise M135, doi: 10.1594/PANGAEA.904009.
- **vmADCP data related to tracer survey:** Visbeck, M., Czeschel, R., and Krahmann, G. (2018): ADCP current measurements (38 and 75 kHz) during METEOR cruise M135, data set, doi: 10.1594/PANGAEA.887131.

Video Supplement

The time development of the modeled lateral tracer distributions shown by the vertical column integral is given as video supplement (SI-videos) in full time resolution. These SI-videos are publicly available at Freund, M. (2020): Time development of modeled lateral tracer distributions in the eastern tropical South Pacific, PANGAEA, doi: 10.1594/PANGAEA.913475 (dataset in review).

Acknowledgements for Chapter 3. Advective Regimes and the Connectivity from the Shelfbreak to the Open Ocean

Thanks to Rena Czeschel and Gerd Krahmann for the contemporary raw data processing and the (internal and external) publication of the ADCP data related to the tracer survey (cruise M135). I appreciate the contribution of Arne Bendinger due to comprehensive plotting of the moTREs which speeded up their analysis. Florian Schütte provided the SLA map (Fig. 3.13) and did the exemplary eddy tracking (eddies A and B in Fig. 3.13). During the early stages of the analyses this chapter's content profited from the helpful discussions with Yonss José and Olaf Duteil.

Acknowledgements for Chapter 4. Upward Tracer Motion

I appreciate the contribution of Arne Bendinger due to comprehensive plotting of the moTREs which speeded up their analysis.

Acknowledgements for Chapter 5. Offshore Diapycnal Diffusivity

The content of this chapter and the sections 1.2.5 & 2.1.1 build a manuscript that was submitted to *Geophysical Research Letters* in November 2018, revised according to the reviewer's comments, and resubmitted in October 2019.
Citation: Freund, M., Visbeck, M., and Tanhua, T. (2019): Eastern Tropical South Pacific Diapycnal Diffusivity within the Offshore Oxygen Minimum Zone, Geophys. Res. Lett., pp. , with Supporting Information containing the processed injection data, declined.
It was declined in November 2019 with the arguments that it "does not merit publication on its own" - without the results shown in the thesis chapters above. Further, it is "a scientifically

correct paper but not obviously a significant advance in a geophysical field" and "does not present sufficient innovation".

While preparing and revising the manuscript of this chapters content, I appreciate the input of two anonymous reviewers. Marcus Dengler, Manuela Köllner, and Jan Lüdke greatly contributed through many helpful discussions. Special thanks to Avan Antia for her help in improving the writing style and structure. The reports of the peer-review process were considered for this version of the chapter.

Expression of Thanks

Many thanks to my thesis committee, Martin, Toste, and Marcus, for your support and advises during the years. It was an exciting and interesting experience to learn from all you.

Many thanks to the colleagues and friends at Geomar, in the PO department, and in the SFB754 community. It was inspiring and nice to work with you. You created a pleasant working atmosphere and I enjoyed our discussions.

Special thanks to Manuela und Donata helping me to be prepared for what to expect and what to come.

Best thanks to Jan and Daniela for your ever lasting cooperation when I was stuck in all-day-issues and -routines.

To my friends, who you are invisible in business and academic live, supporting me since decades as in the times as a doctoral researcher, cheering me up or calming me down - whatever is needed. Thank you for keeping an eye on me.

To Jörg, my husband, thanks for your faith and your patience. Thanks for lending me your ear, especially in the end phase of the thesis writing, and for proofreading the thesis. You have an incredible skill to get IT-systems running at any time, even from remote. You are my anchor to the here and now. Thanks for open up so many possibilities for me.

Declaration

I hereby declare that this thesis is my own work, despite the supervision of my advisors in the thesis committee Prof. Dr. Martin Visbeck, Dr. Toste Tanhua, and Dr. Marcus Dengler. Cooperation with colleagues are acknowledged. I complied with the good scientific practice of the German Research Foundation (DFG).
Neither this thesis nor parts of it nor any similar form of it has been submitted in any other examining body.
An academic degree has been never withdrawn from me.

Declaration in German - Erklärung

Hiermit erkläre ich, dass die vorliegende Dissertation - abgesehen von der Beratung durch meine Betreuer im Thesis Committee Prof. Dr. Martin Visbeck, Dr. Toste Tanhua und Dr. Marcus Dengler - nach Inhalt und Form eine eigenständige und nur mit den angegebenen Hilfsmitteln verfasste Arbeit ist, die unter Einhaltung der Regeln guter wissenschaftlicher Praxis der Deutschen Forschungsgemeinschaft (DFG) entstanden ist. Die Zusammenarbeit mit anderen Wissenschaftlern habe ich kenntlich gemacht.
Diese Arbeit wurde weder gänzlich noch in Teilen noch in ähnlicher Form an anderer Stelle im Rahmen eines Prüfungsverfahrens vorgelegt, veröffentlicht oder zur Veröffentlichung eingereicht.
Mir wurde nie ein akademischer Grad entzogen.

Kiel, 25. April 2020 _____

. (Madeleine Freund)